



**Politecnico
di Torino**

POLITECNICO DI TORINO

Master of Science in Environmental Engineering

Climate Change

A.a. 2020/2021

Graduation Session December 2021

Master Thesis

**Future crop water footprint scenarios
across the African continent**

Assessing the impacts of climate change and advanced management
strategies on agriculture, production and water resources

Supervisors:

Prof. Francesco Laio

Marta Tuninetti Ph.D.

Candidate:

Vittorio Giordano

Abstract

Alarming projections of climate change, increasing aridity and decreasing water availability, coupled with continued population growth, changes in dietary patterns and expanding biofuel use represent some of the heaviest pressures on global agriculture. In addition, crop yields are generally projected to decrease under future climate conditions. All these factors heavily impact food production and constitute worrisome implications for food security. At the same time, to meet the projected demands from population and societal changes, global crop production needs to double globally by 2050, and the commonly preferred solution for achieving such increment is through boosting crop yields. But while western countries are closer to their crop yield potential, Africa still falls behind in crop yield gap closure.

This work develops high-resolution, crop water footprint (*CWF*) scenarios of different crops across the African continent for 2010, 2040, 2070 and 2100, in order to assess the impacts of climate change on African agriculture. In addition, by including crop yield forecasts which project a high input, advanced management agriculture on the continent, it investigates if food security can be achieved by increasing production on the current harvested areas and how this will affect the water resources. Results show that advanced management practices bring crop yields to increase up to three folds, while the water use efficiency also improves - between 2010 and 2040, the average unitary water footprint (*uWF*) decreases by 62% and 74%, in the case of maize and sorghum respectively, over the whole continent. As an example, in Mozambique it decreases by 78% between 2010 and 2040; nevertheless, in Egypt the *uWF* increases by 58%, in the case of maize. At the same time, in both countries, the *CWF* of maize increases from 2010 to 2040, respectively by 58% and 150%. These results show that, when the increment in agricultural production is taken into account, the water volume needed rises - 30% and 25% average increment in volume, respectively for maize and sorghum, between 2010 and 2040 across Africa -, putting a strain on a natural resource already affected by climate change.

Contents

List of Figures	3
List of Tables	8
1 Introduction	9
2 Data	17
2.1 Inter-Sectoral Impact Model Intercomparison Project (ISI-MIP)	18
2.2 Global Gridded Crop Models	20
2.2.1 <i>CLM4.5</i>	21
2.2.2 <i>GEPIC</i>	22
2.2.3 <i>PEPIC</i>	23
2.2.4 <i>LPJmL</i>	23
2.2.5 <i>GAEZ v4</i>	23
2.3 Crop Yield Simulations	25
2.4 Crop Actual Yield	29
2.5 Harvested Areas	31
2.6 Climatic Data	32
2.7 Crop-specific data	35
3 Methodology	37
3.1 Global gridded crop model Validation	38
3.1.1 Models Ensemble spatial variability	38
3.1.2 Temporal variability & Model comparison	39
3.1.3 Country specific procedure	43
3.1.4 Inclusion of <i>GAEZ v4</i> in the validation	44

3.2	<i>GAEZ v4</i> extensive analysis & validation	46
3.3	Crop Water Footprint Model	51
3.3.1	Evaluation of Crop Water Footprint over a single growing season	52
3.3.2	Validation of input climatic variables	53
3.3.3	Model Modifications	55
3.4	Scenarios comparison	59
4	Results	62
4.1	Continent-level aggregated water footprint	63
4.2	Spatial Distribution and Temporal evolution of rainfed water footprint	71
4.3	Spatial Distribution and Temporal evolution of irrigated water footprint	73
4.4	Crop aggregated green water footprint	75
4.5	Crop aggregated blue water footprint	77
5	Discussion	80
6	Conclusion	87
	Bibliography	90
A	Yield spatial variability on Italy and Ethiopia	97
B	Country identifier global grid	100
C	GGCMs Details	101

List of Figures

1.1	Prevalence of Undernourishment, 2020. The prevalence of undernourishment expresses the probability that a randomly selected individual consumes an amount of calories that is insufficient to cover her/his energy requirement for an active and healthy life (FAOSTAT, 2021).	10
1.2	(a) Geographic map of Africa; (b) Major Agricultural Systems, taken from AQUAMAPS (FAO, 2021).	14
1.3	(a) Estimated aridity over Africa; taken from FAO (2021); (b) Area equipped for irrigation (<i>AEI</i>), available from Siebert et al. (2013).	15
2.1	Schematic representation of the scenario design for ISIMIP2b. “Other” includes non-climatic forcing factors such as fertilizer input, irrigation, selection of crop varieties, water abstraction for human use etc. Panel (a) shows model runs that separate the pure effect of the historical climate change from other (human) influences (Group 1). Group 2 consists of model runs to estimate the effect of future climate change assuming fixed year 2005 levels of population, economic development, land use (<i>LU</i>), and management (2005soc). Panel (b) shows Group 3, which consists of model runs that quantify the effects of <i>LU</i> changes and changes in population, GDP and management from 2005 onwards, associated with <i>RCP6.0</i> (no mitigation scenario under <i>SSP2</i>) and <i>RCP2.6</i> strong mitigation scenario under <i>SSP2</i>) (Frieler et al., 2017)	20
2.2	General framework of the <i>GEPIC</i> model, (Liu, 2009)	22
2.3	Overall structure of <i>GAEZ v4</i> , (FAO and IIASA, 2021)	25

2.4	National aggregation of maize yield at 2010, 2040, 2070 and 2100 for <i>RCP2.6</i> , CO ₂ scenario.	27
2.5	Percentage variation maps of (a) 2100 attainable soy yield relative to 2010 actual soy yield, (b) 2100 attainable soy yield relative to 2040 attainable soy yield	29
2.6	Crop actual yield at 2010 for: (a) Maize, (b) Sorghum, (c) Soy, (d) Wheat, source: <i>GAEZ v4</i>	31
2.7	Total harvested areas of: (a) Maize, (b) Sorghum, (c) Soy, (d) Wheat, source: <i>GAEZ v4</i>	32
2.8	Percentage variation maps relative to 2010 of: (a) precipitation at 2100; (b) reference potential evapotranspiration at 2100;	35
3.1	Spatial variability of irrigated Maize (a) average yield, (b) standard deviation across Ethiopia and (c) average yield, (d) standard deviation across Italy for the year 2099, <i>RCP6.0</i>	39
3.2	Individual models, ensemble and FAOSTAT (2021) yearly national maize yield data comparison for (a) Ethiopia and (b) Italy, <i>RCP2.6</i>	40
3.3	Individual models, ensemble and FAOSTAT (2021) yearly national maize yield data comparison for (a) Ethiopia and (b) Italy, <i>RCP6.0</i>	40
3.4	(a) <i>CLM4.5</i> , (b) <i>GEPIC</i> , (c) <i>LPJmL</i> and (d) <i>PEPIC</i> , ensemble and FAOSTAT (2021) yearly national maize yield series, Ethiopia, <i>RCP2.6</i>	41
3.5	(a) <i>CLM4.5</i> , (b) <i>GEPIC</i> , (c) <i>LPJmL</i> and (d) <i>PEPIC</i> , ensemble and FAOSTAT (2021) yearly national maize yield series, Italy <i>RCP2.6</i> . .	41
3.6	(a) <i>CLM4.5</i> , (b) <i>GEPIC</i> , (c) <i>LPJmL</i> and (d) <i>PEPIC</i> , ensemble and FAOSTAT (2021) yearly national maize yield series, Ethiopia <i>RCP6.0</i>	42
3.7	(a) <i>CLM4.5</i> , (b) <i>GEPIC</i> , (c) <i>LPJmL</i> and (d) <i>PEPIC</i> , ensemble and FAOSTAT (2021) yearly national maize yield series, Italy <i>RCP6.0</i> . .	43
3.8	Country specific analysis. Representation of Ensemble, irrigated and rainfed ensemble and FAOSTAT (2021) data of yearly national maize yield for: (a) Ethiopia, <i>RCP2.6</i> ; (b) Ethiopia, <i>RCP6.0</i> ; (c) Italy, <i>RCP2.6</i> ; (d) Italy, <i>RCP6.0</i>	44

3.9	Comparison among Ethiopia yearly national yield as obtained from FAOSTAT (2021), Model Ensemble and <i>GAEZ v4</i> . (a) <i>RCP2.6</i> ; (b) <i>RCP6.0</i>	45
3.10	Comparison among Italy yearly national yield as obtained from FAOSTAT (2021), Model Ensemble and <i>GAEZ v4</i> . (a) <i>RCP2.6</i> ; (b) <i>RCP6.0</i>	45
3.11	<i>GAEZ v4</i> validation with FAOSTAT (2021) national yield values - (a) Sorghum; (b) Maize.	47
3.12	<i>GAEZ v4</i> 2010 wheat actual yield validation with: (a) FAOSTAT national yield values at 2010; (b) Monfreda et al. (2008) yield data set at 2000	48
3.13	<i>GAEZ v4</i> 2040 sorghum yield scenario comparison: (a) with and without CO ₂ fertilization; (b) <i>RCP2.6</i> and <i>RCP6.0</i>	49
3.14	<i>GAEZ v4</i> future attainable soy yield at 2100 compared with: (a) actual soy yield at 2010; (b) attainable soy yield at 2040	50
3.15	<i>GAEZ v4</i> 2010 wheat harvested areas validation with: (a) FAOSTAT national harvested areas values at 2010; (b) Portmann et al. (2010) harvested areas data set at 2000	51
3.16	Climatic variables validation scatter plots. Panel (a): potential evapotranspiration from ISIMIP (2021) against FAO (2014). Panel (b): validation of ISIMIP (2021) precipitatin with New et al. (2002) dataset.	54
3.17	Daily evapotranspiration (a) and precipitation (b) over the growing period of Sorghum in one grid cell of Egypt. Horizon 2070, <i>RCP2.6</i> , CO ₂	55
3.18	Daily evolution of crop coefficient, water content coefficient (a) and irrigation (b) over the growing period of Sorghum in one grid cell of Egypt. Horizon 2070, <i>RCP2.6</i> , CO ₂	56
3.19	Monthly evolution of (a) actual evapotranspiration, (b) green evapotranspiration and (c) blue evapotranspiration over the year for Sorghum crop in one grid cell of Egypt. Horizon 2070, <i>RCP2.6</i> , CO ₂	57
3.20	Monthly evolution of (a) total precipitation, (b) effective precipitation and (c) irrigation over the year for Sorghum crop in one grid cell of Egypt. Horizon 2070, <i>RCP2.6</i> , CO ₂	57

3.21	Comparison of (a) uWF and (b) CWF between 2010 and 2100 for maize, scenario $RCP2.6$, CO_2 fertilization.	60
3.22	Percentage difference map of (a) Maize uWF at 2100 ($RCP2.6$) and (b) wheat CWF at 2100 ($RCP2.6$), relative to 2010	61
4.1	Evolution of average African yield of four crops across the future scenarios. Both $RCPs$ are shown, as well as FAOSTAT (2021) historical yield statistics from 1961 to 2019.	64
4.2	Yield achievement ratio of: (a) maize; (b) sorghum; (c) soy; (d) wheat.	65
4.3	Evolution of uWF averaged over whole Africa across future scenarios. Both $RCPs$ are shown.	67
4.4	Evolution of WF averaged over whole Africa across future scenarios. Both $RCPs$ are shown.	68
4.5	Historical evolution of harvested areas over whole Africa from 1961 to 2019. Future values are kept constant and equal to harvested areas at 2010.	70
4.6	Panel: (a) overall harvested areas in Africa by production type and crop variety; (b) tonnes produced overall by the three major producers of each crop variety at 2010.	71
4.7	Sorghum rainfed uWF across Africa at (a) 2010; (b) 2040, $RCP2.6$; (c) 2100, $RCP2.6$; (d) 2100, $RCP6.0$; Future scenarios are represented as percentage difference maps relative to 2010.	72
4.8	Maize rainfed uWF across Africa at (a) 2010; (b) 2040, $RCP2.6$; (c) 2100, $RCP2.6$; (d) 2100, $RCP6.0$; Future scenarios are represented as percentage difference maps relative to 2010.	73
4.9	Sorghum irrigated uWF across Africa at (a) 2010; (b) 2040, $RCP2.6$; (c) 2100, $RCP2.6$; (d) 2100, $RCP6.0$; Future scenarios are represented as percentage difference maps relative to 2010.	74
4.10	Maize irrigated uWF across Africa at (a) 2010; (b) 2040, $RCP2.6$; (c) 2100, $RCP2.6$; (d) 2100, $RCP6.0$; Future scenarios are represented as percentage difference maps relative to 2010.	75

4.11	Green <i>WF</i> across Africa at 2010. The three countries showing higher values are enlarged. The histogram with the five countries recording higher values is shown as well.	76
4.12	Blue <i>WF</i> across Africa at 2010. The three countries showing higher values are enlarged. The histogram with the five countries recording higher values is shown as well.	77
4.13	Three countries showing higher blue <i>WF</i> values at 2040, in orange, on the left, and at 2100, purple, on the right - <i>RCP2.6</i> . The histogram shows the evolution of the overall blue <i>WF</i> for the respective country between three scenarios.	79
5.1	Evolution of agricultural production for each crop variety.	81
5.2	Prevalence of severe or moderate food insecurity.	83
5.3	Current and projected water stress index in Africa (source: WRI (2021)): (a) Baseline water stress index (2010); (b) Index variation in the projection for year 2040 using the halfway scenario <i>Business as Usual</i>	84
5.4	Map of land and/or water scarcity pressures on agriculture; taken from FAO (2021)	86
A.1	Spatial variability of irrigated Maize (a) average yield, (b) standard deviation across Ethiopia and (c) average yield, (d) standard deviation across Italy for the year 2000	97
A.2	Spatial variability of rainfed Maize (a) average yield, (b) standard deviation across Ethiopia and (c) average yield, (d) standard deviation across Italy for the year 2000	98
A.3	Spatial variability of rainfed Maize (a) average yield, (b) standard deviation across Ethiopia and (c) average yield, (d) standard deviation across Italy for the year 2099, <i>RCP6.0</i>	99

List of Tables

2.1	<i>GGCMs</i> simulations used in this study	28
2.2	Summary of Crop Actual Yield data sets	30
2.3	Summary of Harvested Areas data sets	32
2.4	Summary of Climatic data sets	34
C.1	<i>GGCMs</i> detailed parameters description	101
C.1	<i>GGCMs</i> detailed parameters description	102

Chapter 1

Introduction

Climate change is already affecting every inhabited region across the globe and its impacts are now well documented. Widespread and rapid changes in the atmosphere, ocean, cryosphere and biosphere have occurred; global temperature and precipitation have increased since 1850, the oceans have warmed and the global mean sea level have risen (IPCC, 2021). Human-induced climate change is affecting many weather and climate extremes in every region across the globe and there is evidence of changes in extremes such as heatwaves, heavy precipitation, droughts and tropical cyclones, which are attributed to human influence (IPCC, 2021). Among all of this, climate change also affects food production. Warmer mean and extreme temperatures, altered precipitation regimes and drought patterns, elevated atmospheric CO₂ concentrations, among many other mechanisms, already affect agricultural productivity worldwide (Jägermeyr et al., 2021).

The whole picture, however, is even more daunting, since, in parallel to climate change impacts on agriculture, other pressures affect this sector nowadays. The world is experiencing rising demand for crop production, which stem from increasing human population, meat and dairy consumption, as a consequence of growing affluence, and biofuel consumption (Ray et al., 2013). The demand for food and animal feed is increasing at a historic pace and countries are increasingly turning to agricultural commodities as a solution to high fuel prices, energy security, and growing CO₂ emissions (Elliott et al., 2014). Ray et al. (2013) estimated that the global agricultural production will need to be increased by 60 to 110% in order to

meet such increasing demands as well as to provide food security to the chronically undernourished share of the global population. Yet, this represents a double sided challenge. While climate change is affecting agricultural production, slowing its yearly increment towards 2050, world hunger is on the rise. After remaining stable for few years, the prevalence of undernourishment increased from 8.4 to 9.9% just in 2020. Under the shadow of the COVID-19 pandemic world hunger increased again, between 720 and 811 million people faced hunger in 2020, around 118 million more than in 2019 (FAO et al., 2021).

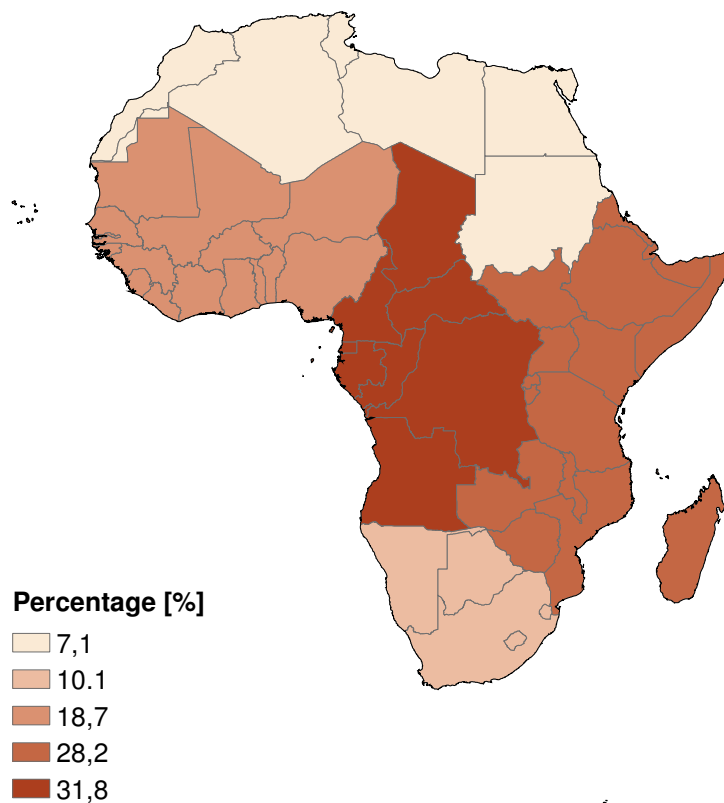


Figure 1.1: Prevalence of Undernourishment, 2020. The prevalence of undernourishment expresses the probability that a randomly selected individual consumes an amount of calories that is insufficient to cover her/his energy requirement for an active and healthy life (FAOSTAT, 2021).

As the availability of land for agricultural uses stagnates or even declines, increased land-use intensification and improved management to increase yields on existing lands have been proposed as possible solutions to meet demand challenges and to attenuate some of the negative impacts of climate change (Elliott et al., 2014). Crop yield growth has been shown as an effective tool for increasing agricultural production and meeting food demand on existing cropland, without further encroachment on natural ecosystems such as forests, wetlands and savannas. Potentially, it can also contribute in reducing global poverty and undernourishment, as farmers constitute a wide share of the poor population (Ray et al., 2013). However, yields are not improving on 24 to 39% of cropland areas in top producing nations with rising population and increasing affluence (Ray et al., 2013). Growing season temperatures, over all harvested areas for the major ten global crops have increased of 0.5 to 1.2 °C and recent research suggests that yields have already been impacted. According to Ray et al. (2019), this has led to a 1% average reduction in consumable food calories in these ten crops. In addition, crop yields are predicted to decrease under future climate conditions; especially at higher levels of warming strong future yield losses are expected (Ray et al., 2019). Also freshwater limitations will take a toll on irrigated production, some regions could necessitate the reversion of 20 to 60 Mha of cropland from irrigated to rainfed management by the end of the century (Elliott et al., 2014).

The largest adverse impacts on yields have been found in low-latitude regions by several studies using Global Gridded Crop Models (*GGCMs*) or linear regression analyses (Jägermeyr et al., 2021; Ray et al., 2019; Elliott et al., 2014; Rosenzweig et al., 2014). Results suggest that climate impacts on tropical croplands are generally more negative than the mid- and high-latitude impacts. Even moderate temperature increases will have negative yield impacts on major crops in tropical regions due to their current proximity to crop-limiting temperatures thresholds for suitable production (Jägermeyr et al., 2021; Rosenzweig et al., 2014). Furthermore, increases in tropical temperatures can lead to shortening of growing periods, greater evaporative demand and, thus, water stress on crops, while CO₂ fertilization effects can not compensate such impacts (Rosenzweig et al., 2014).

Most parts of Africa lie exactly between the tropics. Here, hunger affects 21% of the population, compared with 9% in Asia and 9.1% in Latin American and the Caribbean (FAO et al., 2021). A map of the prevalence of undernourishment in Africa can be seen in figure 1.1. Although food demand is expected to increase more than 60% by 2050, the rise is expected to be much greater in sub-Saharan Africa, a region facing the greatest food security risk, which is expected to see its population double by 2050 and its cereal demand almost triple (van Ittersum et al., 2016). The causes of hunger in Africa are many: poverty, poorly developed agricultural infrastructure, competition for water and other resources, conflicts and natural disasters. Among these, insufficient food supply is one of the main causes (Tian and Yu, 2019). Therefore, increasing food production still plays a central role in eradicating hunger in the continent. This brought to the definition of the focus of this work. The present thesis focuses on the African continent and it explores (i) the dynamics and impacts of climate change over its cultivated areas, and (ii) the implications of the advancement in agricultural management. The investigation has been built around the crop water footprint (*CWF*), as the subject of this work, given the inclusion in such indicator of agriculture-related variables, such as yields and harvested areas indirectly, as well as climatic and water-related ones, namely evapotranspiration and precipitation (D’Odorico et al., 2019, 2018). The concept of “water footprint” provides a framework to analyse the link between human consumption and the direct and indirect appropriation of global freshwater. The water footprint of a product (also known as “virtual water content” (Allan, 2011)), usually expressed in water volume per unit of product is the sum of the water used in the process steps taken to produce such product (Mekonnen and Hoekstra, 2011). By making future projections of this indicator calculated for crops it was possible to investigate the impacts of climate change on agriculture but also the effects of a strong increment of yields on the natural resources. The hypothesis of a strong yield increase thanks to a high input agricultural management projected on the continent represents the conceptual center of this work and defines its underpinning research: (i) What would happen if it was possible to reach an advanced agricultural management on the current cropland by 2040? (ii) Would the production be sufficient to meet the growing food

demand? And (iii) How would this impact the water resources?

This study consisted in an investigation of global gridded crop models (*GGCMs*) (Rosenzweig et al., 2014), to find the most suitable for the purpose of this work. The choice of *GAEZ v4* (FAO and IIASA, 2021) allowed to introduce the assumption of improved agricultural management from 2040 onwards. Most commonly, *GGCMs* used in the literature are merely driven by variable information on weather and atmospheric CO₂ concentrations, whereas assumptions on soil properties and management systems are static (Müller et al., 2017). Therefore, the choice of projecting improved management conditions on agriculture constitutes a new approach in the *CWF* literature. Such strong assumption has been coupled with a constraint: harvested areas have been kept constant at 2010, the last year for which a gridded dataset is available, in order to simulate a form of agricultural intensification over the continent. Global agricultural intensification through ever-increasing resource use is a main driver of current transgressions of ‘planetary boundaries’ and irrigation, which is of paramount importance to increasing productivity on existing agricultural lands, already accounts for more than 70% of human water withdrawals, representing, globally, the largest freshwater user (Jägermeyr et al., 2021). However, African agriculture still relies mostly on rainfall and there are many locations across the African territory where the actual crop yield falls below its potential, due to water stress conditions occurring along the cropping period, and groundwater resources are notably underutilized, despite the potential for sustainable use by taking advantage of the rainfall generated recharge (De Angelis et al., 2021). Therefore, improved water management is a key driver for the closure of the yield gap, since it allows to expand current agricultural production with proper infrastructures for irrigation where the locally generated runoff is large enough, without compromising the environmental flow and the downstream flow towards the other cells of the drainage network (De Angelis et al., 2021). The work proceeded with the adaptation of the model developed by Tuninetti et al. (2015) to work on future *CWF scenarios* for four crops: maize, wheat, sorghum and soy. The first two crops are the principal grains grown on the continent, while sorghum is an important crop in Africa but often disregarded by similar studies performed on a global level, most commonly

substituted by rice. Maize is the most widespread cultivation and it is present in nearly all the ecological zones.

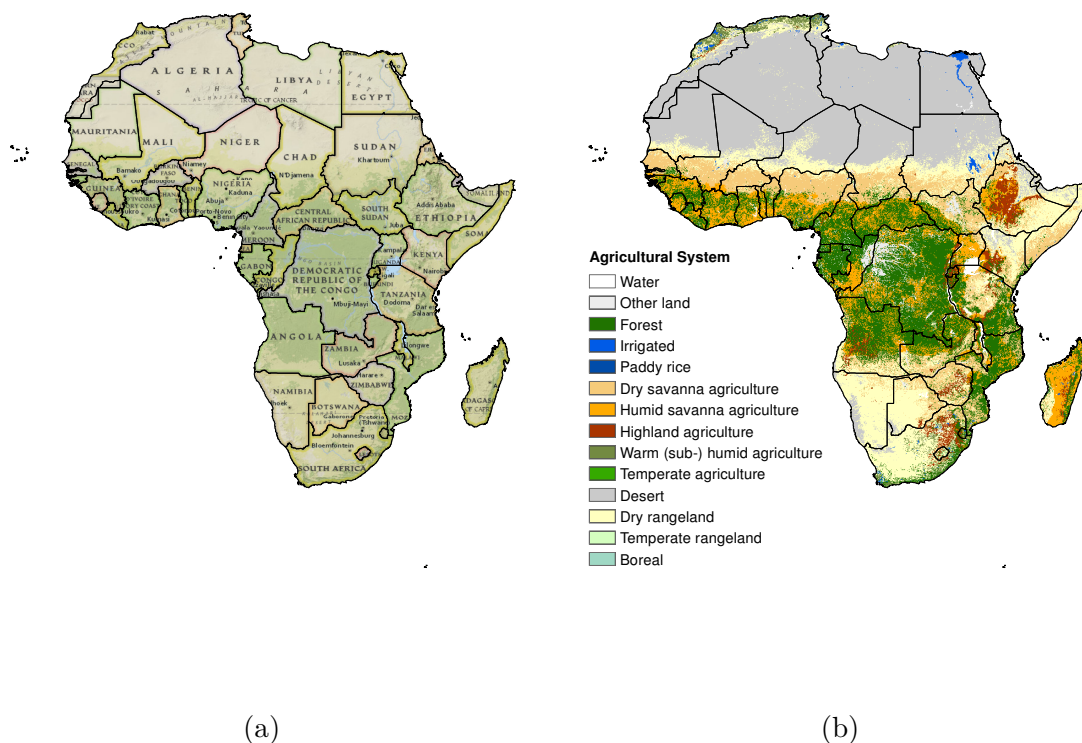


Figure 1.2: (a) Geographic map of Africa; (b) Major Agricultural Systems, taken from AQUAMAPS (FAO, 2021).

Most of the African agricultural production relies upon rainfall along the cropping period to meet its water requirements and only a few locations manage to exploit surface and groundwater bodies for irrigation purposes. This is caused by a lack of proper infrastructures able to transport water towards cultivated areas. Most of the areas equipped for irrigation *AEI* are located in the north, specifically along the Nile river in Egypt and Sudan (De Angelis et al., 2021); *AEI* are shown in figure 1.3b. As a consequence to the strong rely on precipitation, farmers are exposed to climate variability and extreme events, which impact food security and compromise price stability. This is further worsen by the prevalence, in sub-Saharan Africa, of smallholder farmers (i.e., cultivating less than five hectares per household), which produce over 70% of the total food calories, since it increases the single farmer risk of complete crop loss due to climate extremes.

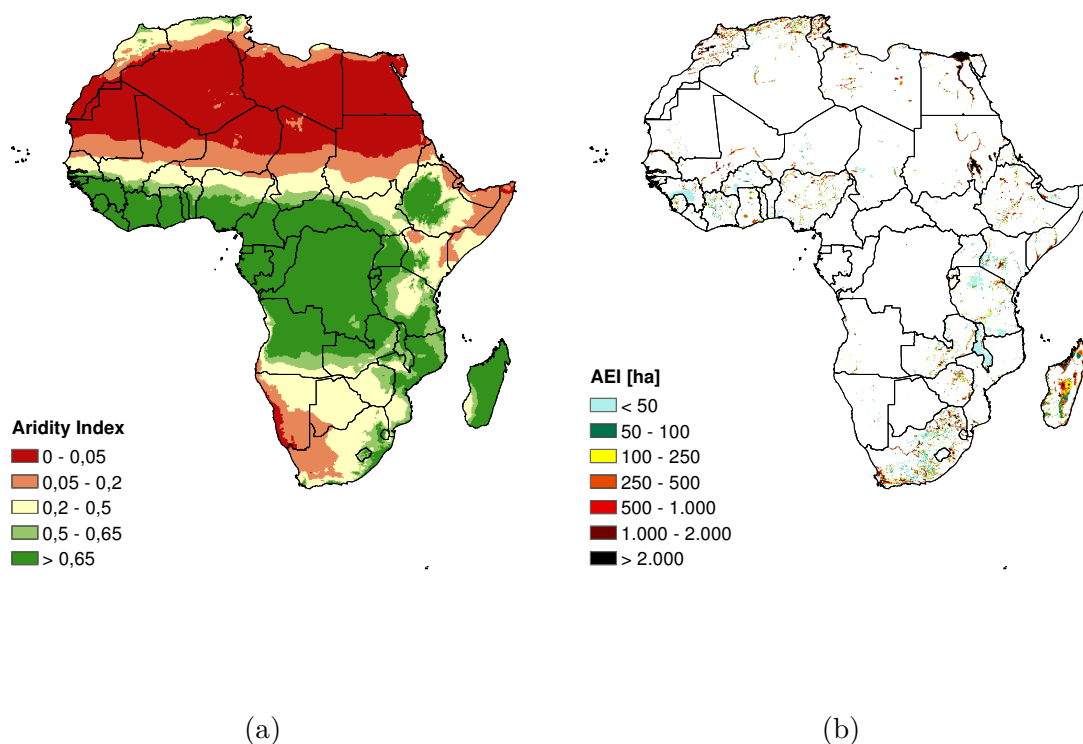


Figure 1.3: (a) Estimated aridity over Africa; taken from FAO (2021); (b) Area equipped for irrigation (*AEI*), available from Siebert et al. (2013).

The Master Thesis is organized in the following chapters: chapter 2 presents the multiple data sets used in the evaluation of the *CWF* scenarios and the *GGCMs* which have been validated before selecting *GAEZ v4*. Chapter 3 introduces the methodology followed by this study. The first section describes the process of *GGCMs* validation and choice. In the second section, the analysis performed on the selected *GGCM* is described. Then, the third section of chapter 3 describes the *CWF* model developed by Tuninetti et al. (2015), its inner workings and the modifications which have been brought for it to work on future scenarios. The fourth sections describes how future scenarios have been compared with the present baseline, in order to represent them in the results. These are illustrated and discussed in chapter 4. First, the results are depicted at the continental-level of aggregation, then their spatial distribution is assessed by keeping the results at the cell-level and representing them on maps. In addition, different configurations of the *CWF* are shown, namely its blue, green, rainfed and irrigated components, in order to high-

light specific aspects better described by each of them. Results are accompanied by comments on the visible effects of climate change or on the effects of the advanced management assumption on the outcomes. Chapter 5 discusses the results in the view of the production increase owed to such assumption and the eventual satisfaction of future demand. In addition, the impacts which such assumptions brings on the water resources is discussed in view of the continent water availability. Finally, the conclusions are drawn in chapter 6.

Chapter 2

Data

As mentioned in the previous section, the purpose of this study is to produce future forecasts of crop water footprint (*CWF*). According to Tuninetti et al. (2015), the *CWF* is defined as the ratio between the water evapotranspired by the crop during the growing seasons of one year and the crop yield. Therefore, data have been gathered with the aim of calculating this indicator. Subnational datasets at high spatial resolution of both actual yield observations and future yield simulations have been employed to design four different Crop Water Footprint Scenarios. *CWF* estimates are referred to four time intervals, each spanning over thirty years, in order to remove the input data dependency of interannual fluctuations and to be consistent with crop yield dataset. Specifically, such intervals are 1981-2010, 2011-2040, 2041-2070, 2071-2100 and are respectively referred to as the present scenario *Horizon 2010*, and the future scenarios *Horizon 2040*, *Horizon 2070* and *Horizon 2100*.

Five different Global Gridded Crop Models (*GGCM*) have been assessed via a validation procedure to select the one providing the most reliable future yield representation. The models analyzed are: *CLM4.5*, *GEPIC*, *PEPIC*, *LPJml* - which belong to the Inter-Sectoral Impact Model Intercomparison Project (*ISI-MIP*) repository (Schellnhuber et al., 2014) - and the Global Agro-Ecological Zoning version 4 (*GAEZ v4*) - developed by the Food and Agriculture Organization (*FAO*) and the International Institute for Applied Systems Analysis (*IIASA*) (FAO and IIASA, 2021). Finally, the choice has fallen on the most recent of these models, *GAEZ v4*, a model and a database which provides fundamental information on the current and

future state of agriculture, on its irrigation demand and production, on development opportunities, risks and adaptation options. Global, regional and sub-regional geospatial data are available for up to 77 different crops (FAO and IIASA, 2021). Specifically, the actual harvested areas for rainfed and irrigated cultivation, for the reference year 2010, of the crops under analysis, provided by *GAEZ v4*, served this study for the calculation of the *CWF*.

To compute the total water evapotranspired by the crop over a single growing season, the model developed by Tuninetti et al. (2015) has been used. This needs additional inputs such as crop specific data, soil properties and climatic data (Tuninetti et al., 2015). Sowing and harvesting dates, which delimit the length of the growing period (*LGP*), have been sourced from Portmann et al. (2010) and the daily crop coefficient ($k_{c,j}$) has been calculated following Allen et al. (1998) and Mekonnen and Hoekstra (2011). The soil available water content (*AWC*), which has been provided by FAO/IIASA/ISRIC/ISSCAS/JRC (2012), the root zone depth, obtained from Siebert and Döll (2010) and the depletion fraction, which values are given by Allen et al. (1998), contribute to the calculation of the daily water stress coefficient ($k_{s,j}$). Finally, fundamental input data for the model to work are Precipitation (P) and reference Potential Evapotranspiration (ET_0), which have been sourced from *ISI-MIP* repository (ISIMIP, 2021).

2.1 Inter-Sectoral Impact Model Intercomparison Project (ISI-MIP)

ISI-MIP is a climate-impacts modelling initiative which aims at advancing comprehensive knowledge of the risks of climate change by integrating impacts across sectors and scales in a multi-impact model framework and by establishing a forum in which researchers from key impact sectors can bring their knowledge together (Schellnhuber et al., 2014; Warszawski et al., 2014). The core product of the *ISI-MIP* is an open repository where a wide range of climate-impact model simulations from different sectors and scales, driven by common climate and socio-economic input are publicly available (ISIMIP (2021); Schellnhuber et al. (2014)). This allows for model

improvement, integration of impacts across sectors in a multimodel context and a multimodel assessment of sector-specific impacts at different levels of global warming (Schellnhuber et al., 2014).

ISI-MIP data sets used in this work belong to the simulation round *ISI-MIP2b*, one of the rounds which *ISI-MIP* is organized into (Frieler et al., 2017). This is not the latest round, but it is the latest in which such data sets are available. *ISI-MIP2b* protocol was developed in response to the IPCC Special Report on the 1.5 °C target. It is designed to allow for separation of historical warming, starting from pre-industrial conditions, from other drivers impacts. In addition, it allows to quantify the impacts of additional warming to 1.5 °C; global mean temperature change projections are based on the low emissions Representative Concentration Pathway *RCP2.6* and on the no-mitigation pathway *RCP6.0*, with socio-economic conditions fixed at 2005. Simulations include long term impacts up to 2299. Furthermore, it also allows the assessment of the climate effects based on the same climate scenarios, while accounting for simultaneous changes in socio-economic conditions, by following the middle-of-the-road Shared Socioeconomic Pathway *SSP2* Frieler et al. (2017). However, this last part is not available for the data sets included in this work.

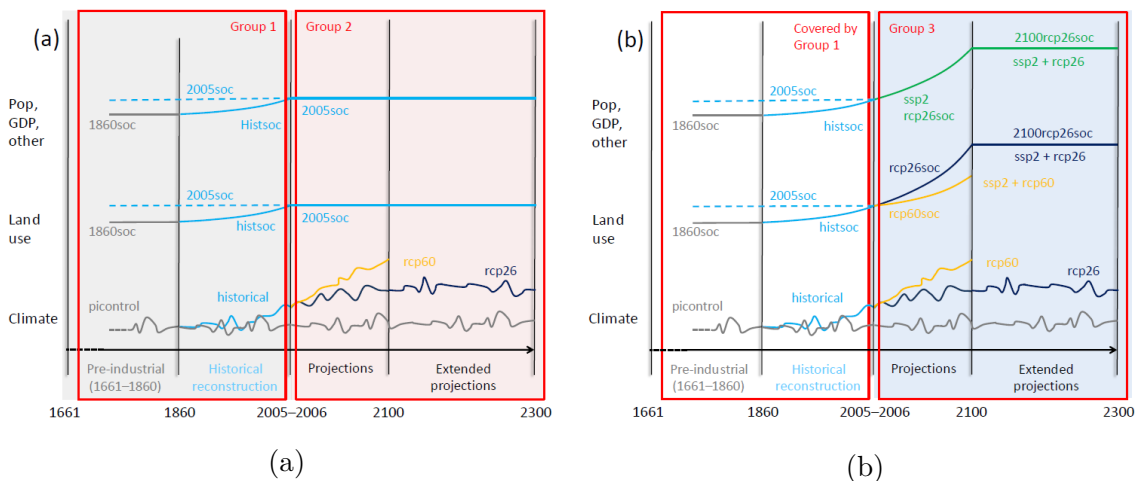


Figure 2.1: Schematic representation of the scenario design for ISIMIP2b. “Other” includes non-climatic forcing factors such as fertilizer input, irrigation, selection of crop varieties, water abstraction for human use etc. Panel (a) shows model runs that separate the pure effect of the historical climate change from other (human) influences (Group 1). Group 2 consists of model runs to estimate the effect of future climate change assuming fixed year 2005 levels of population, economic development, land use (LU), and management (2005soc). Panel (b) shows Group 3, which consists of model runs that quantify the effects of LU changes and changes in population, GDP and management from 2005 onwards, associated with $RCP6.0$ (no mitigation scenario under $SSP2$) and $RCP2.6$ strong mitigation scenario under $SSP2$) (Frieler et al., 2017)

2.2 Global Gridded Crop Models

Numerical crop models have been developed with the aim to better understand agricultural production systems and to predict the effects of changes in climate or management practices by simulating crop yields at the global scale (Müller et al., 2017). The five $GGCM$ analysed in this work may be subdivided into three types according to their structure, processes and original purpose (Rosenzweig et al., 2014):

1. Site-based crop models ($PEPIC$, $GEPIC$)
2. Agro-Ecosystem models ($LPJmL$, $CLM4.5$).
3. Agro-Ecological Zone models ($GAEZ v4$).

Site-based models were developed to simulate processes at the field scale and are often calibrated via agronomic field experiments. Nevertheless, the models belonging to this category, which have been used in this study, have been refined to run simulations on global grids. On the other hand, Agro-ecosystem models were primarily developed to simulate soil water balance, surface energy balance and carbon and nitrogen dynamics. Finally, the agro-ecological zone methodology used by *GAEZ v4* was developed to assess agricultural resources and potential and was later included into models for global environmental change (Rosenzweig et al., 2014).

These models differ in their approach, structure and assumptions; the simulated processes may vary, as well as their parametrization and the management of inputs and outputs. All of these divergences constitute a major source of uncertainty and variability in the projected climate impacts. Thus, GGCMS can show different responses to climate change related effects such as rising temperatures and changes in water availability (Rosenzweig et al., 2014). All of the GGCMS simulate the effects of temperature and water on the plant growth, while most of them reproduce crop processes such as evapotranspiration, leaf area development, light interception and utilization, yield formation, crop phenology, soil–crop–atmosphere water cycle dynamics, soil carbon and nitrogen cycling, and the effect of CO₂ concentration. However, only few models simulate the effects of pests and diseases (*GAEZ v4*) or the effects of water-logging on root functioning (Rosenzweig et al., 2014). In addition, models may differ in the simulation of crop-specific processes and even on their primary output, specifically whether they calculate actual or potential yields.

2.2.1 *CLM4.5*

The Community Land Model (*CLM4.5*) is the land component used in the Community Earth System Model (*CESM*). It is a community-developed model that examines the physical, chemical, and biological processes by which terrestrial ecosystems interact with the climate, across a variety of spatial and temporal scales; since, through their cycling of energy, water, gases and chemical elements, ecosystems are important determinants of the climate (Oleson et al., 2013). The model consists of four components - biogeophysics, hydrologic cycle, biogeochemistry and dynamic

vegetation - and it represents the land surface by five land cover types - vegetated, urban, lake, wetland, glacier - in each grid cell (Oleson et al., 2013).

2.2.2 *GEPIC*

The Geographic Information System (GIS)-based Environmental Policy Integrated Climate crop growth model (*GEPIC*) derives from the integration of the Environmental Policy Integrated Climate model (*EPIC*) with a Geographic Information System. Such procedure allows to increase the range of applicability of the site-based crop model *EPIC*, in order to address the spatial variability of yield as affected by climate, soil and management factors (Liu et al., 2007). The *EPIC* model is a biophysical model designed to simulate crop processes at a daily step for specific sites with site-specific inputs. By integrating *EPIC* with *GIS*, the *GEPIC* model can treat each grid cell as a site and simulate the spatial and temporal dynamics of the soil-crop-atmosphere-management system (Liu, 2009). The general structure of the *GEPIC* model is represented in Fig. 2.2.

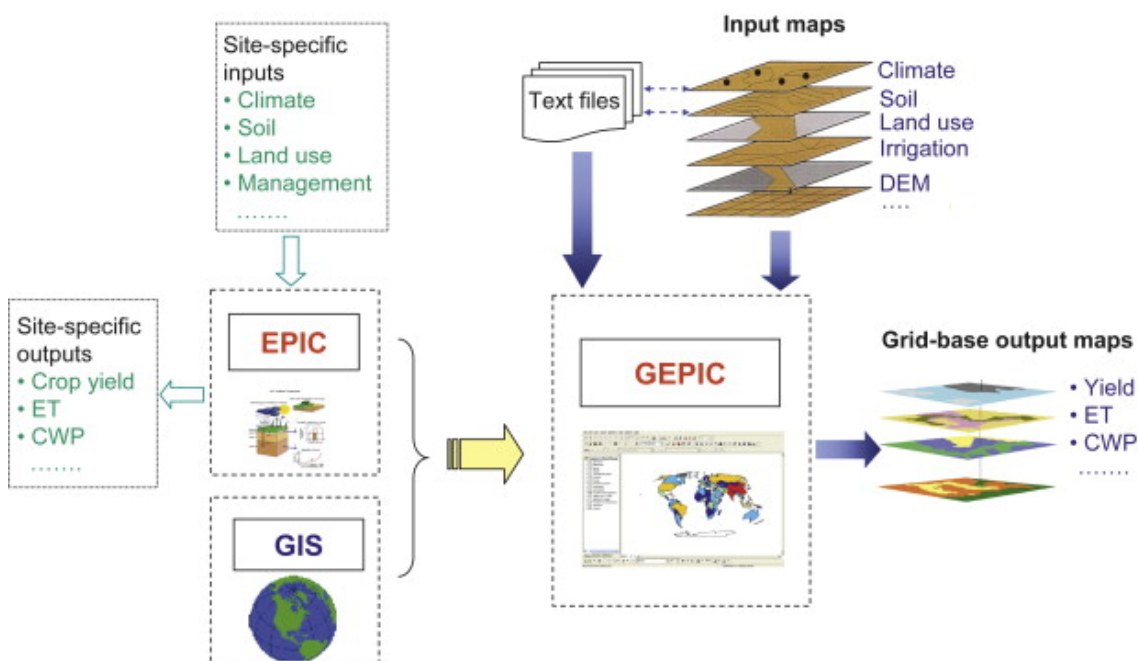


Figure 2.2: General framework of the *GEPIC* model, (Liu, 2009)

2.2.3 *PEPIC*

PEPIC is a Python-based *EPIC* grid-based crop growth model. The integration with a Python framework allows *PEPIC* to be easily applied at different spatial scales (Liu et al., 2016). Refer to subsection 2.2.2 for a description of *EPIC* model.

2.2.4 *LPJmL*

The Lund-Potsdam-Jena managed Land Dynamic Global Vegetation and Water Balance Model (*LPJmL*) is a global Agro-Ecosystem model which aims to address nonlinear biophysical and biogeochemical features of ongoing large-scale replacement of natural vegetation by agro-ecosystems, under climate Change and increasing CO₂ concentration. *LPJmL* simulates the full global carbon and water cycles and their transient changes due to land use. In addition, the model aims to assess future productivity, yield and provision for human societies worldwide, while quantifying drivers such as land management and land use change, climate and CO₂ (Bondeau et al., 2007).

2.2.5 *GAEZ v4*

The Global - Agro Ecological Zone crop growth model (*GAEZ v4*) provides the integrated Agro-Ecological Zones (*AEZ*) methodology, which is used to assess natural resources for identifying suitable agricultural land utilization options, as well as a comprehensive global database for the characterization of climate, soil and terrain conditions relevant to agricultural production. *AEZ* investigates resource limitations and opportunities based on plant eco-physiological characteristics, climatic and edaphic requirements of crops in order to quantify suitability and production potentials for individual crop types under specific input and management conditions, under both rain-fed and irrigation water supply conditions (FAO and IIASA, 2021). *GAEZ v4* estimates such potentials for historical, current and future climatic conditions and presents its results as spatial data at 5 arc-minute resolution grid cells (about 9 x 9 km at the equator). Climatic conditions are represented by a time series of historical data (1961-2010) and a selection of future climate simulations which use the Intergovernmental Panel on Climate Change (*IPCC*) *AR5* Earth System Model

(*ESM*) four *RCPs* (FAO and IIASA, 2021). Moreover, *GAEZ v4* provides a spatial representation of current production statistics for year 2010, which serve as baseline data and comprise current crop areas, yield and production, which represent the most updated actual dataset to my knowledge. Such spatial representation has been obtained by downscaling the annual national average of 2009-2011 FAOSTAT (2021) statistics to individual spatial units (grid cells), coupled with rain-fed and irrigated cropland areas (FAO and IIASA, 2021).

The main difference with the other models is the output, since *GAEZ v4* calculates the potential crop yield instead of the actual one. Potential yield is a constraint-free yield which represents the agronomically possible upper limit of crop production with regard to temperature and radiation regimes prevailing in each grid-cell (FAO and IIASA, 2021). However, the model also computes yield reduction factors, specifically: Temperature and Frost hazards, the damages cause by pests, diseases and weeds on plant growth and on the quality of the product, the climatic factors affecting the efficiency of farming operations. By combining agro-climatic potential yields, the reduction factors and the constraints induced by soil limitations and terrain-slope conditions, *GAEZ v4* estimates agro-ecological attainable yields. Finally, by comparing agro-ecological attainable yield with the actual yield of the year 2000 and 2010, the model computes the yield constraints and gaps, which constitute important information for identifying causes of food insecurity (FAO and IIASA, 2021). See figure 2.3 for a schematic representation of *GAEZ v4* overall structure.

An additional aspect of *GAEZ v4* model, which is particularly relevant for this work, consists in the choice of attributing to all future simulation a high level of input. This represents the assumption of a farming system which is mainly market oriented, fully mechanized and which applies optimal irrigation with a sprinkler system, advanced management strategies and optimum applications of nutrients and chemical pest, disease and weed control; a system where production is based on high yielding varieties (FAO and IIASA, 2021). Such assumption has a very high impact on future yields and it is the core of the investigation performed in this work

about future yield improvement on current cropland.

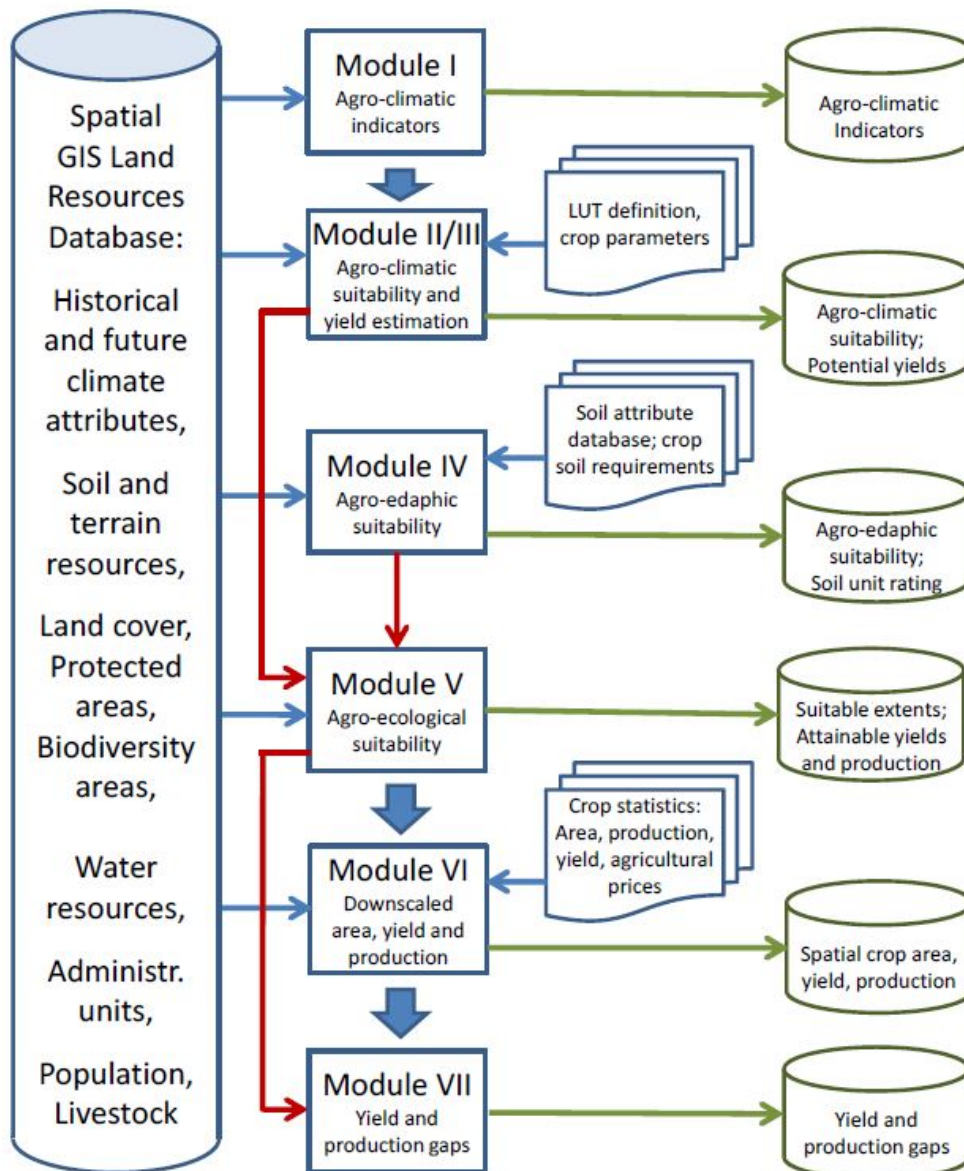


Figure 2.3: Overall structure of *GAEZ v4*, (FAO and IIASA, 2021)

2.3 Crop Yield Simulations

ISI-MIP impact models *CLM4.5*, *GEPIC*, *PEPIC*, *LPJml* provide yield simulations, with a resolution of 30×30 arc min, for four different simulation periods: pre-industrial (1661-1860), historical (1861-2005), future (2006-2099), future (extended) (2100-2299). They are run with four different Global Climate Models (*GCMs*) -

GFDL-ESM2M, HadGEM2-ES, IPSL-CM5A-LR, MIROC5 - and are available as modelled by different climate scenarios which represent the climate of the simulation period, including the CO₂ concentration in the atmosphere. Two are the scenarios for past simulation periods: a control scenario - *picontrol* -, which represents the pre-industrial climate with fixed CO₂ concentration at 286ppm, and the *historical* scenario, which represents the historical climate as simulated by the *GCMs*. Furthermore, *RCP2.6* and *RCP6.0* are the two available future climate scenarios. Regarding the models belonging to the *ISI-MIP* repository, the simulations used in this work span one-hundred years, from 2000 to 2099, they belong to the historical scenario for the years from 2000 to 2005 and to the future one from 2006 onwards. Specifically, both *RCPs* have been used to reproduce future yields. The simulations have been obtained by averaging the outputs of all the four different (*GCMs*) and by including a sensitivity scenario that considers the effects of increasing CO₂ concentration in the atmosphere on plant growth - See Table 2.1 for a summary of the models assessed in this study, with the respective parameters involved.

GAEZ v4 crop model simulations are slightly different. The model provides attainable yield values averaged over thirty years intervals, namely 1961-1990, 1971-2000, 1981-2010, 2011-2040, 2041-2070 and 2071-2100, with a resolution of 5×5 arcmin. While the past scenarios rely on *CRU TS v3.21* (Harris et al., 2014; CRU, 2021) as climate data source, the simulations of future scenarios are run with five *GCMs* - GFDL-ESM2M HadGEM2-ES IPSL-CM5A-LR MIROC-ESM-CHEM NorESM1-M - and with all four *RCPs* as climate scenarios. They even include two sensitivity scenarios, one projecting an increasing CO₂ concentration in the atmosphere and its fertilization effect on plant growth, while the second neglecting CO₂ fertilization effects. The crop yields used in this work have been sourced in two slightly different forms. In the case of soy and wheat, *GAEZ v4* provides the *GCMs* ensemble, while for maize and sorghum, the ensemble has been calculated starting from the outputs of the five *GCMs* provided by *GAEZ v4*. For the Historical assessment, *GAEZ v4* uses time series obtained from the Climate Research Unit (*CRU*) at the University of East Anglia, which provide a globally complete (except the Antarctic) land-only data set for climate variables. The *CRU TS v3.21* gridded

climate data set is constituted by monthly observations at meteorological stations covering the period from January 1901 to December 2012 (Harris et al., 2014). Station anomalies coming from more than 4000 weather stations distributed around the world, are interpolated into 30×30 arc min latitude by longitude grids (i.e., about 55 km at the equator), covering the global land surface (excluding Antarctica), and combined with an existing climatology to obtain absolute monthly values. The data set includes six variables: mean temperature, diurnal temperature range, precipitation, wet-day frequency, vapour pressure and cloud cover (Harris et al., 2014).

The simulations run with *GAEZ v4* used in this work cover the three future time intervals and have been modelled by averaging all five different *GCMs*. To be consistent, only *RCP2.6* and *RCP6.0* have been included in the simulations. In addition, the present scenario has not been simulated, but the actual yield values for the year 2000 and 2010 have been used instead in the comparison. Later on in the development of this study, *GAEZ v4* has been subject to additional analyses and validation procedures - refer to section 3.2 for further information and see Table C.1 in Appendix C for a more detailed description of the models' parameters.

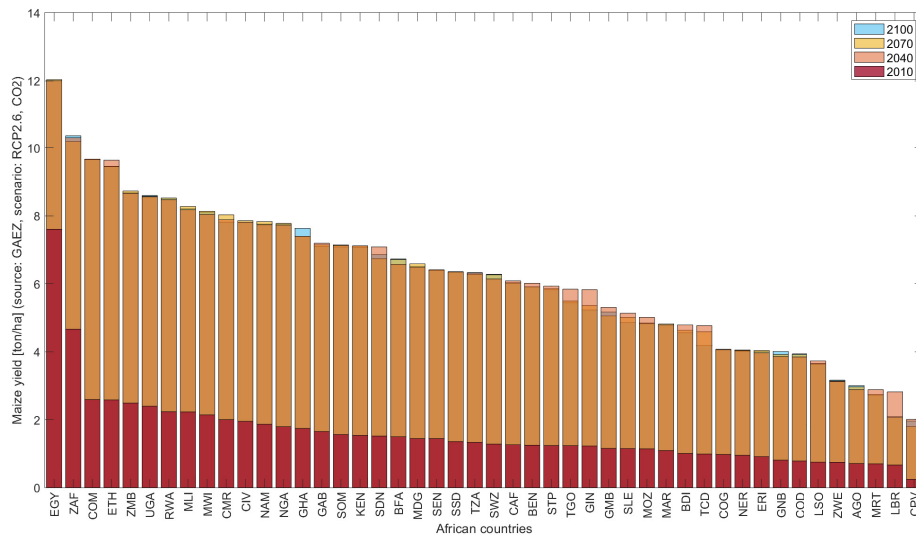


Figure 2.4: National aggregation of maize yield at 2010, 2040, 2070 and 2100 for *RCP2.6*, CO_2 scenario.

Table 2.1: *GGCMs* simulations used in this study

GGCM	Time Interval	Climate Scenario	Climate Forcing	Sensitivity Scenario	Crops
CLM45	2000-2005 2006-2099	Historical RCP2.6 RCP6.0	GFDL-ESM2M HadGEM2-ES IPSL-CM5A-LR MIROC5	CO2	Maize
GEPIC	2000-2005 2006-2099	Historical RCP2.6 RCP6.0	GFDL-ESM2M HadGEM2-ES IPSL-CM5A-LR MIROC5	CO2	Maize
PEPIC	2000-2005 2006-2099	Historical RCP2.6 RCP6.0	GFDL-ESM2M HadGEM2-ES IPSL-CM5A-LR MIROC5	CO2	Maize
LPJmL	2000-2005 2006-2099	Historical RCP2.6 RCP6.0	GFDL-ESM2M HadGEM2-ES IPSL-CM5A-LR MIROC5	CO2	Maize
GAEZ v4	2011-2040 2041-2070 2071-2100	RCP2.6 RCP6.0	GFDL-ESM2M HadGEM2-ES IPSL-CM5A-LR MIROC-ESM- CHEM NorESM1-M	CO2- fertilization, without- CO2- fertilization	Maize Soy Sorghum Wheat

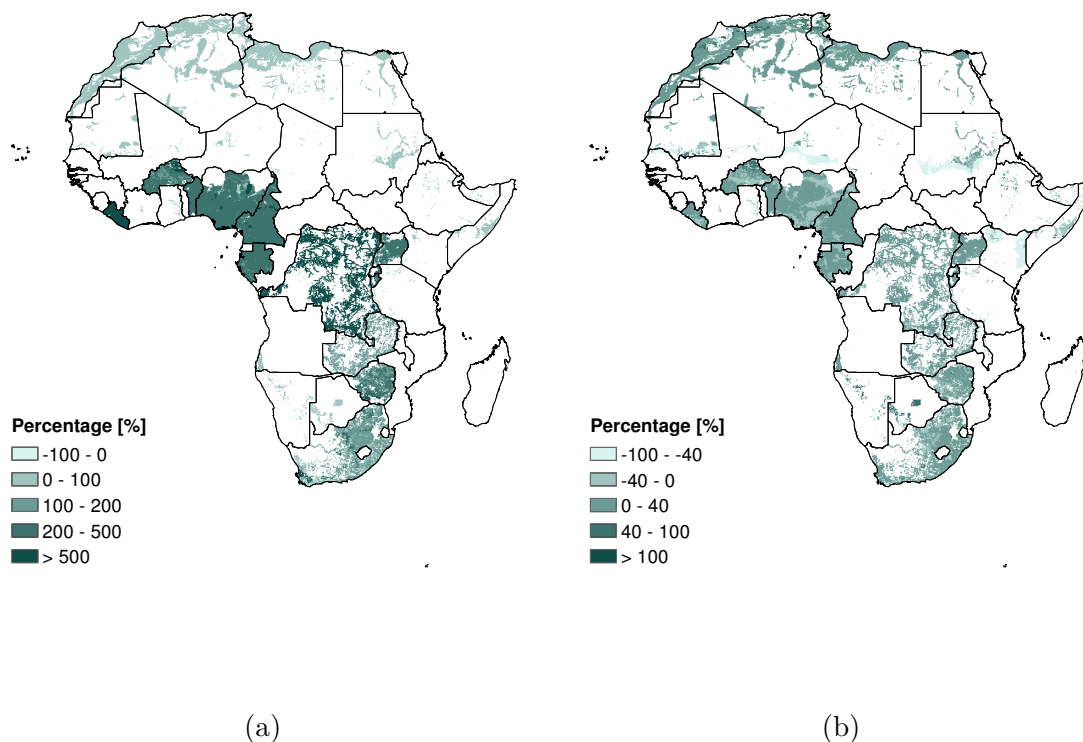


Figure 2.5: Percentage variation maps of (a) 2100 attainable soy yield relative to 2010 actual soy yield, (b) 2100 attainable soy yield relative to 2040 attainable soy yield

2.4 Crop Actual Yield

As mentioned in the section above, the crop actual yield data sets used in this work have been primarily sourced from *GAEZ v4*, since it provides the most updated version of sub-national actual crop yield global grid available in the literature, referring to years 2000 and 2010. *GAEZ v4* actual yield data set has a resolution of 5×5 arc min and is available for 31 crops, for both rainfed and irrigated water supply. It served in the comparison between the five *GGCMs* and as the yield component in the *Horizon 2010 - CWF* baseline scenario. In addition, to validate such data set, the national aggregation of *GAEZ v4* actual yield data over African countries has been compared with FAOSTAT (2021) estimations of annual yield at the country scale and with Monfreda et al. (2008) data set of crop actual yield.

FAOSTAT (2021) database provides annual yields at the country scale from year 1961 to 2019, while Monfreda et al. (2008) data set refers to year 2000 and provides the observed yields of 175 crops on a 5×5 arc min grid. This data set has been widely used across the literature [e.g. Tuninetti et al. (2015); Siebert and Döll (2010)] and since Sub-national data sets of crop yields at high spatial resolution are seldom available, a comparison with the more recent *GAEZ v4* dataset has been performed - See figure 3.12.

Table 2.2: Summary of Crop Actual Yield data sets

Source	Coverage	Spatial Resolution	Crops	Water Supply
FAOSTAT (2021)	1961-2019	National Average	Maize, Sorghum, Soy, Wheat	Average
GAEZ v4	2000, 2010	5×5 arc min	Maize, Sorghum, Soy, Wheat	Irrigated Rainfed
Monfreda et al. 2000	2000	5×5 arc min	Maize, Sorghum, Soy, Wheat	Irrigated Rainfed

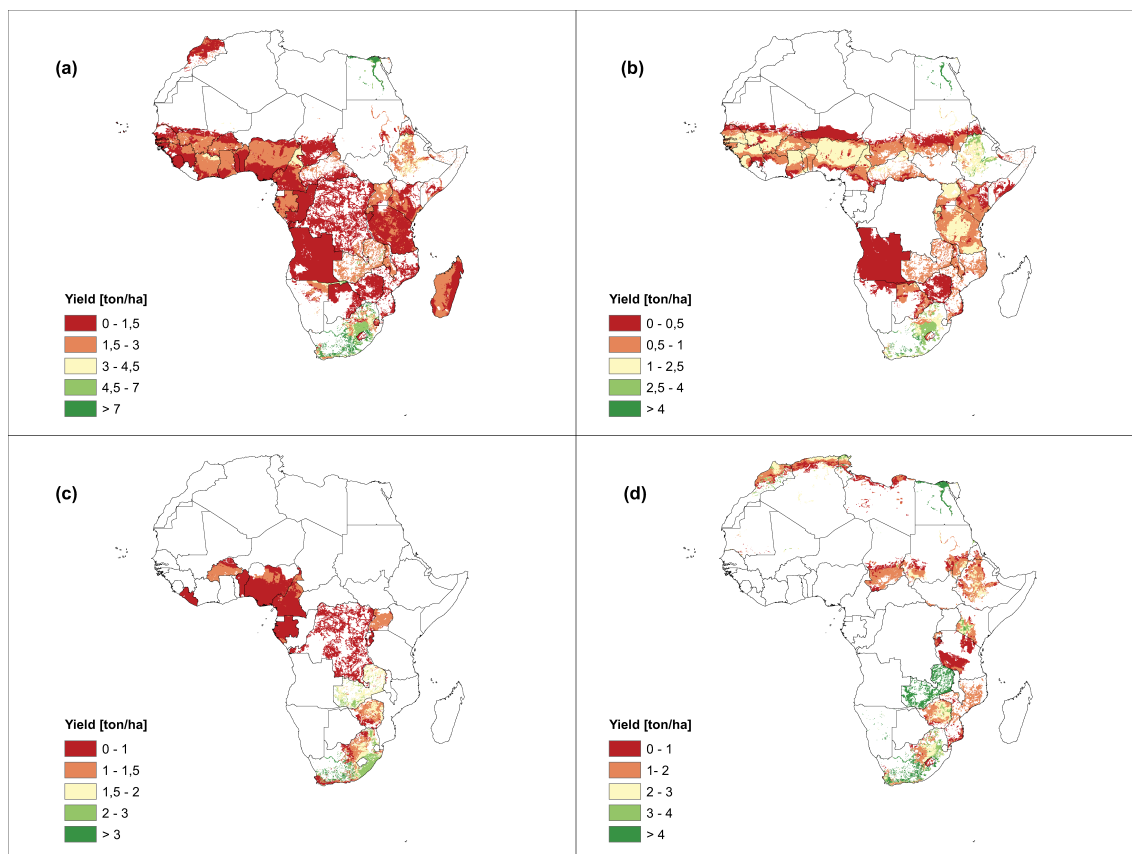


Figure 2.6: Crop actual yield at 2010 for: (a) Maize, (b) Sorghum, (c) Soy, (d) Wheat, source: *GAEZ v4*

2.5 Harvested Areas

As well as for the yield data sets, the harvested areas have been primarily sourced from *GAEZ v4*, which provides actual harvested areas, distinguishing between rain-fed and irrigated water supply; in the former type of production crops are fed only by precipitation, while in the latter, crops are irrigated when necessary in order to prevent the emergence of water stress (Tuninetti et al., 2015). The data set has a resolution of 5×5 arc min and it is referred to the years 2000 and 2010; the latter of which is, to my knowledge, the most updated global grid of harvested areas in the literature. However, since future projections of harvested areas are not available across the literature, the 2010 harvested areas data set has been used in the calculation of all the *CWF* scenarios, including future ones. In addition, it served in this study as a mask for the aggregation to national data, such as national yield and production. A comparison with Portmann et al. (2010) data set can be seen in

figure 3.15.

Table 2.3: Summary of Harvested Areas data sets

Source	Coverage	Spatial Resolution	Crops	Water Supply
Portmann et al. (2010)	2000	5 arc-min	Maize, Sorghum, Soy, Wheat	Irrigated Rainfed
GAEZ v4	2000 2010	5 arc-min	Maize, Sorghum, Soy, Wheat	Irrigated Rainfed

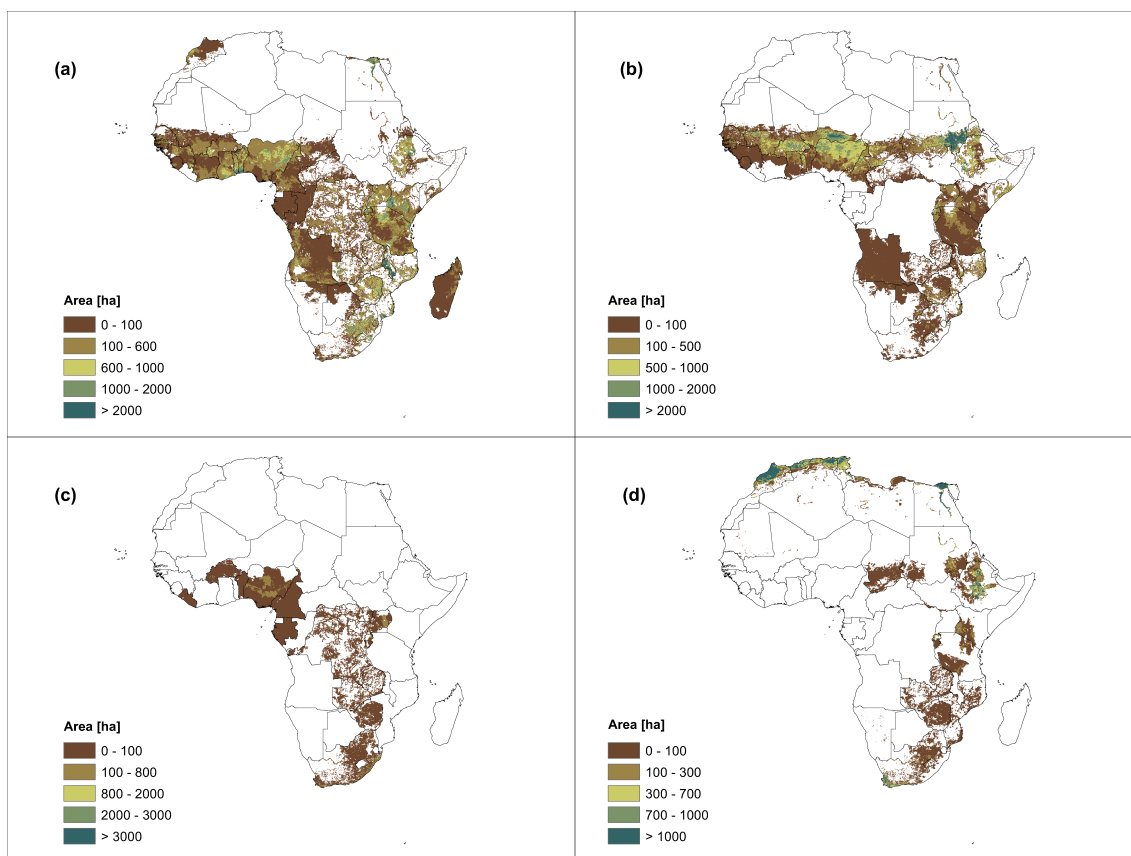


Figure 2.7: Total harvested areas of: (a) Maize, (b) Sorghum, (c) Soy, (d) Wheat, source: *GAEZ v4*

2.6 Climatic Data

The *CWF* model uses Precipitation (P) and reference Potential Evapotranspiration (ET_0) as input data. Both have been sourced from *ISI-MIP* repository - sim-

ulation round *ISI-MIP2b*. Daily precipitation data available on *ISI-MIP* are at 30×30 arc min resolution and are obtained from four different *GCMs* - FDL-ESM2M HadGEM2-ES IPSL-CM5A-LR MIROC5. For the purpose of this study, the output of the *GCMs* have been averaged and downscaled to 5×5 arc min resolution using Nearest Neighbour resampling method. Precipitation data have been organized in four 30-years time intervals - 1981-2005, 2011-2040, 2041-2070, 2071-2100 - and daily averaged in order to obtain a representative average year per each *Horizon*. As the reader can notice, the first interval is not exactly 30 years, because, on *ISI-MIP*, the Historical simulation scenario ends at the year 2005, while, at 2006, the Future simulation scenario starts; therefore, to be consistent, the first time interval used in the simulation for the present baseline *Horizon 2010*, have been cut at year 2005. Intervals covering future time steps have been simulated for both *RCP2.6* and *RCP6.0*.

Monthly long-term average reference evapotranspiration $ET_{0,m}$ data, which refer to a hypothetical well-watered grass surface with fixed crop height, albedo and canopy resistance, have been taken from *ISI-MIP*. They are available at a resolution of 30×30 arc min as the output of *PCR-GLOBWB* global hydrological model (Sutanudjaja et al., 2018). This source was chosen since it uses Penman-Monteith equation, following Allen et al. (1998) approach. Again, all the four *GCMs* have been used as climate forcings and, in this study, the respective realizations have been averaged. In addition, the data have been downscaled to the resolution of 5×5 arc min using Nearest Neighbour resampling method. As precipitation data, $ET_{0,m}$ has been organized in the four 30-years intervals, representing the four *CWF Horizons* and monthly averaged in order to obtain a representative year. $ET_{0,j}$ daily values are then determined through a linear interpolation where the average monthly value is attributed to the middle day of the respective month, as indicated by Tuninetti et al. (2015).

Table 2.4: Summary of Climatic data sets

Variable	Potential Evapotranspiration	Precipitation
Source	ISI-MIP	ISI-MIP
Impact Model	PCR-GLOBWB	-
Simulation Period	1981-2005, 2011-2040, 2041-2070, 2071-2100	1981-2005, 2011-2040, 2041-2070, 2071-2100
Climate Forcing	GFDL-ESM2M HadGEM2-ES IPSL-CM5A-LR MIROC5	GFDL-ESM2M HadGEM2-ES IPSL-CM5A-LR MIROC5
Climate Scenario	RCP2.6, RCP6.0	RCP2.6, RCP6.0
Spatial Resolution	30 × 30 arc min	30 × 30 arc min
Temporal Resolution	Monthly	Daily

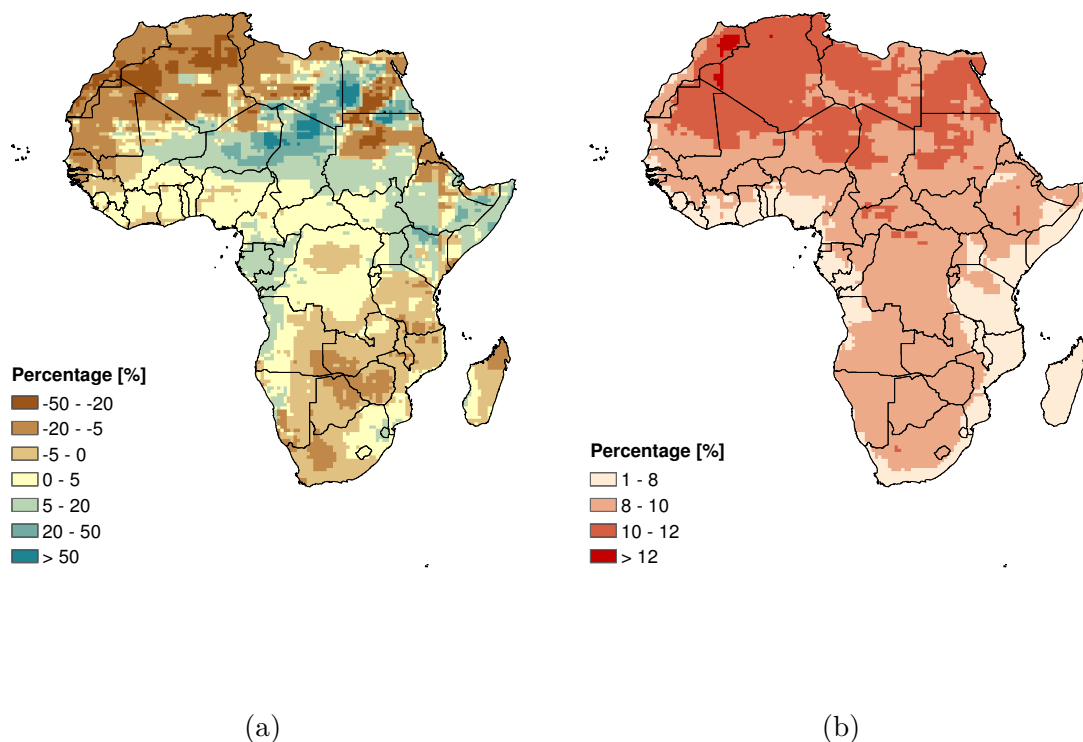


Figure 2.8: Percentage variation maps relative to 2010 of: (a) precipitation at 2100; (b) reference potential evapotranspiration at 2100;

2.7 Crop-specific data

In order to represent specific crop types, the *CWF* model needs crop specific data as input for the calculations. Among these sowing and harvesting dates are necessary, since they delimit the length of the growing period (*LGP*). These have been sourced from Portmann et al. (2010), which provide the month in which the growing period starts and ends. The data set has a resolution of 5×5 arc min, it distinguishes between rainfed and irrigated production and includes multicropping practices. The data set refers to the year 2000.

The daily crop coefficient, $(k_{c,j})$, is used in the calculation of actual evapotranspiration. It depends on crop characteristics and it is influenced by crop height, albedo, evaporation from bare soil and canopy resistance (Tuninetti et al., 2015). During the growing period, $k_{c,j}$ varies with a characteristic curve shape which is divided into

four growing stages - initial phase, development stage, midseason and late season - each with its specific length. Tuninetti et al. (2015) defined the functions of these curves, in which the constant values relative to the stage are taken from Allen et al. (1998). Moreover, the length of each stage is calculated as a fraction, p_{st} , of the *LGP*. This is defined according to Mekonnen and Hoekstra (2011), which provide specific values for different climatic regions.

The daily water stress coefficient, $k_{s,j}$, contributes as well to the calculation of the actual evapotranspiration. Depending on the available soil water content during the growing period, it assumes a value between 0 (maximum water stress) and 1 (no water stress) Allen et al. (1998). It is evaluated considering both irrigated and rainfed production; in the first type $k_{s,j}$ is equal to 1 throughout the growing period, while in rainfed production $k_{s,j}$ is computed daily according to Tuninetti et al. (2015). In its calculation, the 30 arc sec maps of the available water content (*AWC*), provided by FAO/IIASA/ISRIC/ISSCAS/JRC (2012) are used, together with precipitation data, the root zone depth, obtained from Siebert and Döll (2010), and the depletion fraction, which values are given by Allen et al. (1998).

Chapter 3

Methodology

The methodology developed in this work has been proposed to produce and investigate future scenarios of crop water footprint across the African continent at the sub-national scale. The *CWF* model has been analyzed and modified to be run on high spatial and temporal resolution data, to represent monthly averaged results and to produce future forecasts of *CWF*. Thus, a present baseline *CWF* scenario and three future ones, until the end of the century, have been designed. The comparison of these scenarios allows to assess the impacts of climate change on the African agriculture. Since future crop yield simulation are needed to produce these *CWF* scenarios, it was necessary to select one *GGCM* among those presented in section 2.2. Therefore, a thorough model validation has been performed, which has led to the selection of *GAEZ v4* model as the source of the yield data sets. By including such yield forecasts, which simulate the effects of a high input, advanced management agriculture, the study aims to investigate the potential production increment and the respective stress imposed on the water resources. This process required an extensive analysis of *GAEZ v4* crop model and its validation with other data sets by means of graphs and scatter plots. Moreover, a deep understanding of the Tuninetti et al. (2015) model was necessary before including new variables and future forecasts data - which have been validated as well - and in order to modify the model itself, to adapt it to future *CWF* scenarios.

3.1 Global gridded crop model Validation

In order to select the most suitable model for the purpose of this study, a validation procedure has been performed. It consists of multiple steps. At first, only the crop models belonging to the *ISI-MIP* repository (simulation round *ISIMIP2b* (Frieler et al., 2017)) - *CLM4.5*, *GEPIC*, *PEPIC*, *LPJml* - were included, since *GAEZ v4* was not yet accessible (website online since June 17, 2021). *ISI-MIP* crop models provide future yield simulations run with four *GCMs* - GFDL-ESM2M, HadGEM2-ES, IPSL-CM5A-LR, MIROC5 - over the period 2000-2099, for both *RCP2.6* and *RCP6.0*. Maize has been chosen as the representative crop, since its yield values were available for all of the models. The validation has been performed across two countries, Italy and Ethiopia, to evaluate how the models would represent the future yield changes in a European country, with modern agricultural management, and in a country belonging to the continent of interest. After having assessed both the spatial and the temporal variability of these models and their ensemble, an additional step, which included *GAEZ v4* model, has been added to the procedure.

3.1.1 Models Ensemble spatial variability

The harvested areas-weighted yield, Y_a , has been computed for each grid cell belonging to the respective country - Italy and Ethiopia - by performing a weighted average between the actual (for the baseline scenario) or attainable (in the case of future scenarios) irrigated, Y_a^I and the rainfed, Y_a^R production yields:

$$Y_a = \frac{Y_a^R \times A^R + Y_a^I \times A^I}{A^R + A^I} \quad \left(\frac{\text{ton}}{\text{ha}} \right) \quad (3.1)$$

where A^R and A^I are, respectively, the rainfed and irrigated harvested areas, here used as weights, sourced from *GAEZ v4*, as described in section 2.5.

The calculation was performed for every *GGCM*, each of which was available in the *ISI-MIP* repository with four *GCMs*, for a total of 16 different yield realizations. By averaging such data sets the model ensemble has been computed. Finally, the harvested areas-weighted yield values and the standard deviation across the realizations have been represented on the respective country map for two reference years,

2000 and 2099, and distinguishing between irrigated and rainfed water supply - see image 3.1 below (images showing year 2000 and rainfed conditions can be found in appendix A).

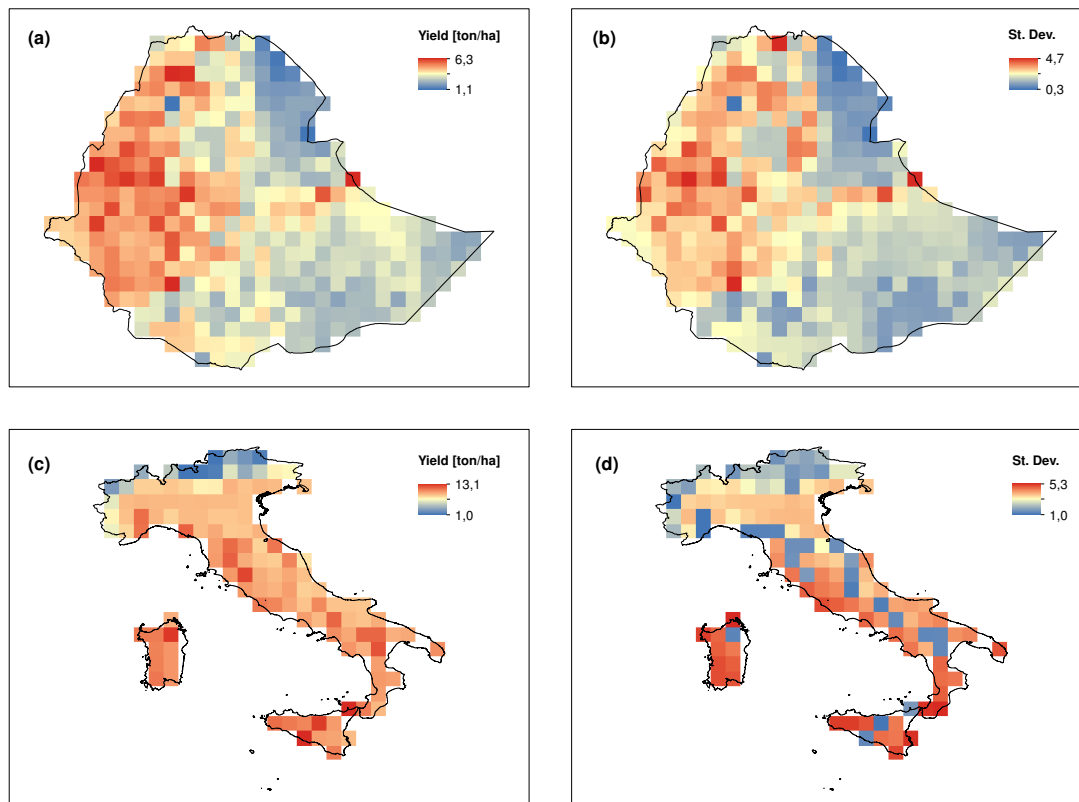


Figure 3.1: Spatial variability of irrigated Maize (a) average yield, (b) standard deviation across Ethiopia and (c) average yield, (d) standard deviation across Italy for the year 2099, *RCP6.0*

3.1.2 Temporal variability & Model comparison

After assessing the spatial variability of the data sets, the yield values have been nationally aggregated and yearly values have been computed from 2000 to 2099. The procedure has been performed for every model individually, as well as for their ensemble, as a mean of comparison. In addition, to validate the data series, FAO-STAT (2021) actual data, ranging from 2000 to 2019 (the last available year), has been added to the comparison. Again, the comparison has been performed for both countries and for both *RCPs*. Below, the comparison plot can be seen in figure 3.2 and 3.3

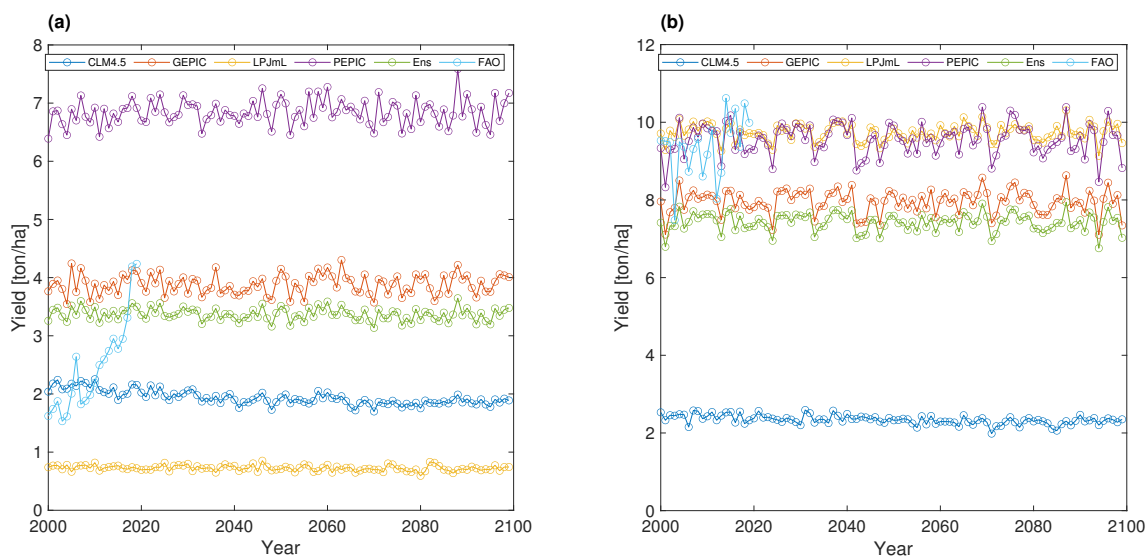


Figure 3.2: Individual models, ensemble and FAOSTAT (2021) yearly national maize yield data comparison for (a) Ethiopia and (b) Italy, *RCP2.6*

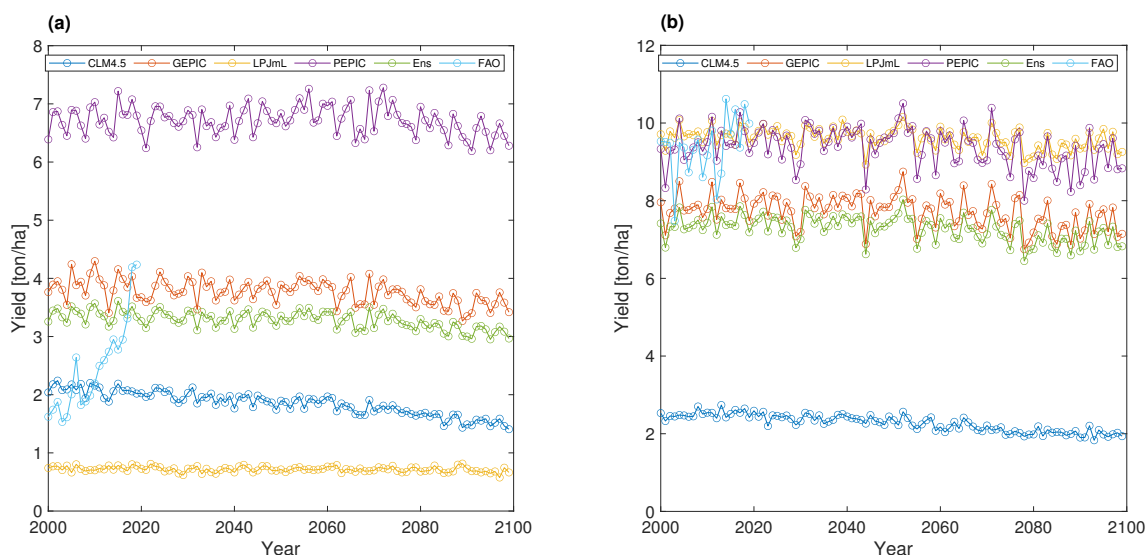


Figure 3.3: Individual models, ensemble and FAOSTAT (2021) yearly national maize yield data comparison for (a) Ethiopia and (b) Italy, *RCP6.0*

While in the case of Italy *PEPIC* and *LPJmL* models fit well the early 2000's FAOSTAT (2021) data series, as can be seen in panel (b) of both figure 3.2 and 3.3, the same does not occur for Ethiopia. No model fit the step increment in yield shown by FAOSTAT (2021) series. As can be observed in chapter 4, all Africa shows an increment in maize yield, mainly due to a consistent expansion of harvested areas. Moreover, the four crop models are quite discordant with each other.

To facilitate the visualization of the models' performances, each of them has been individually plotted with the ensemble and FAOSTAT (2021) data.

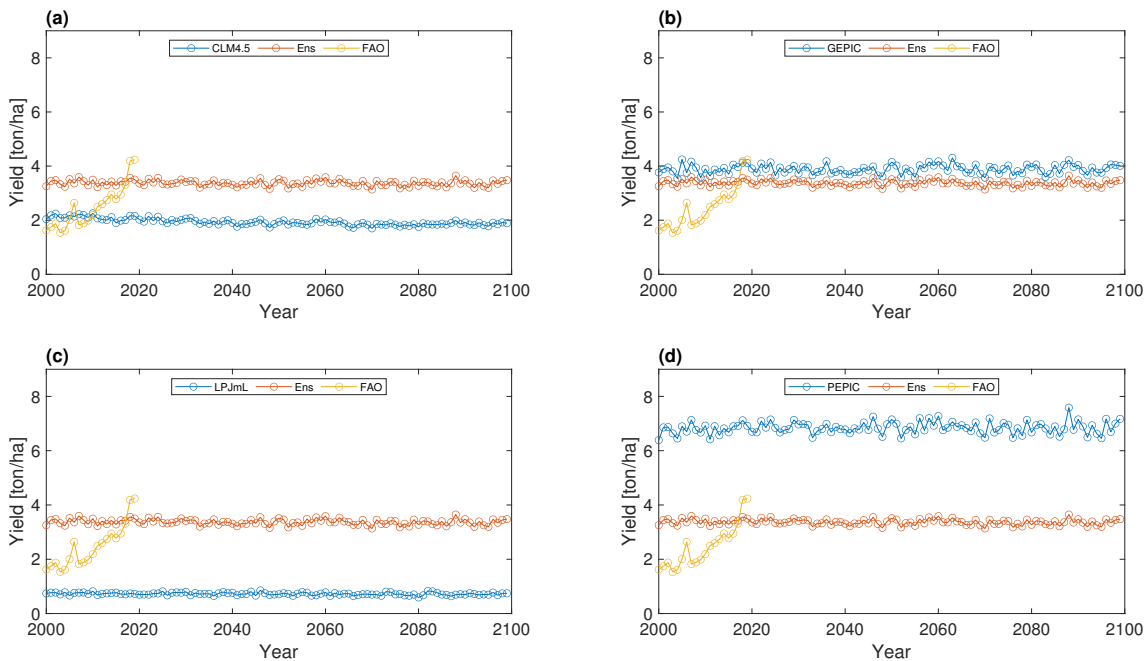


Figure 3.4: (a) *CLM4.5*, (b) *GEPIC*, (c) *LPJmL* and (d) *PEPIC*, ensemble and FAO-STAT (2021) yearly national maize yield series, Ethiopia, *RCP2.6*

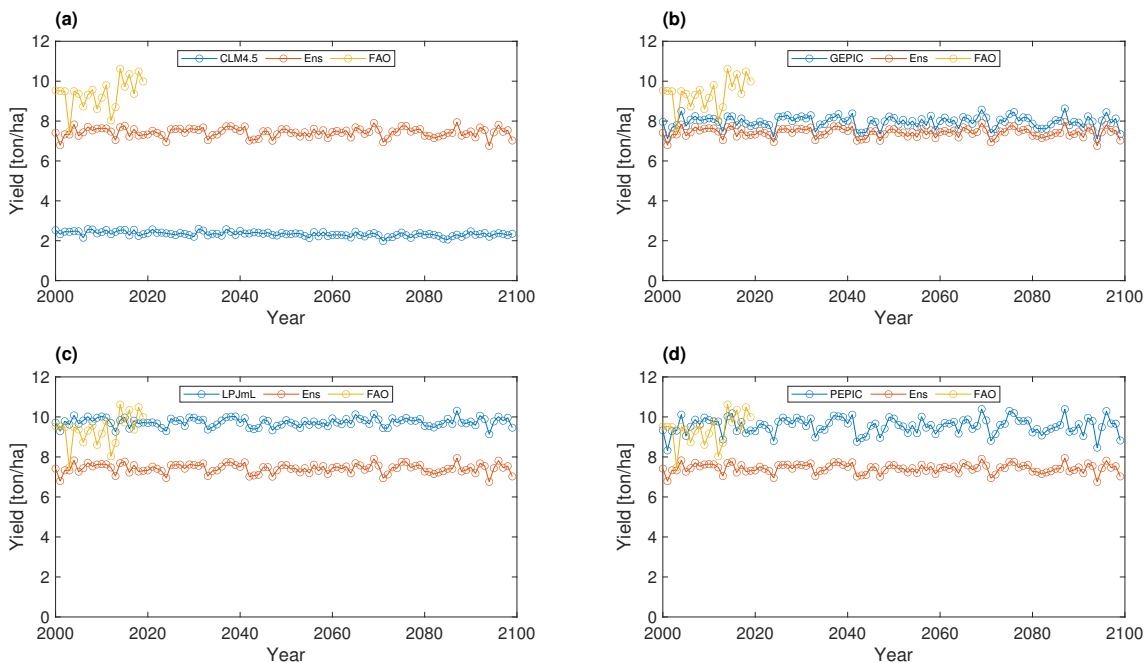


Figure 3.5: (a) *CLM4.5*, (b) *GEPIC*, (c) *LPJmL* and (d) *PEPIC*, ensemble and FAO-STAT (2021) yearly national maize yield series, Italy *RCP2.6*

Figure 3.5 and the following figure 3.7 confirm *LPJmL* and *PEPIC* as the best

models in the case of Italy, even though they diverge more from the ensemble than *GEPIC* model. Regarding Ethiopia, no model fits the trend shown by FAOSTAT (2021) actual yield, however, somehow the models ensemble is in line with 2017/2018 national yield values - figures 3.4 and 3.6.

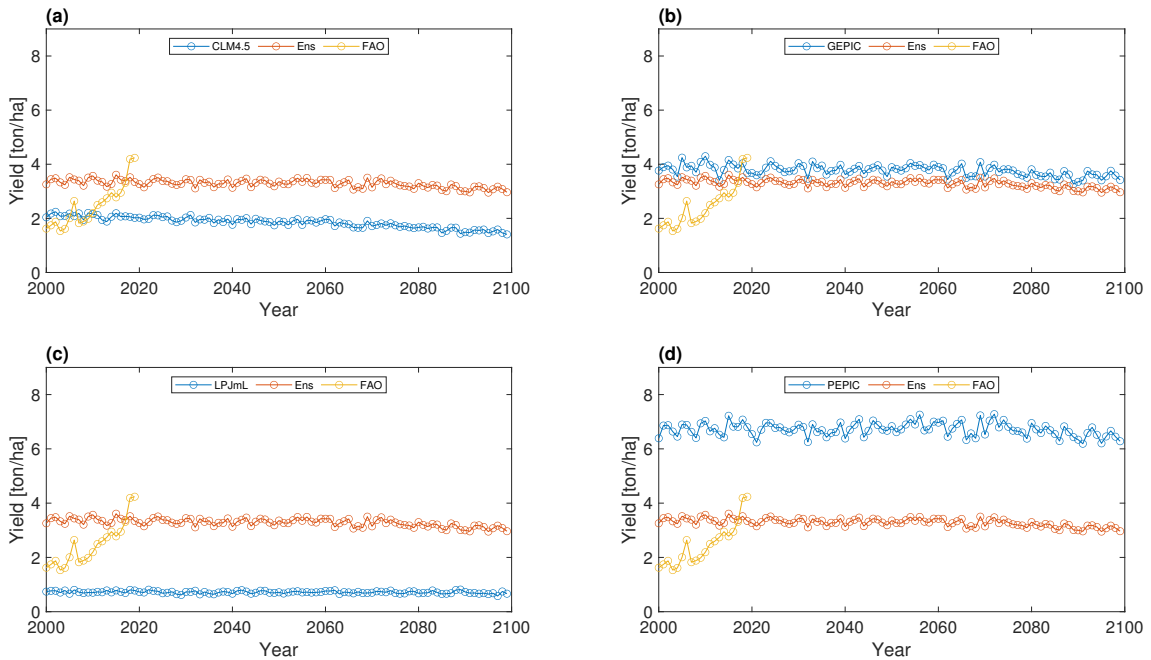


Figure 3.6: (a) *CLM4.5*, (b) *GEPIC*, (c) *LPJmL* and (d) *PEPIC*, ensemble and FAO-STAT (2021) yearly national maize yield series, Ethiopia *RCP6.0*

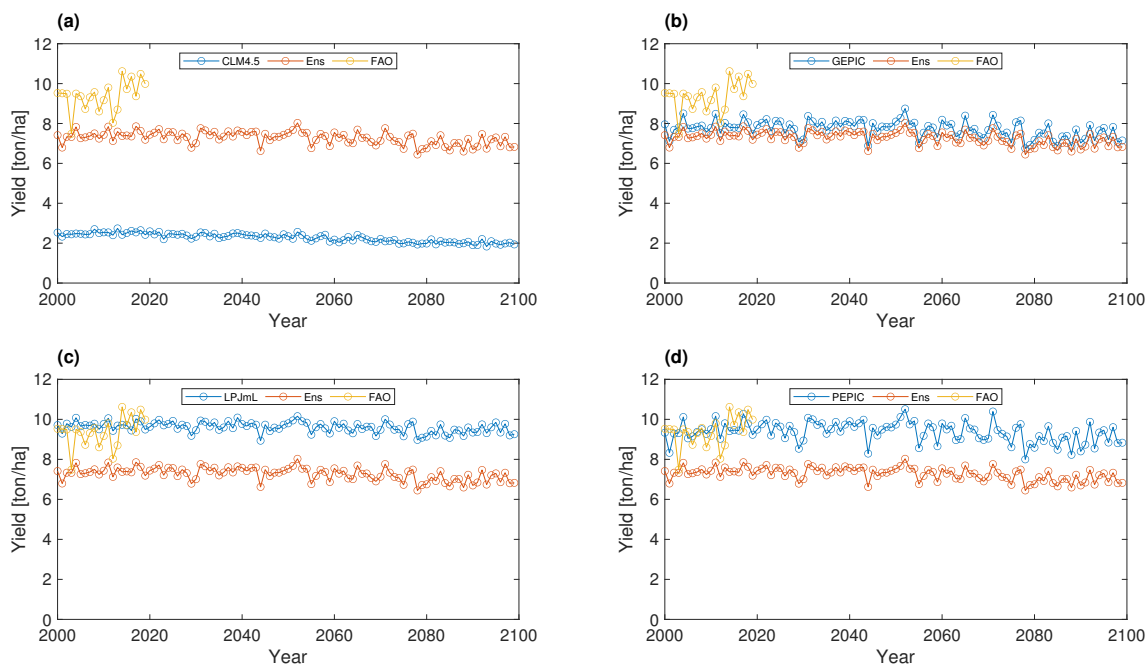


Figure 3.7: (a) *CLM4.5*, (b) *GEPIC*, (c) *LPJmL* and (d) *PEPIC*, ensemble and FAO-STAT (2021) yearly national maize yield series, Italy *RCP6.0*

For both countries, the simulations following *RCP6.0* show a more accentuated decreasing trend towards 2100 than simulations following *RCP2.6*, see figures 3.6 and 3.7 compared to figures 3.4 and 3.5

3.1.3 Country specific procedure

After visualizing the results of the previous steps, it has been decided to slightly modify the procedure and make it specific to the respective country, in order to find the models ensemble which could better fit FAOSTAT (2021) data. Regarding Italy, only *LPJmL* and *PEPIC* have been used to compute the ensemble. While in the case of Ethiopia all the four models have been used to calculate the final ensemble. In figure 3.8 the country specific ensemble can be seen as plotted together with its rainfed and irrigated components and FAOSTAT (2021) data. Rainfed and Irrigated ensemble components have been obtained by considering only the agricultural production obtained with the respective water supply practice. Both *RCP2.6* and *RCP6.0* simulations are present in the figure below.

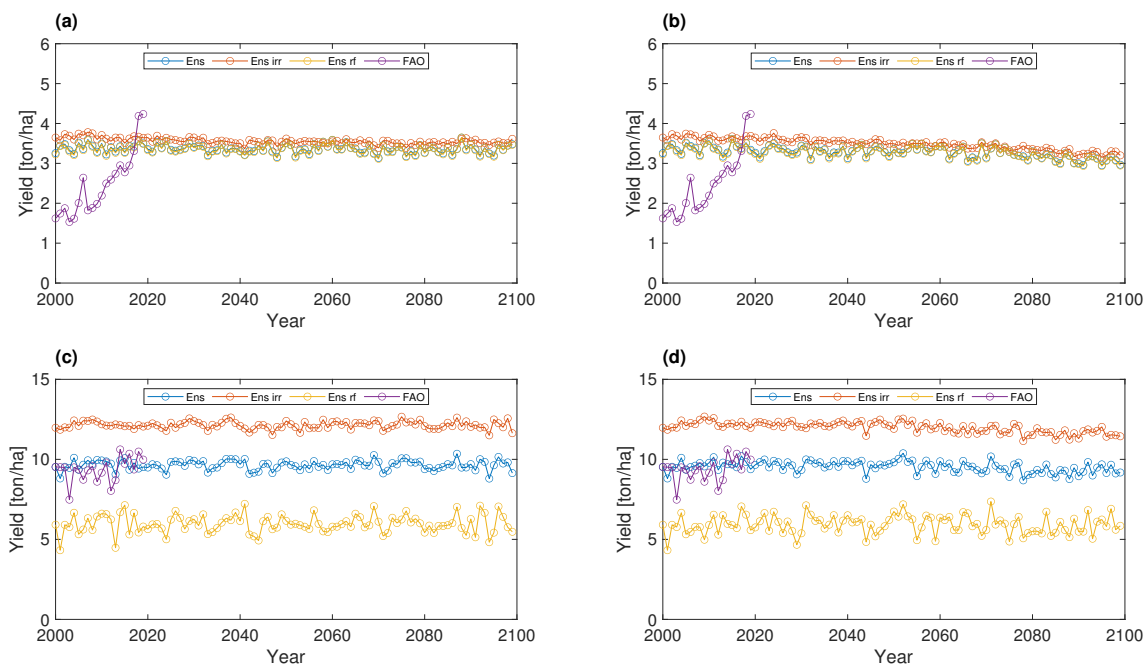


Figure 3.8: Country specific analysis. Representation of Ensemble, irrigated and rainfed ensemble and FAOSTAT (2021) data of yearly national maize yield for: (a) Ethiopia, *RCP2.6*; (b) Ethiopia, *RCP6.0*; (c) Italy, *RCP2.6*; (d) Italy, *RCP6.0*

Still, the results were unsatisfactory regarding the representation of Ethiopia national yield

3.1.4 Inclusion of *GAEZ v4* in the validation

When *GAEZ v4* database became accessible, it was decided to investigate it as well, by including it into the validation procedure. Therefore, an additional step has been added in the validation procedure, which has resulted in the figures 3.9 and 3.10. These figures show the country specific ensemble, as obtained from the previous steps, and FAOSTAT (2021) data plotted together with *GAEZ v4* maize yield data. Regarding the latter, for the years 2000 and 2010, the national actual maize yield has been plotted as provided by *GAEZ v4*, while, for future years, the national attainable maize yield has been used, which has been obtained by averaging over five *GCMs* provided by the database, as described in table 2.1. The same has been done for sorghum, while in the case of soy and wheat the ensemble was directly provided by the crop model. *GAEZ v4* provides future yields averaged over 30 years intervals - 2011-2040, 2041-2070, 2071-2100 - therefore the values provided have been

plotted and kept constant over the respective interval. Again, this has been done for both Italy and Ethiopia and for both *RCP2.6* and *RCP6.0*. Three *GAEZ v4* data series can be seen which correspond, respectively, to irrigated production yield (blue), rainfed production yield (green) and harvested areas-weighted average yield (red).

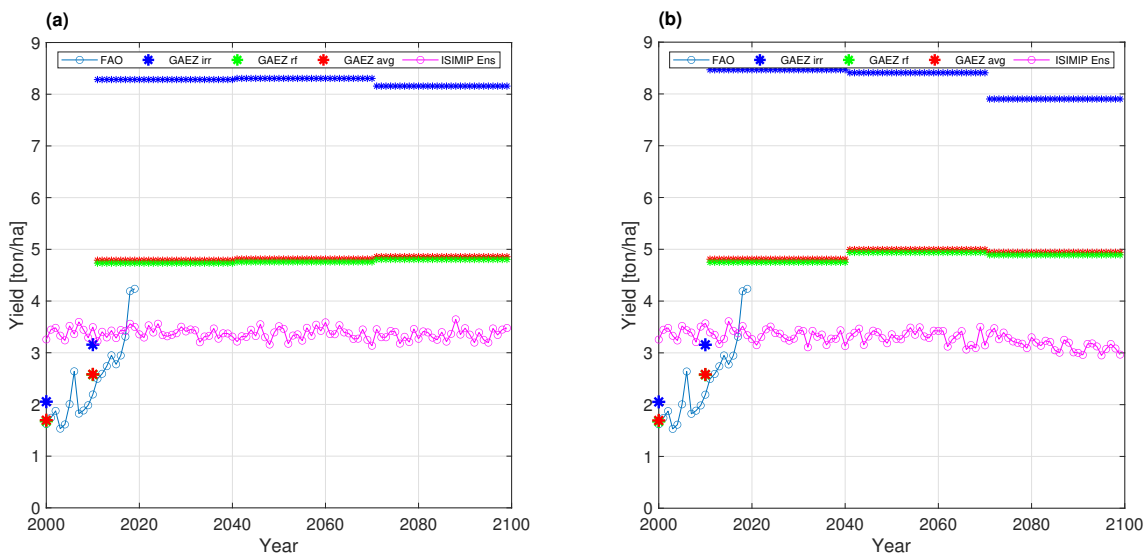


Figure 3.9: Comparison among Ethiopia yearly national yield as obtained from FAOSTAT (2021), Model Ensemble and *GAEZ v4*. (a) *RCP2.6*; (b) *RCP6.0*

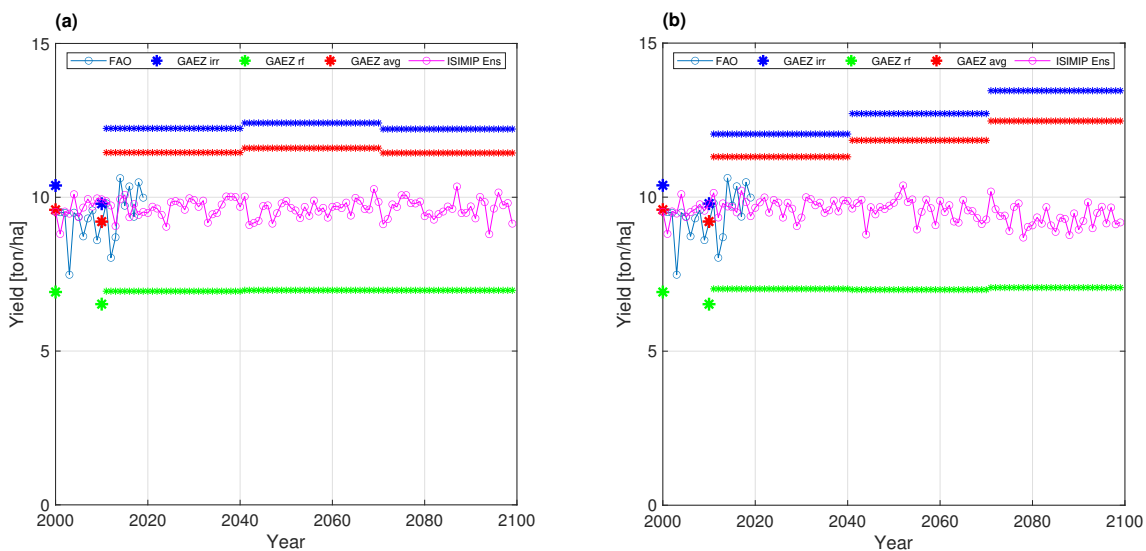


Figure 3.10: Comparison among Italy yearly national yield as obtained from FAOSTAT (2021), Model Ensemble and *GAEZ v4*. (a) *RCP2.6*; (b) *RCP6.0*

This time, as can be seen in figure 3.9, the *GAEZ v4* actual yield resembles closely FAOSTAT (2021) data series for Ethiopia, while average future attainable

yield shows values which seems in line with the last FAOSTAT Ethiopia national yield values referring to 2018/2019; even though *GAEZ v4* assumes advanced management strategies and high input levels for future scenarios. Although this is mostly evident in the irrigated production yield series values, the fact that the rainfed production yield and the weighted average yield are nearly overlapping shows a strong prevalence, among the harvested areas, of rainfed agriculture. In addition, *GAEZ v4* provides 30 years-average attainable crop yield, which remove the simulated inter-annual fluctuations, which are evident in *ISI-MIP* models (additional information about *GAEZ v4* simulations can be found in section 2.3).

This last step of the validation procedure has brought to the selection of *GAEZ v4* as the crop *GFCM* of choice for the provision of crop yield data sets and simulations.

3.2 *GAEZ v4* extensive analysis & validation

Once *GAEZ v4* had been selected as the model of choice, it was still necessary to investigate its parameters and the data sets it provides - specifically, this study has made a wide use of actual and attainable crop yields data sets and of actual harvested areas (irrigated, rainfed and total) at the year 2010. Therefore, national average yield scatter plots have been generated to evaluate the model performance on national yield aggregation over African countries. These have been produced for all the four crops included in this study - maize, sorghum, soy, wheat - and they have been used to compare the different data sets of the same crop, such as those including *RCP2.6* and *RCP6.0*, or those assuming the fertilization effect of CO₂ with those that do not. Furthermore, they have been used to validate *GAEZ v4* data sets by comparing them with FAOSTAT (2021) yield and areas national statistics or with other data sets that are widely used in the literature - namely Monfreda et al. (2008) gridded crop actual yield - see figure 3.12, panel (b) - and Portmann et al. (2010) gridded harvested areas.

Every dot on the scatter plots identifies one African country and the three lines are the bisectors (1x, 2x and 3x). They have been produced for all the crops included

in this work and for each scenario available: *RCP2.6*, *RCP6.0*, CO_2 fertilization and no CO_2 fertilization. Figure 3.11 below shows *GAEZ v4* attainable crop yield scenarios validation with FAOSTAT (2021) 2019 actual national average yield statistics.

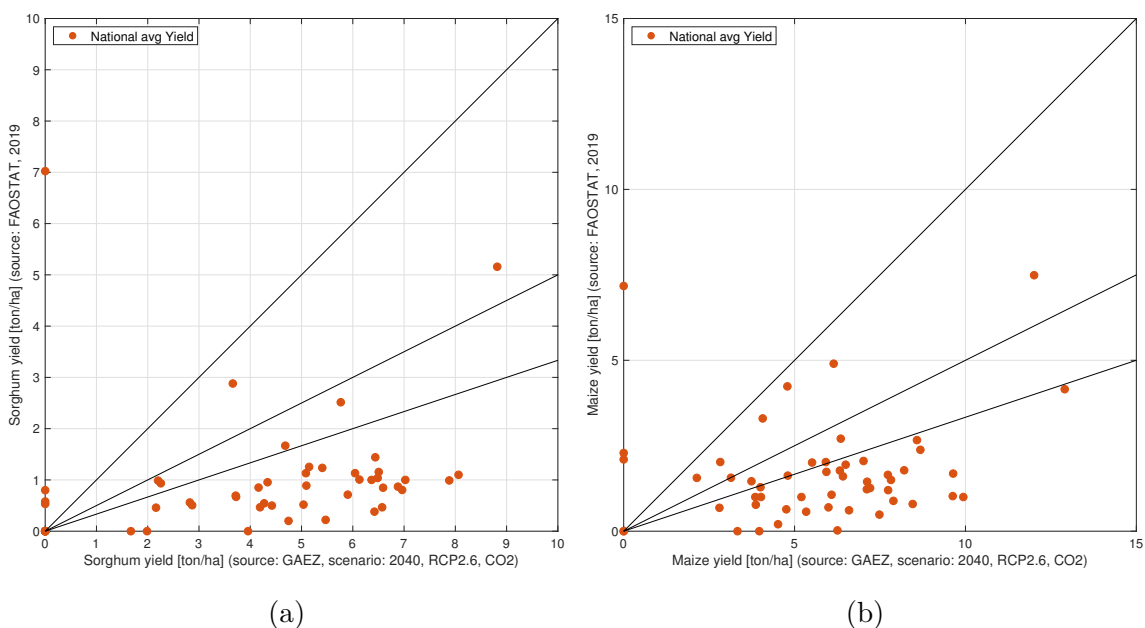


Figure 3.11: *GAEZ v4* validation with FAOSTAT (2021) national yield values - (a) Sorghum; (b) Maize.

It can be seen that, except for countries with a null yield value, *GAEZ v4* aggregated national attainable yield at 2040 is higher than FAOSTAT (2021) values for all African countries, for both Maize and Sorghum crops. Furthermore, most countries show a national attainable yield at 2040 which is more than three times bigger than FAOSTAT (2021) national statistics. This is mainly due to the assumption of high input, advanced agricultural management *GAEZ v4* applies to future attainable yields. This is confirmed by the validation of *GAEZ v4* national actual yield at 2010 with FAOSTAT (2021) national yield values at 2010, which can be seen in figure 3.12, panel (a). *GAEZ v4* actual yield is not subject to such assumption. Indeed, national yield values are closer to the 1x bisector. Only *GAEZ v4* national actual yield values of Eswatini and Angola are, respectively, two and three times bigger than the corresponding FAOSTAT (2021) values.

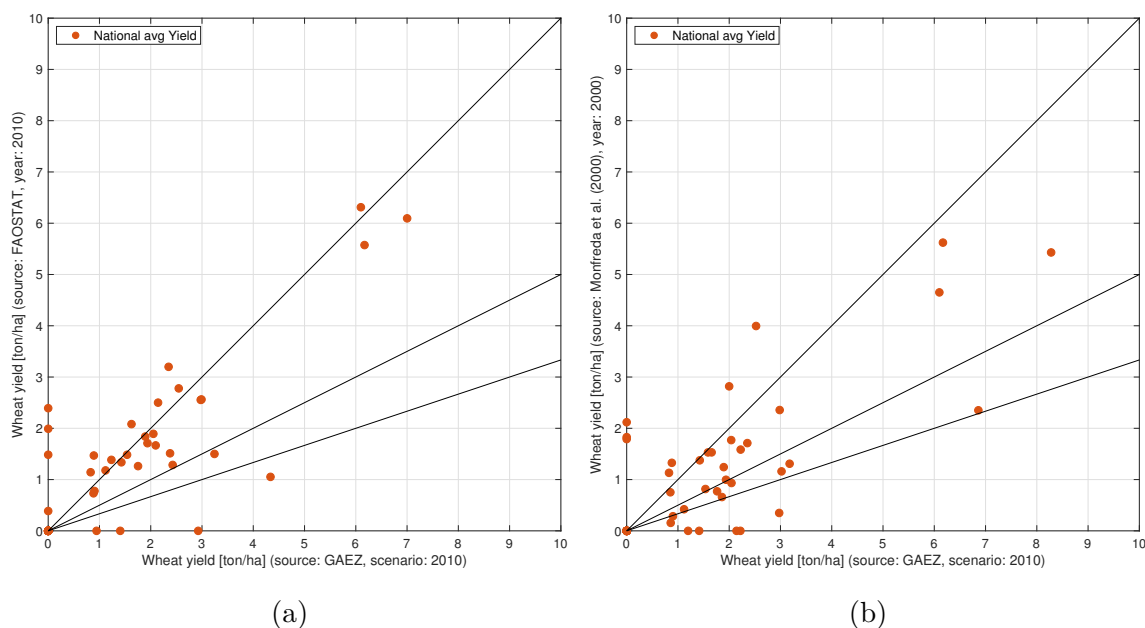


Figure 3.12: *GAEZ v4* 2010 wheat actual yield validation with: (a) FAOSTAT national yield values at 2010; (b) Monfreda et al. (2008) yield data set at 2000

The effects of CO_2 fertilization or of the *RCPs* are definitely less evident than those of high input assumption. As it can be seen in figure 3.13, the effect of CO_2 fertilization sensitivity scenario is minimal with respect to the scenario which does not include CO_2 effects. National yields barely diverge from the 1x bisector; however, a small trend towards the axis representing the scenario which include CO_2 effect can be noticed. This suggests a low influence of carbon dioxide on Sorghum crops in Africa. This partly explains the panel (b) of figure 3.13, where the effects of *RCP2.6* and *RCP6.0* on Sorghum yield at 2040 are compared. Since *RCPs* represent future scenarios of green house gas (*GHG*) emissions and atmospheric concentrations, air pollutant emissions and land use (IPCC, 2014), the small influence of $[\text{CO}_2]$ on crops can justify the small differences between *RCP2.6* and *RCP6.0* on Sorghum yield.

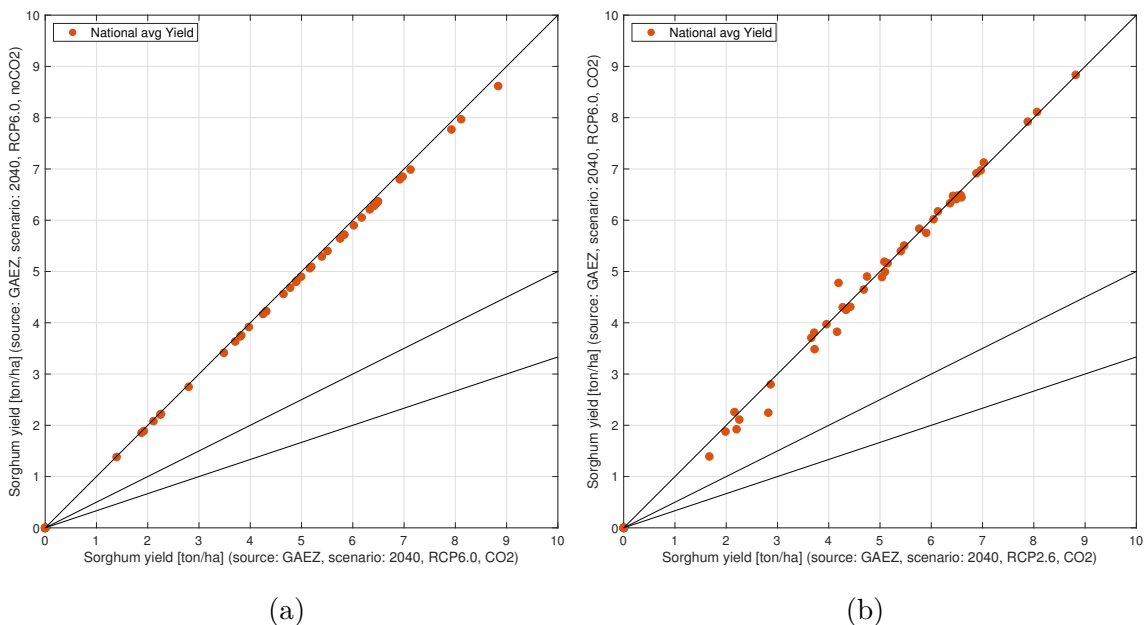


Figure 3.13: *GAEZ v4* 2040 sorghum yield scenario comparison: (a) with and without CO₂ fertilization; (b) *RCP2.6* and *RCP6.0*

The assumption of advanced management agriculture produces very high crop yield compared to actual ones, as mentioned above; thus, the effects of climate change between future scenarios and the present baseline one are hidden and difficult to assess. However, when comparing two future scenarios, the assumption is valid for both, therefore, other influences on crop yields become more visible, as can be noticed from figure 3.14. Panel (a) shows the comparison between *GAEZ v4* national soy yields at 2100 with national soy actual yields at 2010 and, as well as for figure 3.11, for all countries, future yields are around three times higher than present ones. However, in panel (b) The assumption is valid in both, therefore the slight yield increment in 2100 compared to 2040 can be attributed to the changes in climatic conditions and atmospheric CO₂ concentration.

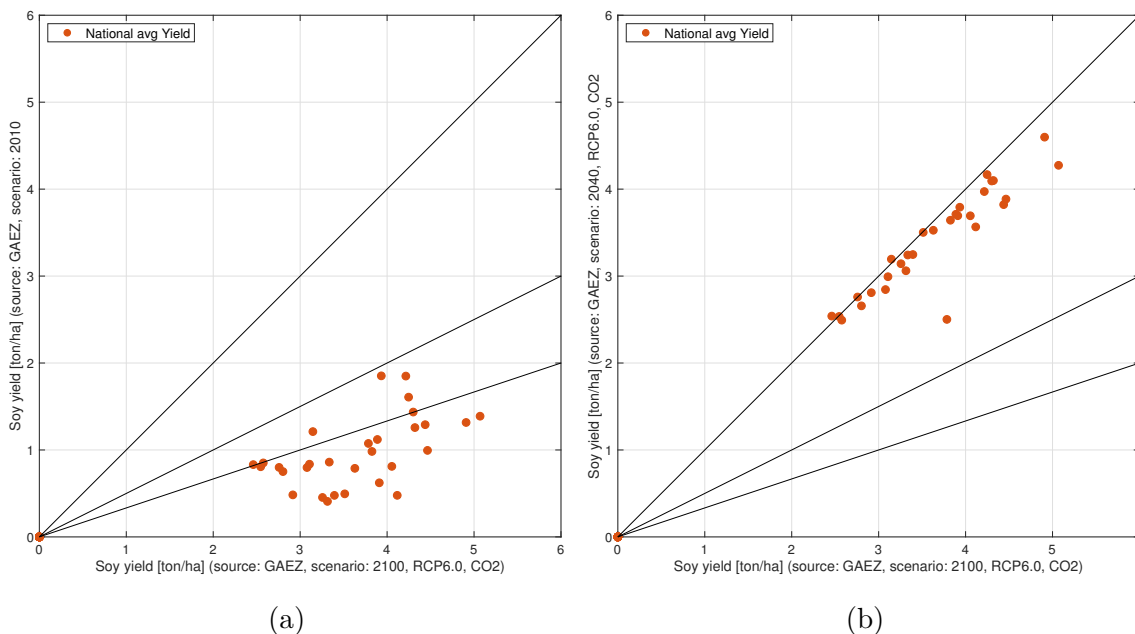


Figure 3.14: *GAEZ v4* future attainable soy yield at 2100 compared with: (a) actual soy yield at 2010; (b) attainable soy yield at 2040

GAEZ v4 national harvested areas at 2010 have been validated with both FAO-STAT (2021) national harvested areas statistics and with Portmann et al. (2010) harvested areas at 2000. In both cases - respectively panel (a) and (b) in figure 3.15 - the strongest divergence from the 1x bisectors can be noticed for countries with around 1000 ha of harvested areas or less. This agreement between the two validation suggests a possible underestimation by *GAEZ v4* model.

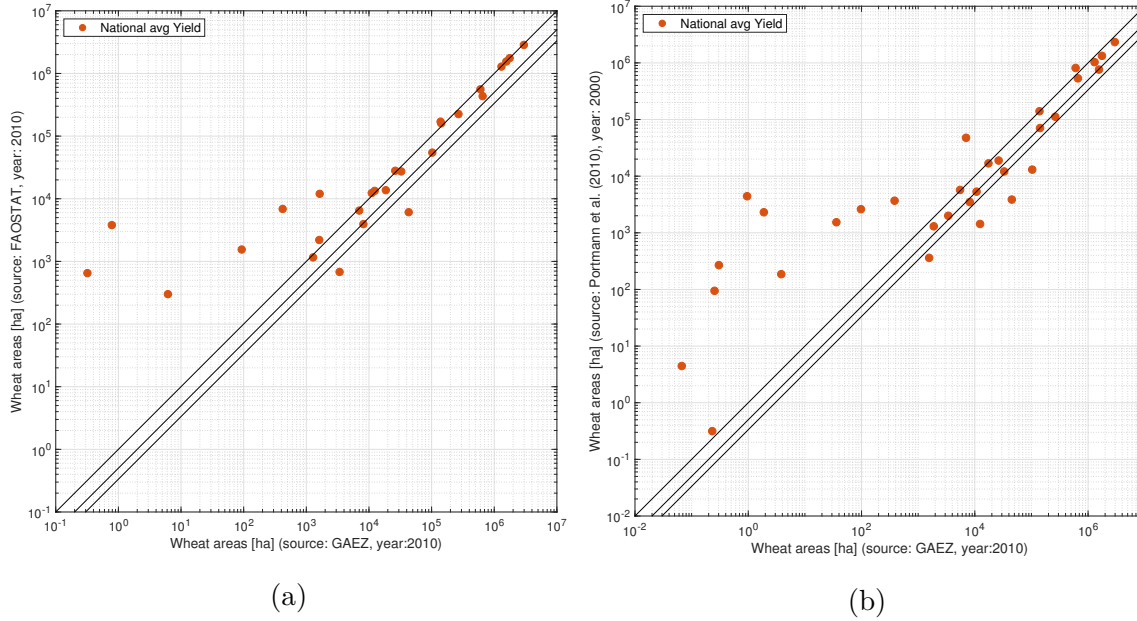


Figure 3.15: *GAEZ v4* 2010 wheat harvested areas validation with: (a) FAOSTAT national harvested areas values at 2010; (b) Portmann et al. (2010) harvested areas data set at 2000

3.3 Crop Water Footprint Model

Once the validity of *GAEZ v4* crop model had been confirmed, the harvested areas and the yield data sets have been given as inputs to Tuninetti et al. (2015) *CWF* model. The model evaluates the virtual water content of crops at the spatial resolution of 5×5 arcmin, which corresponds to 9 Km by 9 Km pixels at the equator (Tuninetti et al., 2015). Both rainfed and irrigated production conditions are considered. The *CWF* estimates refers to thirty years time intervals - 1981-2010, 2011-2040, 2041-2070, 2071-2100 - as previously mentioned, to get rid of the inter-annual fluctuations by averaging over the intervals. This explains why the results are organized in four *Horizons* - 2010, 2040, 2070, 2100. The present interval, represented by the year 2010, is the reference period or baseline scenario with which to compare the future ones.

The crop *CWF* is defined in each cell as the ratio between the water evapotranspired by the crop during the growing seasons of a year y , $ET_{a,y}$ (mm), and the crop actual yield, Y_a (ton ha^{-1}), or attainable yield, in the case of future scenarios, as:

$$WF = \frac{10 \times ET_{a,y}}{Y_a} \quad \left(\frac{m^3}{ton} \right) \quad (3.2)$$

where the factor 10 converts the evapotranspired water height expressed in mm into a water volume per land surface expressed in $m^3 \text{ ha}^{-1}$ (Tuninetti et al., 2015). It must be noted that only the first growing season of the year has been considered in this work. Additionally, the total water evapotranspired by the crop can be written as the sum of a green and a blue component (Tuninetti et al., 2015):

$$ET_{a,y} = ET_{g,y} + ET_{b,y} \quad (3.3)$$

3.3.1 Evaluation of Crop Water Footprint over a single growing season

Monthly long-term average reference evapotranspiration data, $ET_{0,m}$ at 30×30 arc min resolution are converted to 5×5 arc min data grids, as explained in section 2.6. Then, daily $ET_{0,j}$ values are determined through a linear interpolation of monthly climatic data in which the monthly $ET_{0,m}$ value is attributed to the middle of the month Tuninetti et al. (2015). For sake of simplicity, months are considered to be 30 days long. Even though these conversions introduce uncertainties in the calculations, they are necessary because of the lack of 5×5 arc min resolution daily evapotranspiration data (Tuninetti et al., 2015).

Daily crop evapotranspiration, $ET_{a,j}$, is then calculated following Allen et al. (1998) approach for the virtual water content assessment [Mekonnen and Hoekstra (2011); Siebert and Döll (2010); Tuninetti et al. (2015)]. According to such approach, $ET_{a,j}$ is defined as:

$$ET_{a,j} = k_{c,j} \times ET_{0,j} \times k_{s,j} \quad \left(\frac{mm}{d} \right) \quad (3.4)$$

where $k_{c,j}$ is the daily crop coefficient, $ET_{0,j}$ is the daily reference evapotranspiration (mm d^{-1}) and $k_{s,j}$ is the daily water stress coefficient (Tuninetti et al., 2015), as explained in section 2.6.

The total water evapotranspired by the crop over a single growing season, $ET_{a,lgp}$ (mm), is obtained by summing up the daily actual evapotranspiration, $ET_{a,j}$, over

the length of the growing period (LGP) (Tuninetti et al., 2015) :

$$ET_{a,lgp} = \sum_{j=1}^{LGP} ET_{a,j} \quad (mm) \quad (3.5)$$

$ET_{a,j}$, which is the sum of green and blue actual evapotranspiration, differs between rainfed and irrigated production, since the growing period can have different planting dates between the two. In the case of rainfed crops, the green component, $ET_{g,j}^R$, is equal to the total evapotranspiration, $ET_{a,j}^R$, while the blue component $ET_{b,j}^R$ is equal to zero. However, for irrigated crops, the blue component, $ET_{b,j}^I$, equals the amount of irrigation water provided to the crop, while the green component is the difference between $ET_{a,j}^I$ and $ET_{b,j}^I$ values (Tuninetti et al., 2015). The total green and blue evapotranspiration, are the sum of daily values over the growing period, for both rainfed ($ET_{g,LGP}^R$) and irrigated conditions ($ET_{g,LGP}^I$ and $ET_{b,LGP}^I$).

Following Tuninetti et al. (2015), in order to compute the overall green and blue evapotranspiration over the growing period per each cell, $ET_{g,LGP}$ and $ET_{b,LGP}$, the weighted average of the rainfed and irrigated component is performed:

$$ET_{g,LGP} = \frac{ET_{g,LGP}^R \times A^R + ET_{g,LGP}^I \times A^I}{A^R + A^I} \quad (3.6)$$

$$ET_{b,LGP} = \frac{ET_{b,LGP}^I \times A^I}{A^R + A^I} \quad (3.7)$$

where A^R and A^I are the harvested areas, here used as weights, sourced from *GAEZ v4*, as described in section 2.5.

Finally, $ET_{g,LGP}$ and $ET_{b,LGP}$ are inserted in equation 3.2, and the blue and the green components, respectively, of the crop *CWF* are determined in each grid cell. The total water footprint of the cell is the sum of the green and blue *CWF* (Tuninetti et al., 2015). Results have a yearly temporal resolution.

3.3.2 Validation of input climatic variables

This study represents the first application of Tuninetti et al. (2015) *CWF* model to future time intervals. The climatic variables ET_0 and P , presented in the section

2.6, have been included as model inputs in order to produce such future scenarios; although, they had to be validated before. This has been performed by comparing the new data sets with those used in Tuninetti et al. (2015) for previous simulation. In their work, the monthly average reference evapotranspiration was sourced from FAO (2014), while monthly precipitation was given by New et al. (2002). National aggregation of monthly average precipitation and reference evapotranspiration have been compared by means of scatter plot where every dot identifies one African country and the three lines are the bisectors (0.5x, 1x and 2x). In figure 3.16, panel (a) the comparison between potential evapotranspiration data sets by ISIMIP (2021) and FAO (2014) can be seen. The latter data set produces higher values for most countries, however the values never double *ISI-MIP* results. In panel (b), precipitation data sets by ISIMIP (2021) and New et al. (2002) are compared. In this case the values align well along the 1x bisector, except for Gabon, which precipitation value by ISIMIP (2021) is nearly the double of that by New et al. (2002). In addition, the Democratic Republic of Congo shows a value of precipitation which is way higher than those of all the other countries, however, the two data sets are consistent on such result.

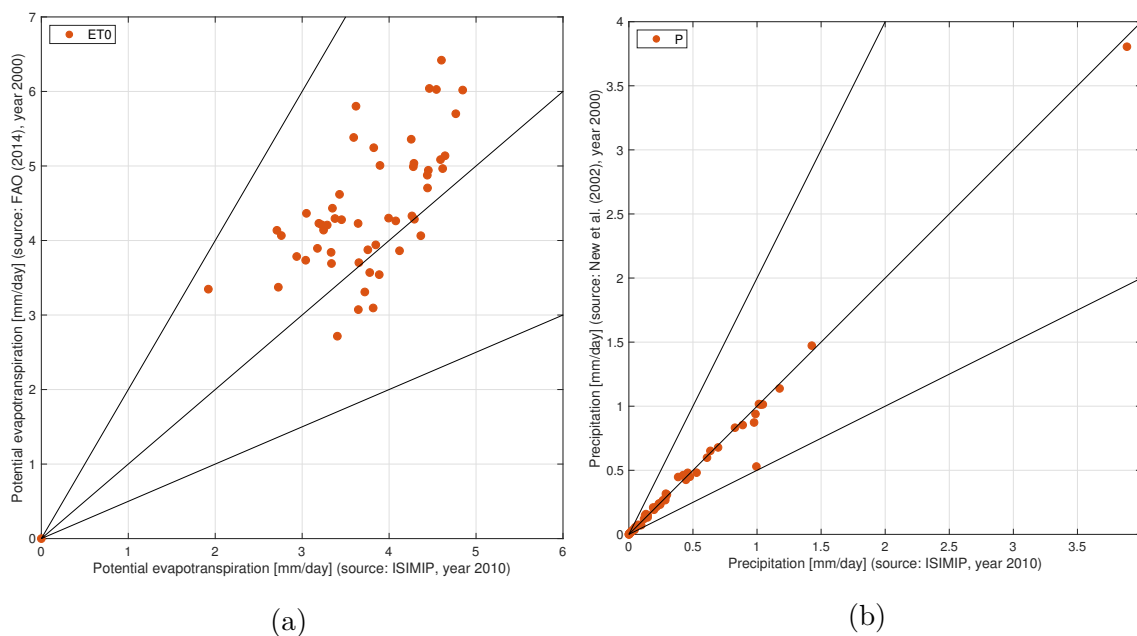


Figure 3.16: Climatic variables validation scatter plots. Panel (a): potential evapotranspiration from ISIMIP (2021) against FAO (2014). Panel (b): validation of ISIMIP (2021) precipitation with New et al. (2002) dataset.

The precipitation data set daily resolution represents a step forward in the model precision, since it is the first time daily data are provided directly as input and not obtained by interpolation of coarser data sets, as it still occurs for the ET_0 . To include such data set, the model algorithm have been modified accordingly, as it is explained in the following section.

3.3.3 Model Modifications

In addition to the climatic variables, to which the model has been adapted to, other data sets, such as *GAEZ v4* harvested areas and crop yields, have been included in the model as new input, specific to this work. Still, a thorough investigation of the algorithm workings was necessary before bringing further changes. Therefore, a short change in the algorithm has been compiled for the *CWF* model to compute and plot the daily evolution of output variables in single grid cells along the growing period, as a way to visualize the model functioning. Figures 3.17 and 3.18 show the daily evolution of the model outputs for the sorghum crop in one grid cell belonging to Egypt territory. It can be notice how the evolution of the climatic variables, P and ET_0 , and the change in the crop coefficients drive the plant growth, its water consumption and irrigation requirements.

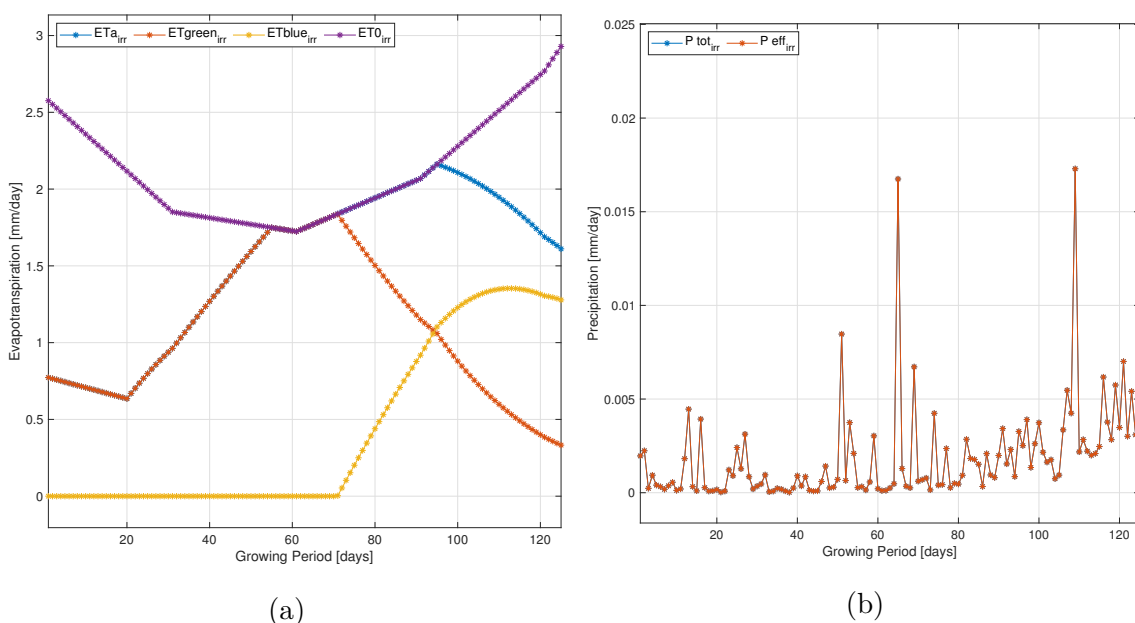


Figure 3.17: Daily evapotranspiration (a) and precipitation (b) over the growing period of Sorghum in one grid cell of Egypt. Horizon 2070, *RCP2.6*, CO_2

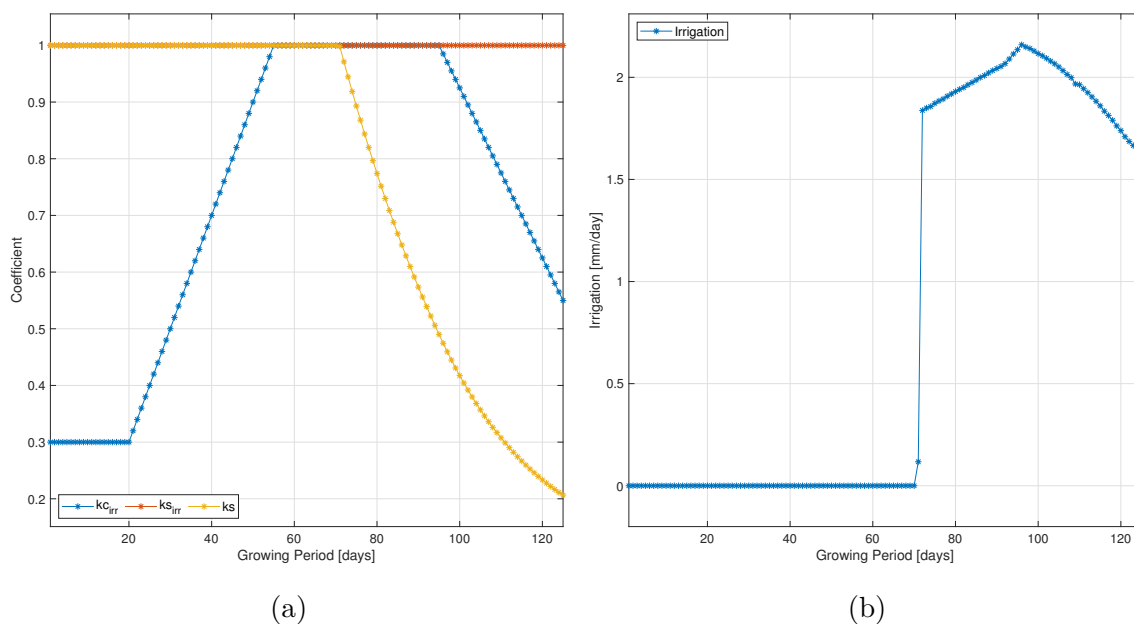


Figure 3.18: Daily evolution of crop coefficient, water content coefficient (a) and irrigation (b) over the growing period of Sorghum in one grid cell of Egypt. Horizon 2070, *RCP2.6*, CO_2

Once the results have been deemed satisfying, as well as the comprehension of the model, another, more significant, modification has been performed. The daily values over the *LGP* have been ordered along the year, so to correctly position the growing season. Then, monthly values have been aggregated to show the monthly evolution of the outputs along the representative year of each scenario compiled. While the daily scale was only available for single cells' outputs, because of computational costs, the monthly scale allows the model to cover the whole globe, by working on the whole matrix extension (5×5 arc min resolution, 2160×4320 grid cells). Each output variable, for every representative *Horizon*, is stored in 12 maps, one per each month, with a resolution of 5×5 arcmin. Below, figures 3.19 and 3.20 show the monthly evolution of climatic variables and irrigation requirement of the same crop and in the same grid cell as before. The shapes are consistent in the two representations, but here the position of the growing period is identifiable along the year and the values are monthly aggregated.

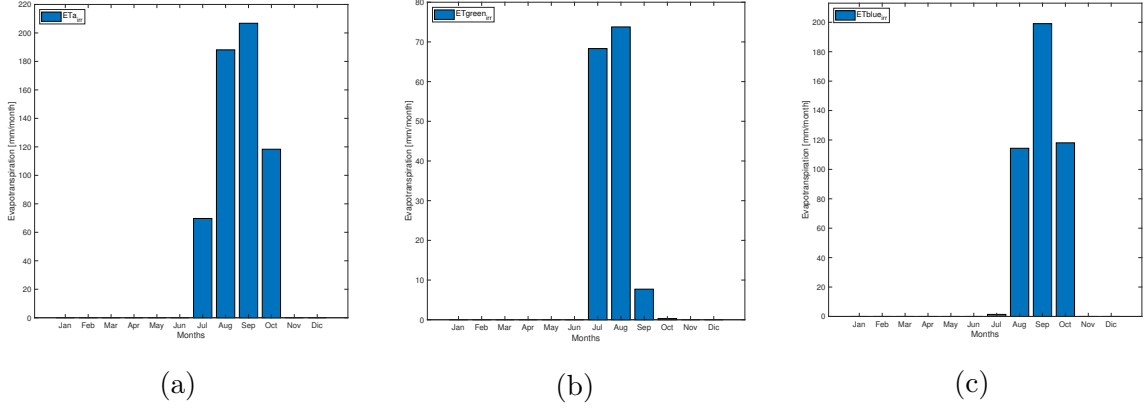


Figure 3.19: Monthly evolution of (a) actual evapotranspiration, (b) green evapotranspiration and (c) blue evapotranspiration over the year for Sorghum crop in one grid cell of Egypt. Horizon 2070, *RCP2.6*, CO_2

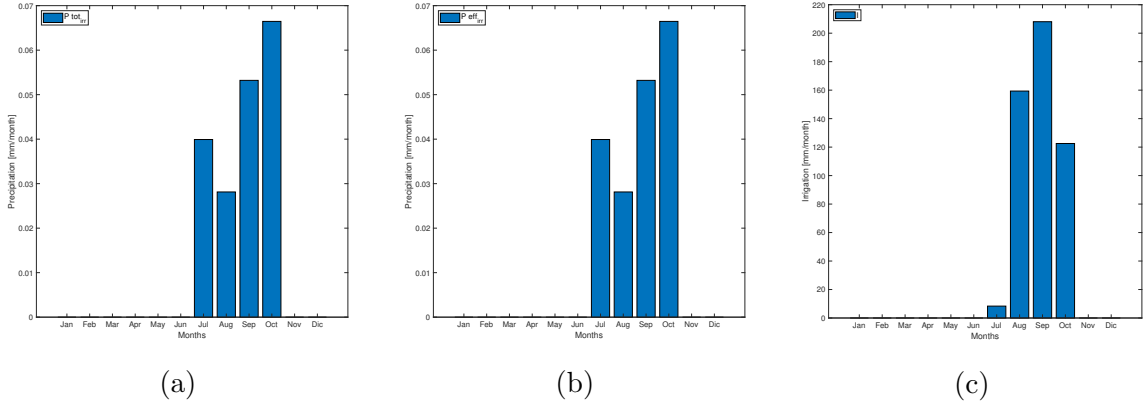


Figure 3.20: Monthly evolution of (a) total precipitation, (b) effective precipitation and (c) irrigation over the year for Sorghum crop in one grid cell of Egypt. Horizon 2070, *RCP2.6*, CO_2

The outputs compiled by the *CWF* model are:

- Crop actual evapotranspiration for rainfed and irrigated production, $ET_{a,j}^R$ and $ET_{a,j}^I$;
- Crop actual green and blue evapotranspiration for irrigated production, $ET_{b,j}^I$ and $ET_{g,j}^I$, which are the components of $ET_{a,j}^I$;
- The total precipitation along the growing period for irrigated and rainfed production;

- The effective precipitation along the growing period for irrigated and rainfed production, which means only the component of the precipitation which is used by the plants and it is not lost as runoff;
- The water used for irrigation, which corresponds to $ET_{b,j}^I$ in the irrigated production;
- The green, the blue and the total crop CWF , but also the rainfed and irrigated production CWF ;

The rainfed and irrigated production CWF represent the last modification introduced in the model. While the blue and the green CWF distinguish between the contributes of precipitation and irrigation water on the two types of production together - as can be understood from equation 3.6 and 3.7 -, the rainfed and irrigated CWF distinguish between the two production types. Specifically, the rainfed CWF only includes green evapotranspiration over the growing period of the rainfed production and the respective crop yield. While the irrigated CWF includes both contributes of blue and green evapotranspiration over the growing period of irrigated production, with the crop yield associated to this type of production. The computation of irrigated and rainfed CWF is the following:

$$WF_{rf} = \frac{10 \times ET_{g,LGP}^R}{Y_{rf}} \quad \left(\frac{m^3}{ton} \right) \quad (3.8)$$

$$WF_{irr} = \frac{10 \times (ET_{b,LGP}^I + ET_{g,LGP}^I)}{Y_{irr}} \quad \left(\frac{m^3}{ton} \right) \quad (3.9)$$

Where Y_{rf} and Y_{irr} are, respectively, the rainfed and irrigated components of the actual or attainable yield, depending on the scenario of interest.

Finally, the model has been calibrated to work on the African continent, in agreement with the purpose of this work, and both unitary water footprint uWF and total water volume maps have been produced for four crops - maize, wheat, sorghum, soy - and for four Horizons - 2010, 2040, 2070, 2100 -, following both $RCP2.6$ and $RCP6.0$ and including both sensitivity scenario with and without CO2 fertilization. Below the total maize uWF map of Africa can be seen. The maize

harvested areas filter the cells where the *CWF* is computed and the colors indicate its magnitude. The darker the colour, the higher the amount of water m^3 used for one *ton* of maize. Here, the representative year is 2070 and the *RCP* is 6.0, CO₂ fertilization effect is included.

3.4 Scenarios comparison

Once all the *CWF* maps have been produced for all the scenarios, they have been compared by means of percentage variation maps and national scale scatter plots. Specifically, all the future scenarios have been compared with the baseline scenario, in order to assess the impact of advanced agricultural management on future yields and water consumption. Moreover, future scenarios have been compared among themselves to evaluate the effects of climate change along the years, when Harvested areas and agricultural practices assumptions are fixed. The steep yield increment induced by high input advanced agricultural management produces an increase in agricultural production over the same extension of harvested areas. This translates in a increment of water use, to support such production, up to three times, in the case of 3.21, panel **(b)**. However, the water use efficiency improves, which can be seen from the decrease in the *uWF* in panel **(a)**. The most impressive results is the nearly 92% reduction of maize *uWF* in Capo Verde from 2010 to 2100.

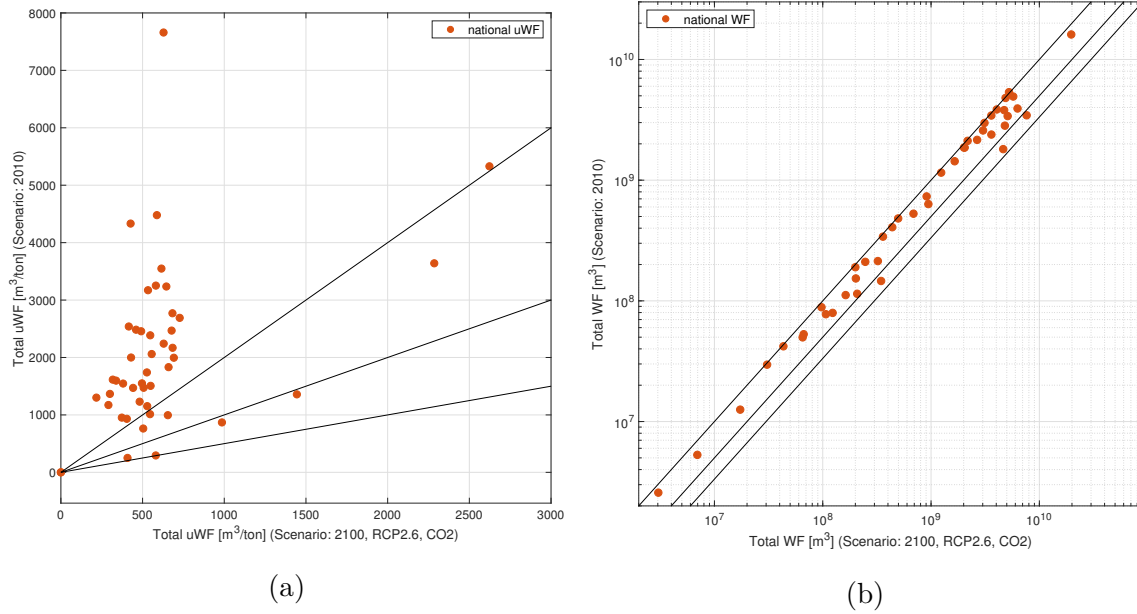


Figure 3.21: Comparison of (a) uWF and (b) CWF between 2010 and 2100 for maize, scenario $RCP2.6$, CO_2 fertilization.

The same comparison is presented in percentage difference map form in figure ???. Here, the percentage change between 2100 and 2010 can be appreciated cell by cell by multiple colour intervals. The prevalence of red cells identifies the only four countries where water use efficiency got worse from 2010 to 2100 - Comoros, Egypt, Namibia and South Africa.

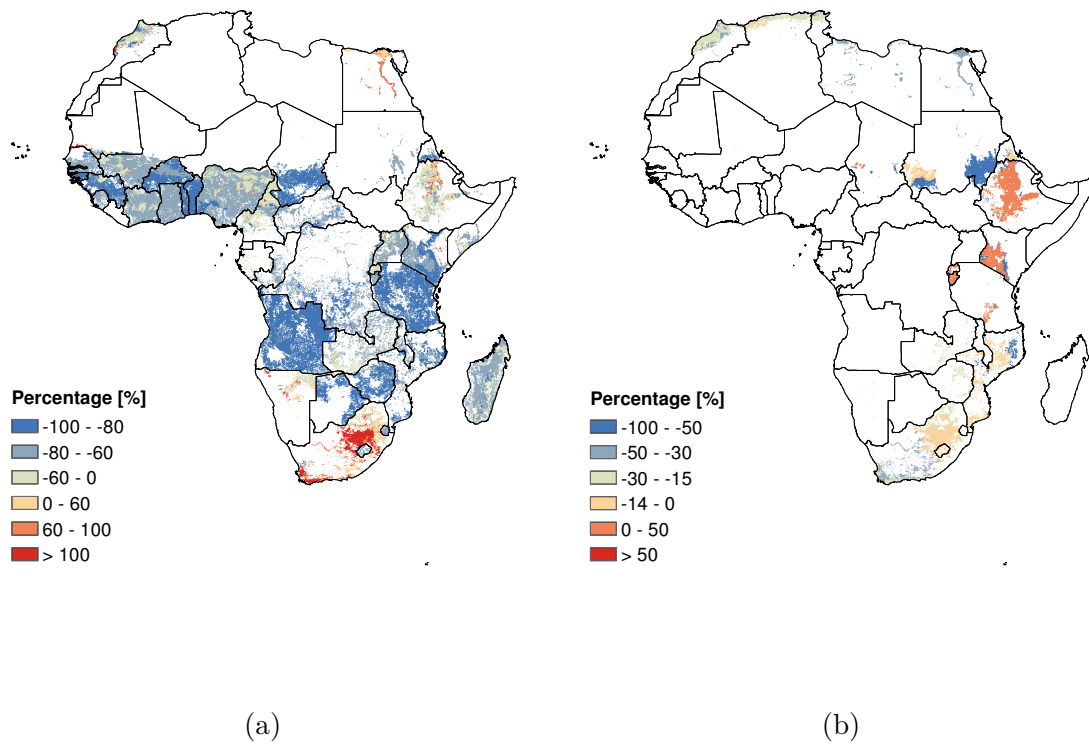


Figure 3.22: Percentage difference map of (a) Maize uWF at 2100 ($RCP2.6$) and (b) wheat CWF at 2100 ($RCP2.6$), relative to 2010

Chapter 4

Results

The work described in this thesis allowed to simulate and represent future scenarios of *CWF* over the African continent, in order to investigate such indicator in its different forms to finally draw insights about the possible future evolution of African agriculture. The main directions of this investigation are two: on one hand, the concerning impacts of climate change on the agricultural sector and, on the other hand, the opportunities and the drawbacks of an advancement in the African agricultural management, in terms of technologies and inputs employed, over the current cropland extension. The results are presented in a way that highlights the directions of the investigation, but, at the same time, the discussion develop along different levels of meaning, in an effort to disentangle the density of significance that the *CWF* indicator encompasses.

Firstly, the continental-level aggregation of the results is presented; this allows the reader to grasp the magnitude of the variables in question and its temporal evolution along the future scenarios. In addition, it permits the immediate comparison with the baseline scenario and with historical values belonging to the period 1961-2019, which have been plotted together with the results. The variables represented in this section are: aggregated crop yields and harvested areas, unitary water footprint and crop water footprint. The following two sections are dedicated to the *uWF* and, specifically, to its irrigated and rainfed components. The baseline 2010 scenario is presented in absolute values, while *Horizons 2040* and *2100* are shown as percentage variation maps relative to 2010. In the case of end-of-century

scenario, both *RCP2.6* and *RCP6.0* are displayed. Such representation has been performed for Maize and Sorghum crops, since they show the highest levels of *CWF* and the most extended harvested areas among the crops under analysis. Sections 4.4 and 4.5 are dedicated to the green and blue component of the crop-aggregated *WF*. The spatial distribution of these variables across the continent is represented through detailed maps for the baseline scenario, where their magnitude is indicated by colour coding. In addition, enlargement of the three countries showing the highest *CWF* values of the continent are shown. In section 4.5 future scenarios of blue *WF* are compared with the baseline scenario for each of these three countries. This connects the discussion to the last section where the evidence of climate change in the previously represented results is highlighted.

4.1 Continent-level aggregated water footprint

Tuninetti et al. (2015) model computes the results in the form of 5×5 arc min grids which cover the entire African continent. In order to highlight the general trend of the evolution of each crop along the four *Horizons*, the results have been aggregated at the continental level. Crop yield and Harvested areas are not outcomes of the model, however, they support the analysis of the results. Figure 4.1 shows the evolution of, respectively, maize, sorghum, soy and wheat yields from 1961 to 2019 - as reported by FAOSTAT (2021) - and along the four *Horizons* developed in this study. Both *RCPs*' trends are shown, even though they become distinguishable generally after 2040. The most surprising feature is the increment shown by all crops' yields from 2010 to 2040. As mentioned before, this is explained by the assumption of advanced management applied by *GAEZ v4* on the future scenarios. Such hypothesis produces an increment in yield of 244.6%, between 2010 and 2040, in the case of maize, which shows the widest absolute gap. Nevertheless, such increasing trend is not constant along the future scenarios, since they all share the same assumption; therefore, other influences on yields become more visible, such as the effect of CO₂ concentration, which produces the gap between *RCP2.6* and *RCP6.0* trends.

It is worth to notice the coherence between the historical series at 2010 and the

baseline 2010 scenario, since 2010 is the only scenario in which actual yield values have been used, instead of attainable ones, and they represent the most recent actual yield data set in the literature. In addition, 2010 is the year to which the harvested areas used throughout all future scenarios are referred to.

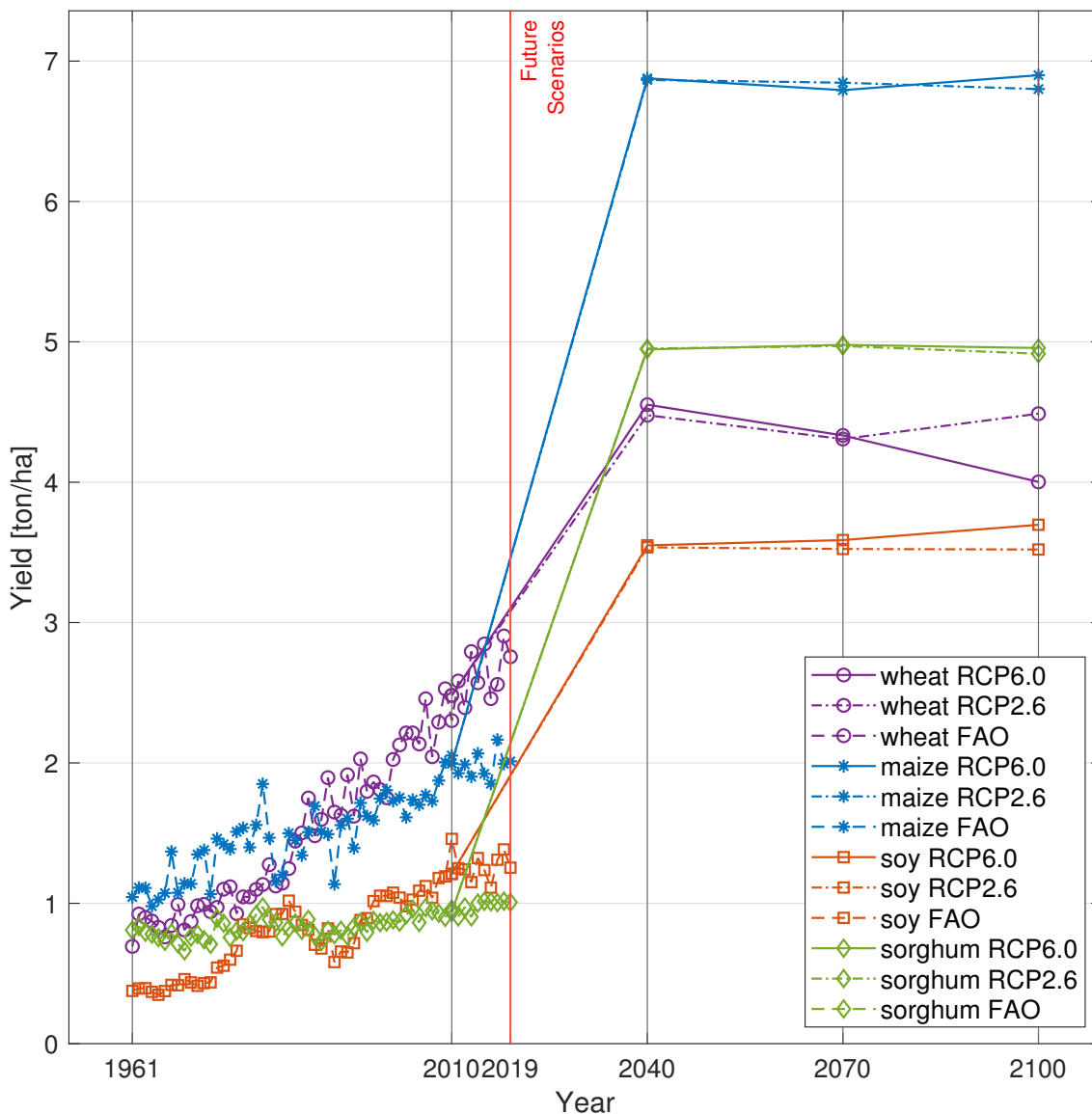


Figure 4.1: Evolution of average African yield of four crops across the future scenarios. Both *RCPs* are shown, as well as FAOSTAT (2021) historical yield statistics from 1961 to 2019.

While the step increment in sorghum, soy and maize yields seems the artificial effect of an hypothetical assumption, hardly achievable in such a short time interval, wheat yield shows a unique trend. Between 2010 and 2040 the yield trend obtained from the interpolation of *Horizons 2010* and *2040* is coherent with the trend that

can be identified in the FAOSTAT (2021) data serie. No matter the hypothesis of high input, advanced management agriculture, maize yield trend is coherent between actual data and simulated attainable values. This means that the actual yield is close to its attainable value - namely its potential limit, taking into account the reduction factors of temperature and frost hazards, pests, diseases and weeds, soil limitations, terrain slope conditions and cimatic factors - and the assumption of advanced mangement seems not to further improve yield growth beyond its current trend. This could mean that wheat is, generally, on track to reach its upper yield limit and to the closure of its yield-gap, which seems achievable by 2040. A narrower gap with respect to the other crops, where it seems still very wide. This is reflected in figure 4.2, which shows the yield achievement ratios (*YAR*) of the four crops. *YAR* is estimated by dividing downscaled actual yields with agro-ecological attainable yield simulated under high input/advanced management assumptions. *YAR* is closely related to yield gap, as both variables together sum up to 100 percent.

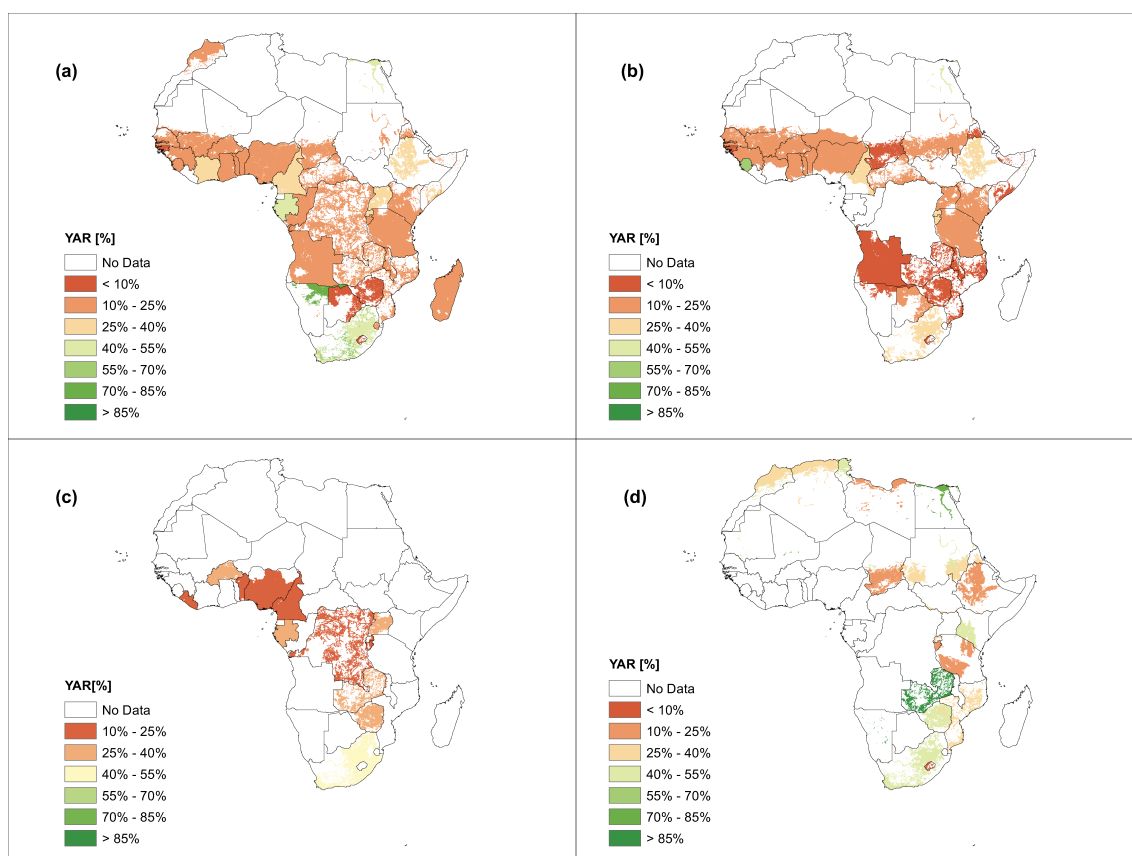


Figure 4.2: Yield achievement ratio of: (a) maize; (b) sorghum; (c) soy; (d) wheat.

Given the tighter yield gap and the milder effect of the high input assumption,

future climatic impacts on wheat yield are more evident in figure 4.1. Wheat is the crop which shows the wider discrepancy between the two *RCPs* and the more accentuated yield reduction - specifically, between 2040 and 2100, *RCP6.0* it records a 12.1% reduction. The evolution of yields affects and is reflected by the *uWF* trends. Especially, in their general decrease, identifiable both in historical data, provided by Tamea et al. (2021), and in future scenarios. A decrease in *uWF* means that a higher efficiency in water use is gained. This is mainly due to the yield increment that allows a higher production on the same cropland area. Nevertheless, by zooming in on the future *Horizons* in figure 4.3, it can be noticed that the *uWF* increases again for all crops according to *RCP6.0*, while soy and wheat show a further decline between 2070 and 2100 according to *RCP2.6*. Wheat is, again, the crop which shows the broadest gap between the 2 *RCPs*, with *RCP2.6* decreasing by 2.7% between 2070 and 2100, while *RCP6.0* shows a 11.6% in the same interval, the steepest among the four crops. This reflects the trend of wheat yield between 2070 and 2100. Such a coherent future increase among the four crops is definitely linked with the corresponding trends observed in the yields and could be attributed to an effect of climate change. As discussed above, in low-latitudes regions, even moderate temperature increases will negatively impact crop yields, due to the current proximity of such regions to crop-limiting temperature thresholds for suitable production (Jägermeyr et al., 2021; Rosenzweig et al., 2014). Furthermore, temperature increases can lead to growing periods shortening and greater evaporative demand, while CO₂ fertilization effect cannot compensate for such impacts (Rosenzweig et al., 2014).

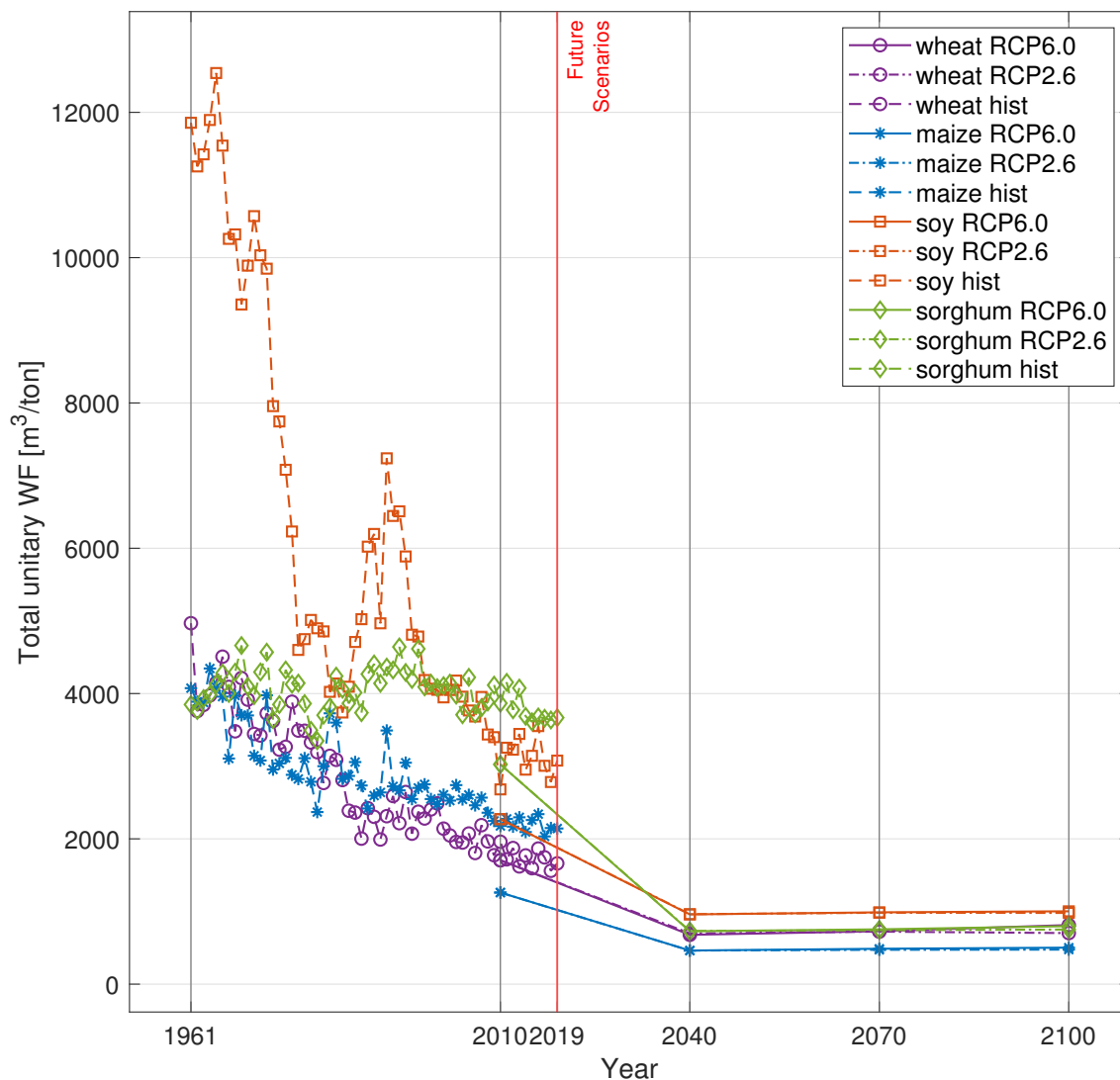


Figure 4.3: Evolution of uWF averaged over whole Africa across future scenarios. Both $RCPs$ are shown.

Even though the water use efficiency improves, to a higher production corresponds a higher water requirement, as it is shown in figure 4.4. Therefore, wheat excluded, the volumetric WF shows a future growing trend for maize, sorghum and soy, even if less accentuated for the latter. Growing trends are present even in historical values, even though they show low coherence with the future scenarios. Maize shows a much steeper increase, starting around 2000 until 2019, then what is projected by its future scenarios. Maize and sorghum also show values at 2010 which are much higher than those obtained in the baseline scenario. As discussed below, this could be due to the difference in the $ET0$ data sets used in this study and in the historical series and to the fact of considering only the first growing season of the year. On

the other hand, wheat and soy CWF values at 2010 are in agreement between the two data series. Nevertheless, even for these two crops, the trend observed in the historical data between 2010 and 2019 is not represented by the simulated future values.

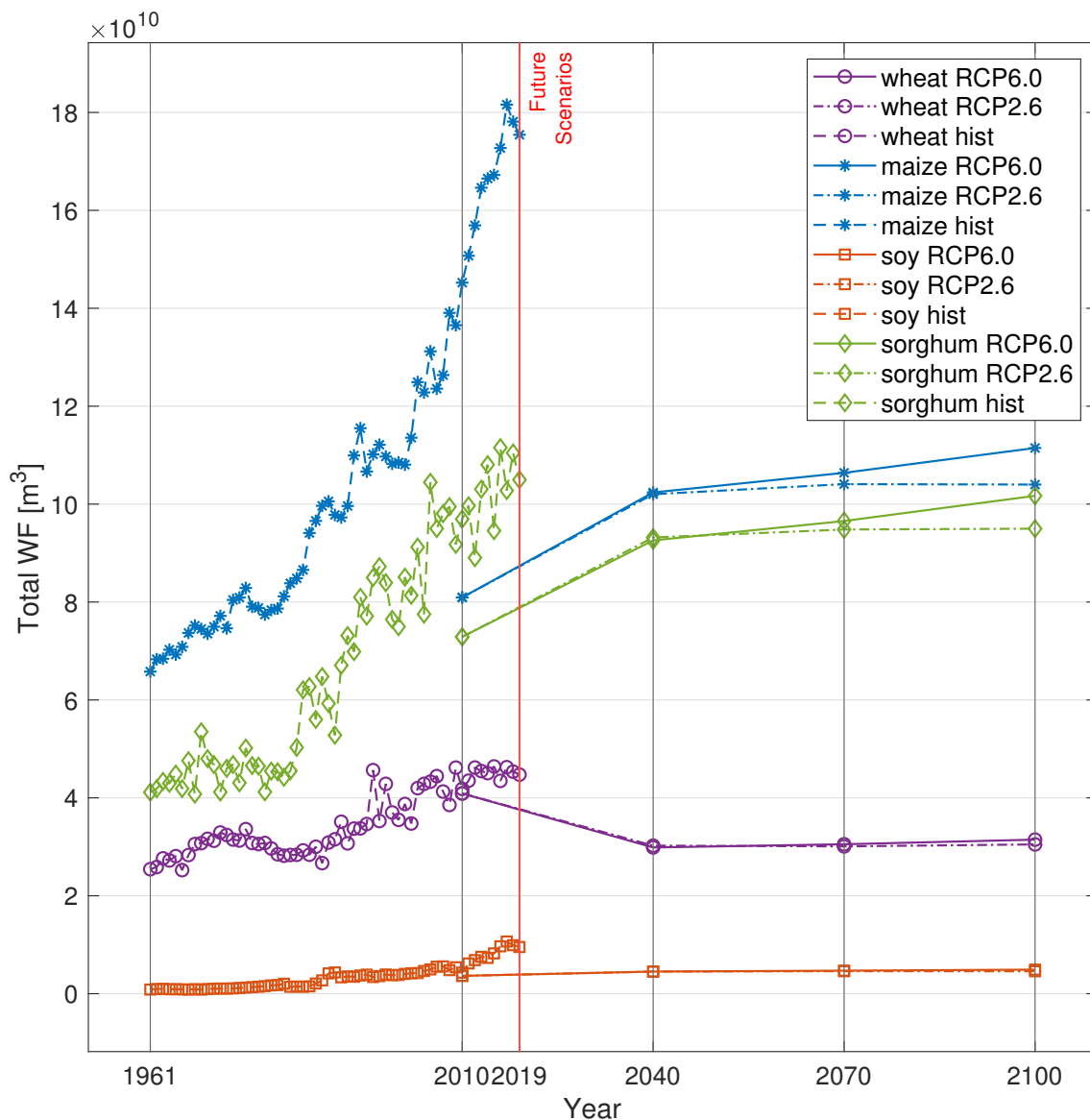


Figure 4.4: Evolution of WF averaged over whole Africa across future scenarios. Both $RCPs$ are shown.

After 2040, $RCP6.0$ of every crop shows a positive trend, even though less steep than that between 2010 and 2040. But in this case, the trend could be attributed to a future temperature increase, which would enhance the evaporative demand and the crop water requirements, but also to a positive effect of a higher CO_2 concentration in the atmosphere on yields. If the increasing trend is evident for the $RCP6.0$, it is

not the same for *RCP2.6*. Indeed, between 2070 and 2100, for this scenario, sorghum shows a very modest growth, while maize and soy *CWF* even decrease, although almost insignificantly. Once again, wheat shows a different behaviour. Between 2010 and 2040 wheat *CWF* declines of 27%, then it slightly grows until 2100 in the case of *RCP6.0*, while *RCP2.6* further decreases until 2070, before growing towards 2100.

The choice of keeping constant the harvested areas at 2010, which was necessary given the lack of a gridded data set of present and future harvested areas in the literature, can explain the divergence in *CWF* trends between historical values and future projections, in the interval going from 2010 to 2019. As can be seen in figure 4.5, where FAOSTAT (2021) historical values of harvested areas for the four crops have been plotted together with *GAEZ v4* 2010 continental aggregation of cropland areas, the shapes of the *CWF* closely resembles the shape of the harvested areas historical series. By keeping areas constant at 2010, the expansion in harvested areas recorded between 2010 and 2019 has remained neglected from the simulations of future scenarios. However, the discordance between *uWF* and *CWF* values at 2010 cannot be attributed to the constant areas. Indeed, this might be linked to the potential evapotranspiration data used in this work, which gives generally lower values per African country with respect to FAO (2014) data set, as can be observed in figure 3.16a, which was previously used to run the model by Tuninetti et al. (2015).

The difference in wheat behaviour might be linked to the fact that this crop shows the highest amount of harvested areas supplied with irrigation water, 25% of the total extension, with respect to maize, sorghum and soy, and a considerable total production in the top three producers countries - see figure 4.6 -, comparable to the respective production of maize and sorghum, which, although, show a way larger extension of harvested areas across the continent. In addition, wheat shows the highest actual yield until 2019. All these factors suggest a more effective agricultural management for this crop and support the hypothesis advanced above about wheat being on track to reach its potential yield. Nevertheless, the impacts of climate change could pose a threat to this process and negatively impact wheat production.

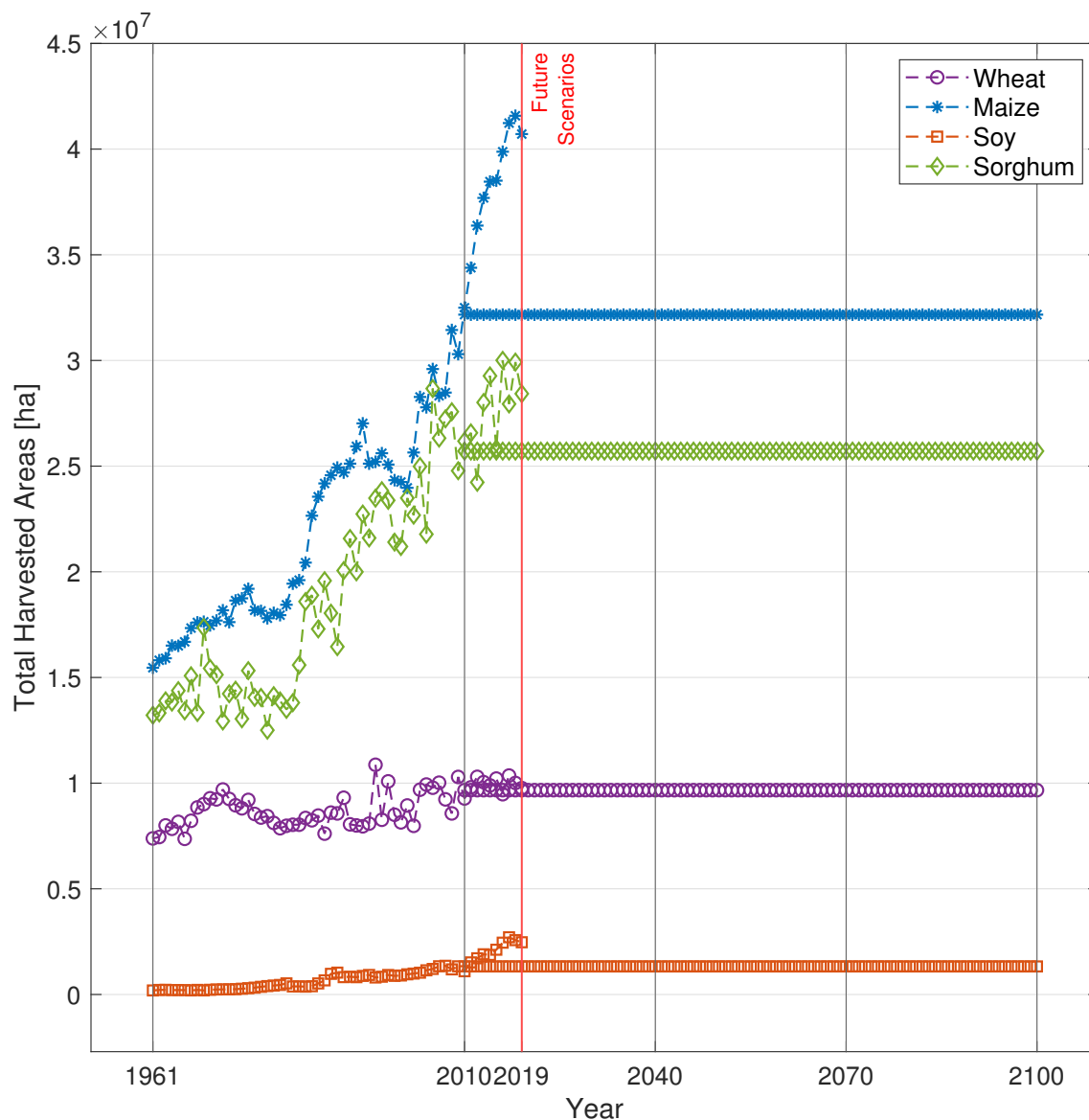


Figure 4.5: Historical evolution of harvested areas over whole Africa from 1961 to 2019. Future values are kept constant and equal to harvested areas at 2010.

The share of irrigated areas with respect to the total cropland extension is very limited for maize, sorghum and soy, which record, respectively, 6%, 4.7% and 2.6% as illustrated in figure 4.6a.

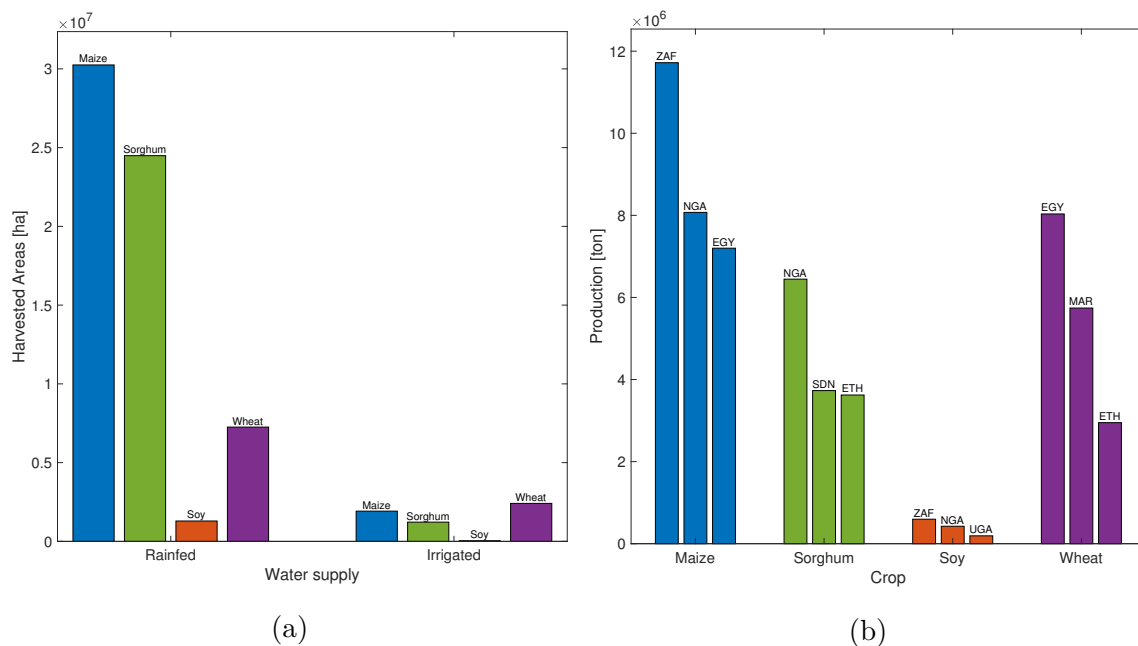


Figure 4.6: Panel: (a) overall harvested areas in Africa by production type and crop variety; (b) tonnes produced overall by the three major producers of each crop variety at 2010.

4.2 Spatial Distribution and Temporal evolution of rainfed water footprint

Rainfed uWF is obtained from equation 3.8 and includes only green water from rainfall evapotranspired by rainfed crops divided by their respective yield. Therefore, rainfed uWF can be used for assessing the water use efficiency of rainfed agriculture. Here, maize and sorghum crops are used to illustrate the results of this section, since they present the largest cropland areas and the highest water use, among the four crops considered in this study. Sorghum rainfed uWF is quite heterogeneous on the continent and shows marked higher values in correspondence of the arid subtropical zones, which can be seen in figure 1.3a. Future scenarios report a general decrease of rainfed uWF , except in Ethiopia and South Africa, where it is expected to increase. In addition, the most evident divergence between $RCP2.6$ and $RCP6.0$ at 2100 is expected precisely in South Africa, where the area reporting an increment bigger than 100% considerably expands in the case of $RCP6.0$.

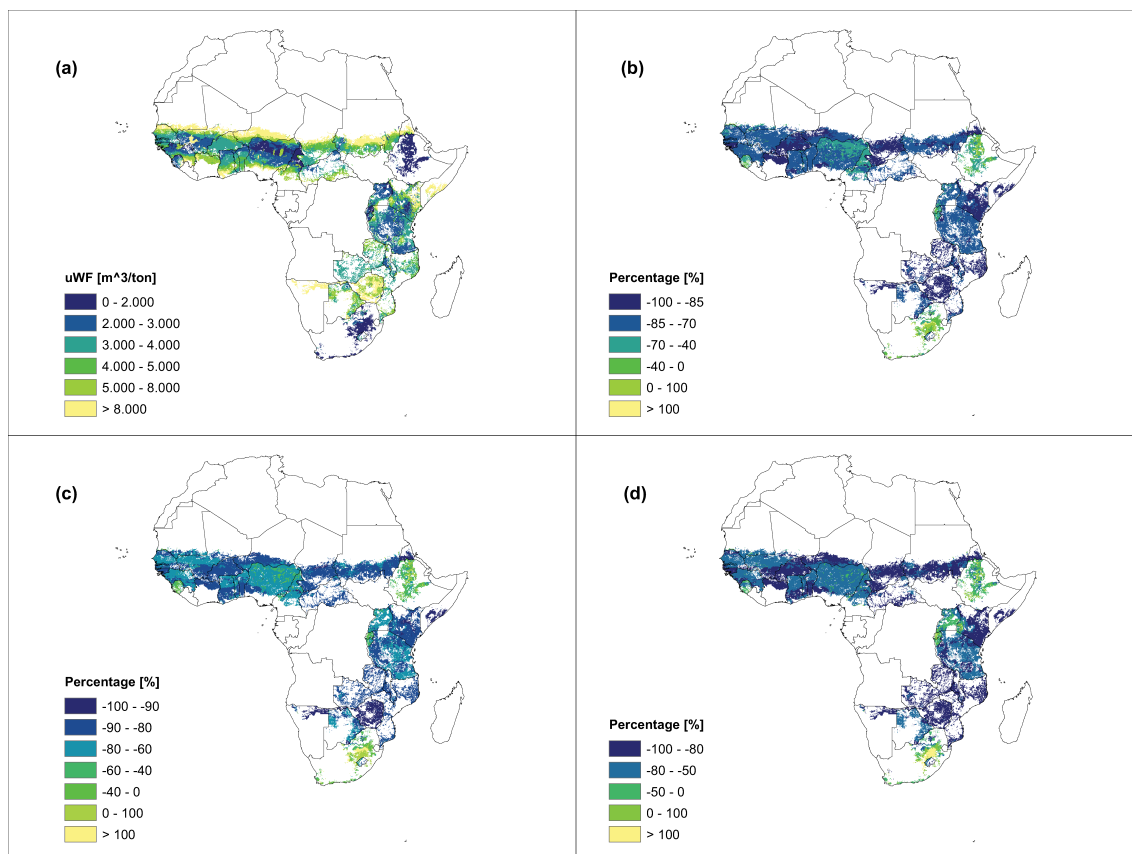


Figure 4.7: Sorghum rainfed uWF across Africa at (a) 2010; (b) 2040, $RCP2.6$; (c) 2100, $RCP2.6$; (d) 2100, $RCP6.0$; Future scenarios are represented as percentage difference maps relative to 2010.

Such characteristic behavior of Ethiopia and South Africa observed in figure 4.7, is present in the case of maize as well, as shown in figure 4.8. Maize rainfed uWF also shows higher values in correspondence with the arid zones at the tropics. However, Angola and the Democratic Republic of Congo, which belong to the humid tropical zone, also show discretely high values, as compared to other countries with more arid climates. Therefore, this fact might be less related to the climate and more to the efficiency of the agricultural management, which is expressed by the yield component of the uWF . More notably, Namibia shows an overall positive change only according to $RCP6.0$ at 2100, while $RCP2.6$ shows a more widespread negative change, in the range of -60 to 0%, for both 2100 and 2040 Horizons. In addition, it is only $RCP6.0$ to show a strong decrease of uWF along a tract of the Moroccan coast, while nothing similar is reported by the other scenarios.

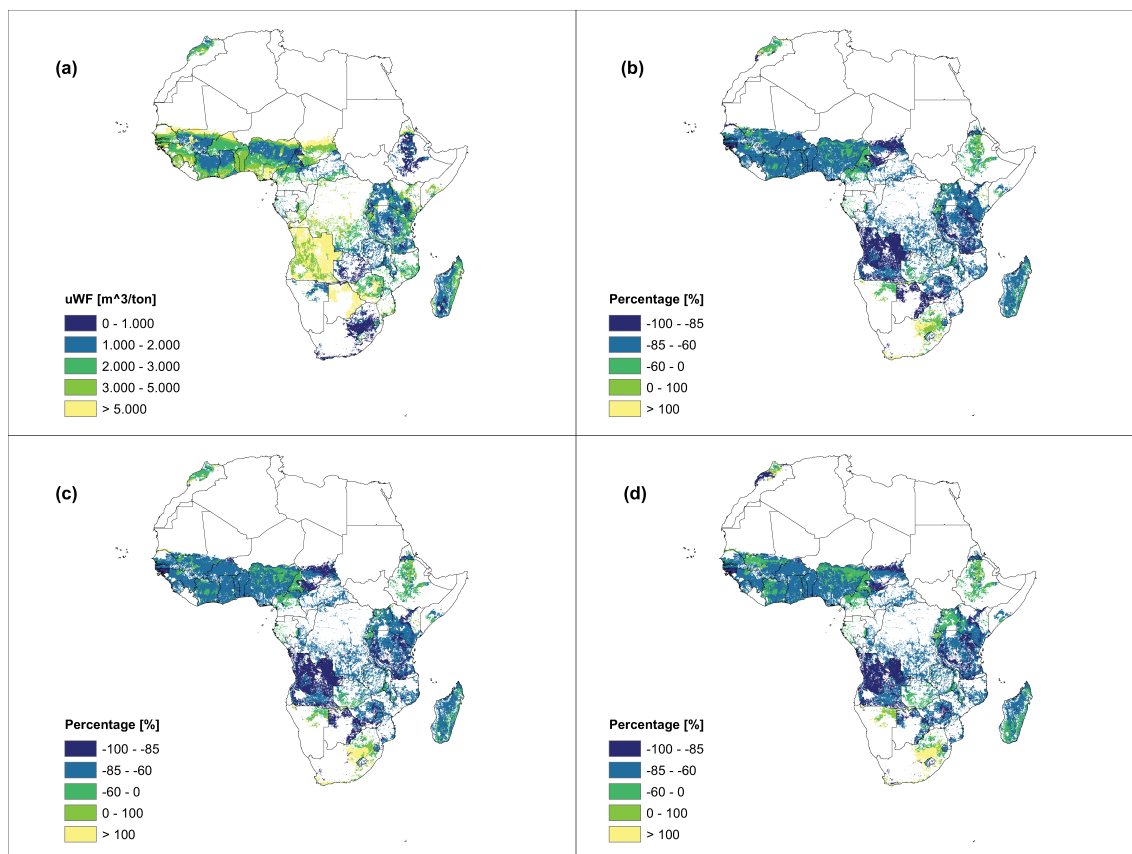


Figure 4.8: Maize rainfed uWF across Africa at (a) 2010; (b) 2040, *RCP2.6*; (c) 2100, *RCP2.6*; (d) 2100, *RCP6.0*; Future scenarios are represented as percentage difference maps relative to 2010.

4.3 Spatial Distribution and Temporal evolution of irrigated water footprint

Irrigated uWF derives from equation 3.9 and includes both green and blue water evapotranspired by irrigated crops divided by their respective yield. Therefore, irrigated uWF can be used for assessing the water use efficiency of irrigated agriculture. Here, once again, maize and sorghum crops are used to illustrate the results of this section. The most prominent feature in the figures of this paragraph is the extremely limited extension of irrigated cropland areas, with respect to rainfed ones (refer to figure 1.3b for a detailed description of *AEI*). They are mostly located in western Africa, specifically, in Egypt, along the river Nile, and in South Africa.

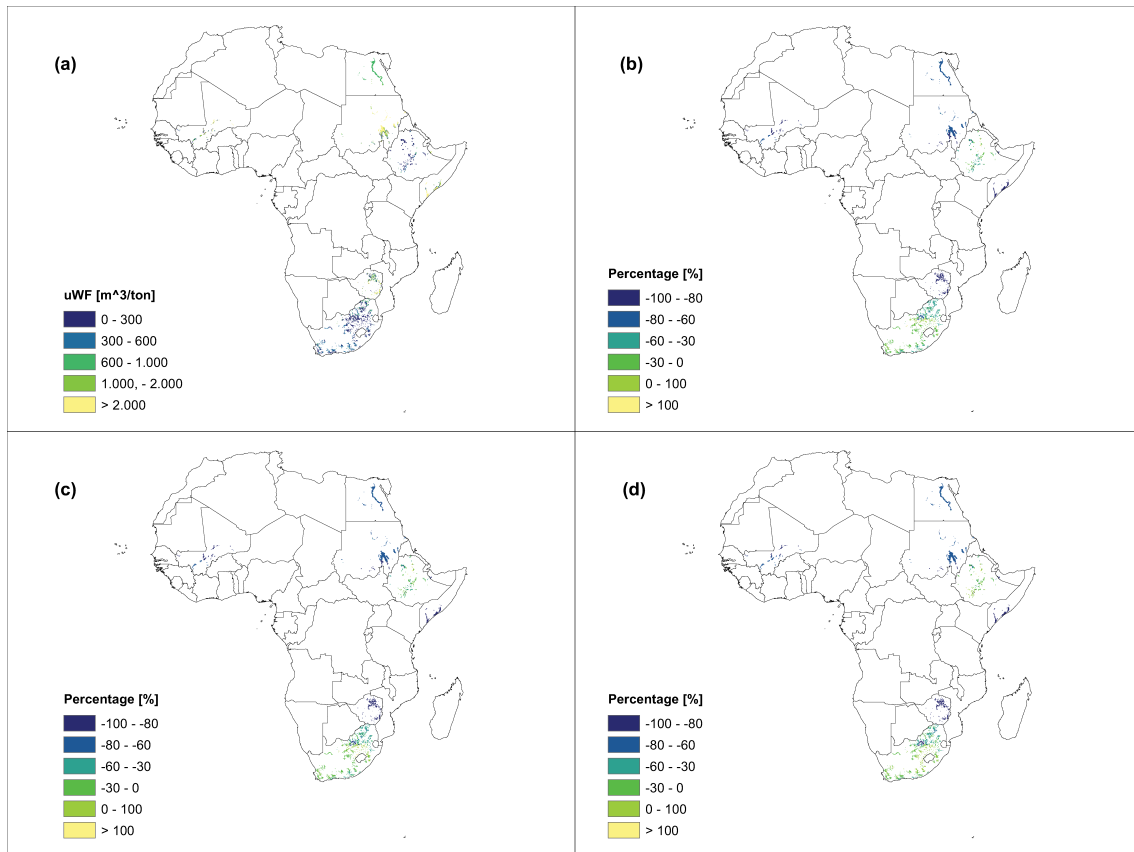


Figure 4.9: Sorghum irrigated uWF across Africa at (a) 2010; (b) 2040, $RCP2.6$; (c) 2100, $RCP2.6$; (d) 2100, $RCP6.0$; Future scenarios are represented as percentage difference maps relative to 2010.

South Africa shows again a widespread increase in irrigated uWF for both maize and sorghum and low water use efficiency is reported in Sudan, however it is expected to improve in the future scenarios. Maize and Sorghum shows opposite irrigated uWF trends in two countries: Egypt and Ethiopia. Sorghum irrigated uWF is expected to improve in Egypt in the future, but to get worse and increase in Ethiopia. On the contrary, as observed in figure 4.10, maize irrigated uWF is reported to increase in the future in Egypt, but to decrease, or improve, in Ethiopia.

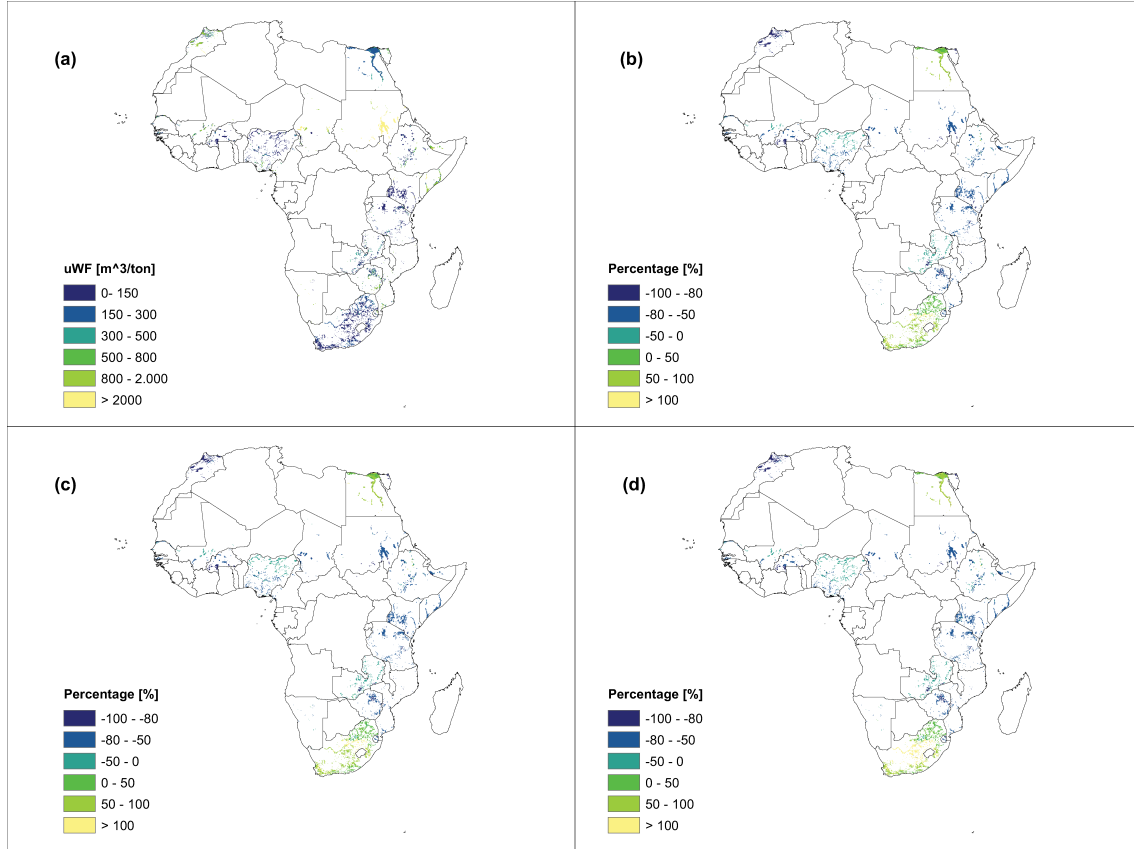


Figure 4.10: Maize irrigated uWF across Africa at (a) 2010; (b) 2040, $RCP2.6$; (c) 2100, $RCP2.6$; (d) 2100, $RCP6.0$; Future scenarios are represented as percentage difference maps relative to 2010.

4.4 Crop aggregated green water footprint

In this and in the following section CWF results are reported as the combined WF of the four crops considered in this work. In addition, the green and the blue components of the WF have been separated in order to investigate the use of, respectively, rainfall and irrigation water and its evolution in the future scenarios. Green WF is obtained as:

$$WF_g = \frac{10 \times ET_{g,LGP}}{Y_a} \quad \left(\frac{m^3}{ton} \right) \quad (4.1)$$

where $ET_{g,LGP}$ is calculated following equation 3.6. Thus, green WF includes the overall rainfall water evapotranspired by both rainfed and irrigated agriculture.

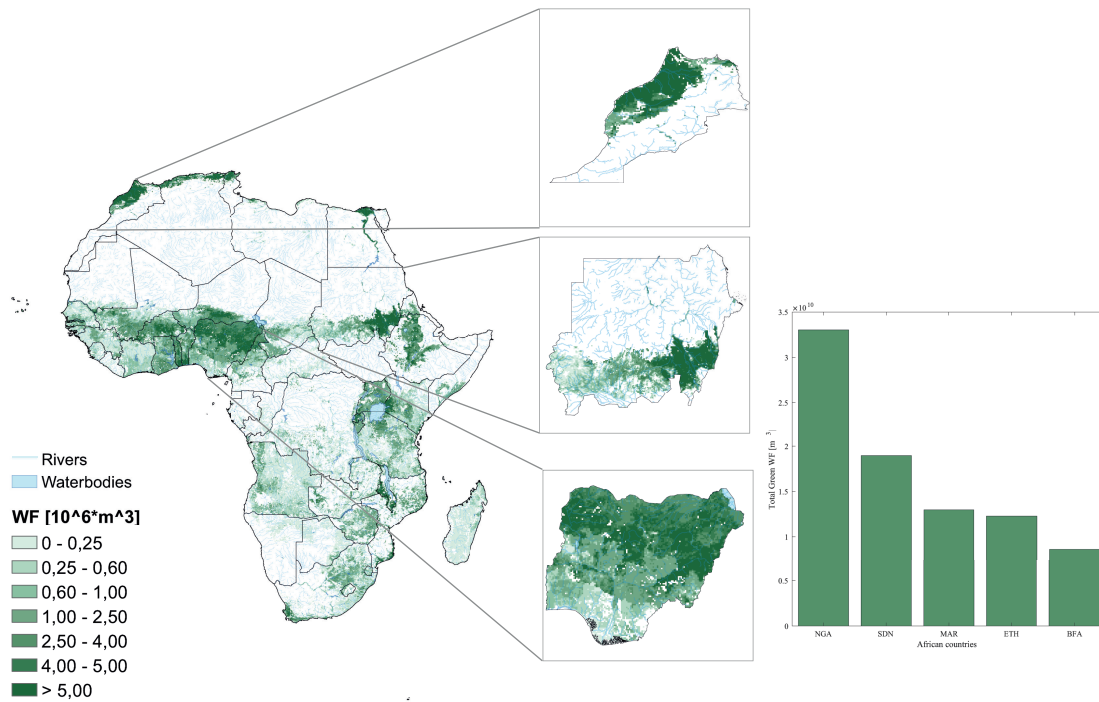


Figure 4.11: Green WF across Africa at 2010. The three countries showing higher values are enlarged. The histogram with the five countries recording higher values is shown as well.

As it can be inferred from equation 3.6, $ET_{g,LGP}$ includes the total harvested areas, rainfed and irrigated, therefore, in figure 4.11, the spatial extension of green WF corresponds to the total harvested areas of the four crops together. This is why the shape of the Nile river is so clear, from north of Egypt across Sudan. Below the Sahara desert, the semi-arid region stretching longitudinally from Senegal in West Africa to Sudan and Ethiopia in East Africa, called Sahel, is clearly evident. Here, agriculture is strongly dependent on rainfall which, however, is erratic and highly variable and the whole region is prone to droughts and often addressed as a climate change hotspot (Turco et al., 2015), where the increase in mean temperature, the intensification of extreme hot-season occurrence and a precipitation decrease define the hotspot. Even though farming systems are adapted to such variability, for example through forms of seasonal nomadism, recent climate variations and their complex interactions with socio-economic factors are increasing the pressure on the region which is experiencing widespread impoverishment, growth of terroristic or-

ganizations, increment of conflicts and migration towards wealthier countries (Aime and de Giorgio, 2021). It is worth to notice that the two countries reporting the highest green WF in Africa - namely Nigeria and Sudan - belong to this region, a fact which confirms the strong dependency of their agricultural systems on rainfall.

4.5 Crop aggregated blue water footprint

Blue WF is defined as:

$$WF_b = \frac{10 \times ET_{b,LGP}}{Y_a} \quad \left(\frac{m^3}{ton} \right) \quad (4.2)$$

where $ET_{b,LGP}$ is calculated following equation 3.7. Thus, blue WF includes the overall irrigation water evapotranspired by irrigated agriculture. its spatial extension coincides with that of irrigated harvested areas, as showed below.

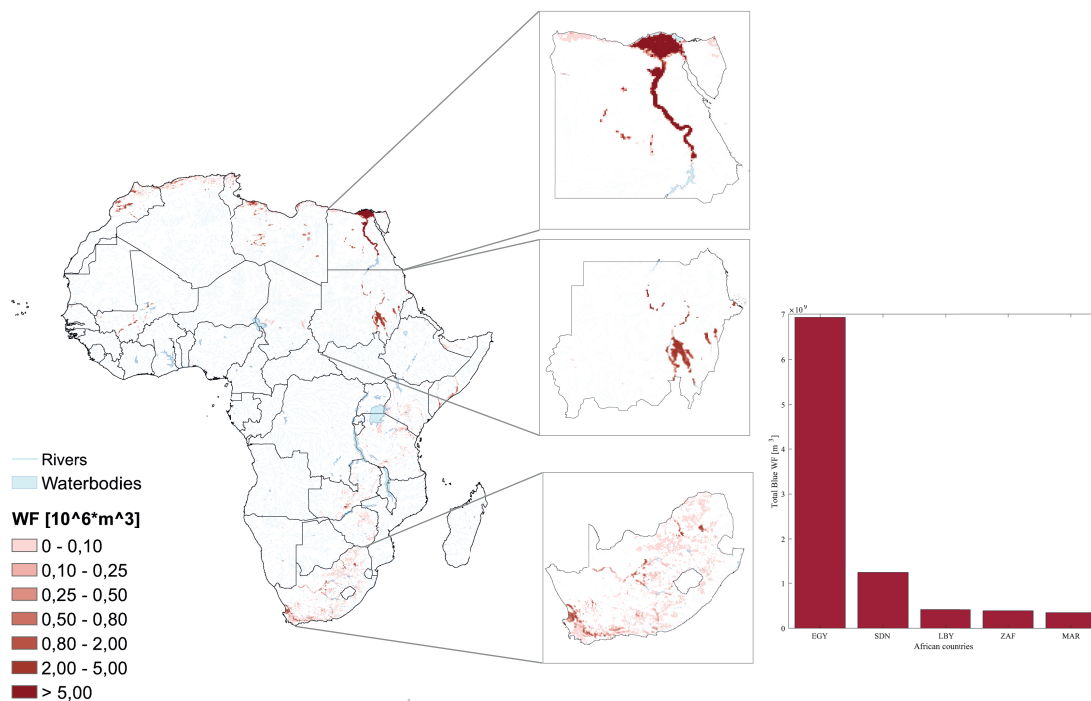


Figure 4.12: Blue WF across Africa at 2010. The three countries showing higher values are enlarged. The histogram with the five countries recording higher values is shown as well.

The highest concentration of irrigated areas appears to be along the Nile river and around its delta especially, on the coast of Egypt. The course of the river can be followed southwards, across Sudan, until Khartoum, its capital city, where the Blue Nile and the White Nile meet. South of the confluence point, the red coloured area enclosed by the two rivers is a vast agricultural scheme, the Gezira, which exploits their waters as its source of irrigation. It is not surprising that Egypt and Sudan are the countries showing the highest blue WF . At 2010, the third country on the list is Libya, however, it is South Africa to be enlarged in figure 4.12, since its blue WF is expected to overcome Libya's from 2040 onwards. Nevertheless, figure 4.13 reports a decline in South Africa's blue WF , which logically is to be expected from Libya as well. This trend, coupled with the evidence brought in the sections above of an expected increment in maize and sorghum rainfed and irrigated uWF in South Africa, can be explained by a better synchrony in the future between these crops' growing seasons and the rainfall, which allows to exploit more green water and reduce the dependency from blue water without losing in production amounts. Another interesting result shown in figure 4.13 is the expected progressive increment in Sudan blue WF in the future scenarios. As explained before, Sudan strongly depends on the Nile river as a source of irrigation water, therefore, such result implies incremental abstractions of Nile waters. Moreover, Sudan is located downstream with respect to Egypt, of which 70% of water demand relies on water bodies, Nile included (De Angelis et al., 2021). It is not a novelty that the Nile is a controversial trans-boundary river, but these projections could pose as additional sources of tensions among the two countries in the future. The situation is further complicated by the construction project of the Grand Ethiopian Renaissance Dam, which Ethiopia is building on the Blue Nile river, just on the border in common with Sudan. Supporters claim that the project could improve the flood control and reduce the sediment deposition, however, critics maintain that there are risks of reduced downstream water availability, a likely recession in Sudan agriculture and losses for Egyptian hydropower (Wheeler et al., 2016).

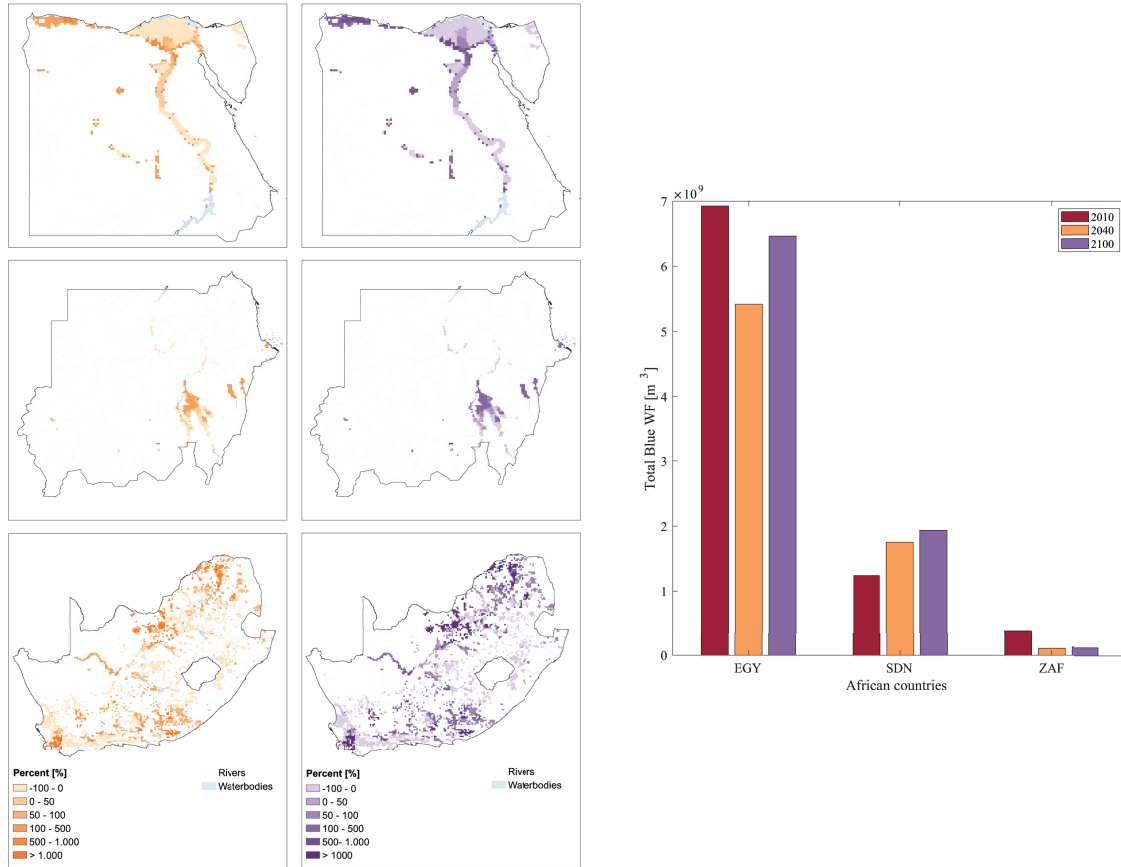


Figure 4.13: Three countries showing higher blue WF values at 2040, in orange, on the left, and at 2100, purple, on the right - $RCP2.6$. The histogram shows the evolution of the overall blue WF for the respective country between three scenarios.

Chapter 5

Discussion

The main and most evident outcome of the previous chapter is the effect of the advanced management assumption on crop yields, which produces an impressive increment by 2040. Even though this is a very optimistic hypothesis, it is fair to believe that, at some point in time, an agricultural management more similar to that of western countries will be achieved across all the African continent. The consequences of such scenario are immense, incredibly complex and impossible to be made into generalizations across the whole continent; moreover, they largely exceed the scope of this work and the capabilities of its author. However, the results presented in the previous chapter, by limiting the range of the possibilities with the assumption of constant harvested areas along the future scenarios, highlight some of the possible consequences that could occur. Moreover, the magnitude of the change introduced by the high input assumption between 2010 and 2040 partly obscures the impacts ascribable to climate change. Still, some trends can be identified between different future time steps and the divergences between the *RCPs*, which generally widens approaching 2100, are meaningful. This work also evidences different dynamics between the two categories of impacts on agriculture - climate change and management modernization -, however, in the long term they would definitely interact with each other and, if climate change would take a negative toll on the agricultural sector, an improved management could definitely represent a reliable mitigation strategy.

In Africa, crop yields may have stagnated due to a complex combination of factors, environmental and socio-economic. Specific constraints to crop yield increases

include variability of dry spells and lack of field-water management strategies, absence of significant irrigation infrastructure, low nutrient application and absence of fallows to restore soil fertility levels (Ray et al., 2012). However, biophysical limitations can be overcome and significant yields gains achieved: according to Ray et al. (2012), even fairly small increase in inputs is sufficient to double maize yields in Africa. Thanks to the yield increment recorded in this work, between 2010 and 2040, the production of the four crops considered is expected to increase by 244.6% for maize, 427.7% for sorghum, 193.5% for soy and 83.5% in the case of wheat. Basically, maize and sorghum production is projected to more than triple, nearly triple in the case of soy and nearly double for maize - as illustrated in figure 5.1.

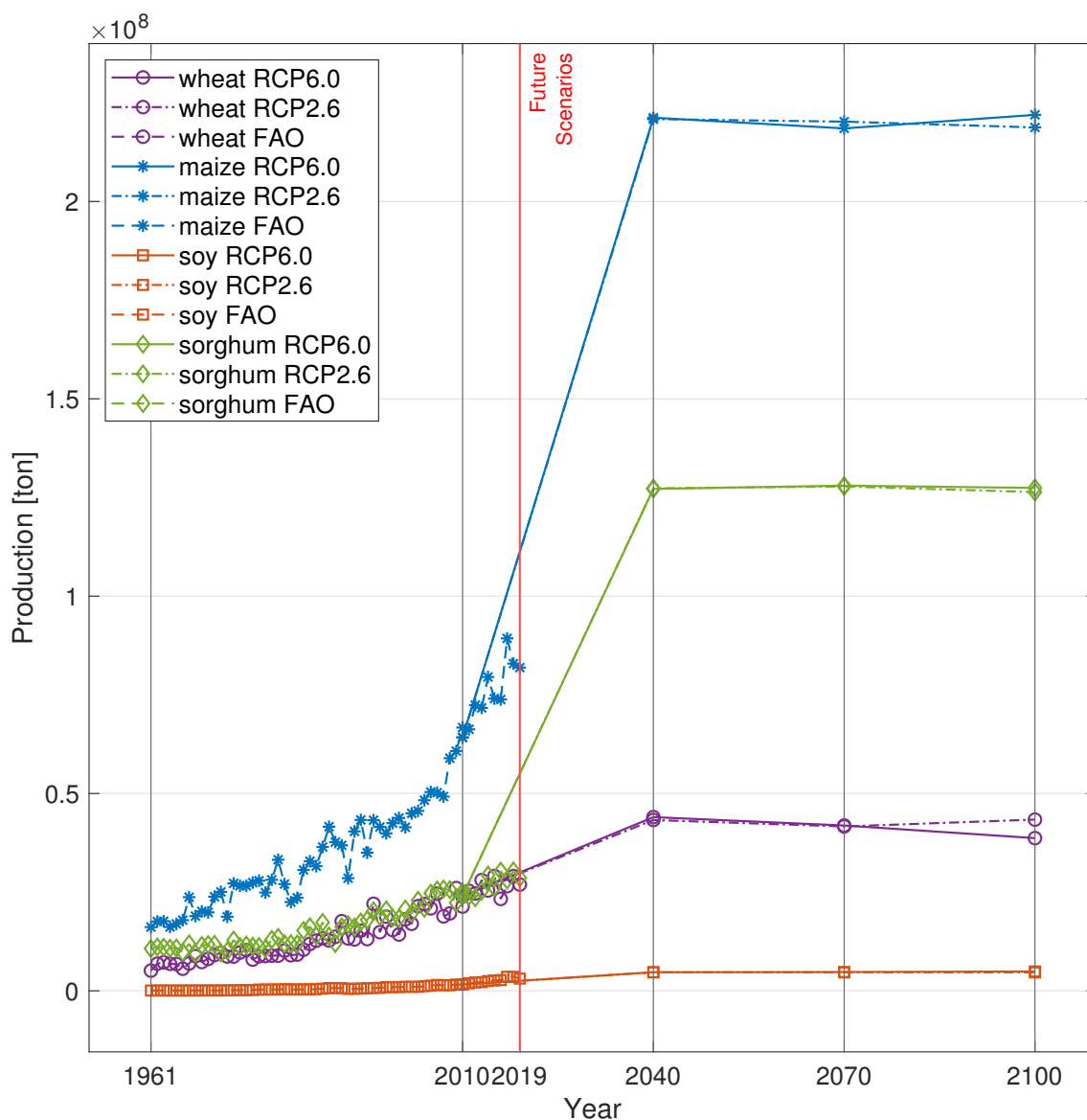


Figure 5.1: Evolution of agricultural production for each crop variety.

These projections are in line with the need expressed by Ray et al. (2013) of doubling global food production by 2050. Nevertheless, according to van Ittersum et al. (2016), a three folds increase of food demand in sub-Saharan Africa is to be expected by 2050. But even in this case maize, soy and sorghum would be on track to successfully reach the goal, even assuming no cropland expansion. These are optimistic projections which allow to hope for the abatement of the widespread food insecurity on the continent, even though it is not only a question of total amount produced. Nowadays, food insecurity is still high across the continent and affecting large shares of the population, as can be observed in figure 5.2. Here, the prevalence of severe food insecurity is represented as the percentage of people in the population who live in households classified as severely food insecure. A household is classified as severely food insecure when at least one adult in the household has reported to have been forced to reduce the quantity of the food, to have skipped meals, having gone hungry, having to go for a whole day without eating because of a lack of money or other resources or exposed to other severe experiences as such, at times during the year. It is an indicator of lack of food access (FAOSTAT, 2021). Even if this sudden advancement in management seems unlikely, it is not the only opportunity to improve crop yields. According to Elliott et al. (2014), semiarid regions where crop are mainly cultivated under rainfed conditions, typically show the greatest yield increase when irrigation water is supplied. Therefore, the expansion of the irrigation infrastructure, supported with a sustainable water management represents a step towards the strengthening of food security across the continent.

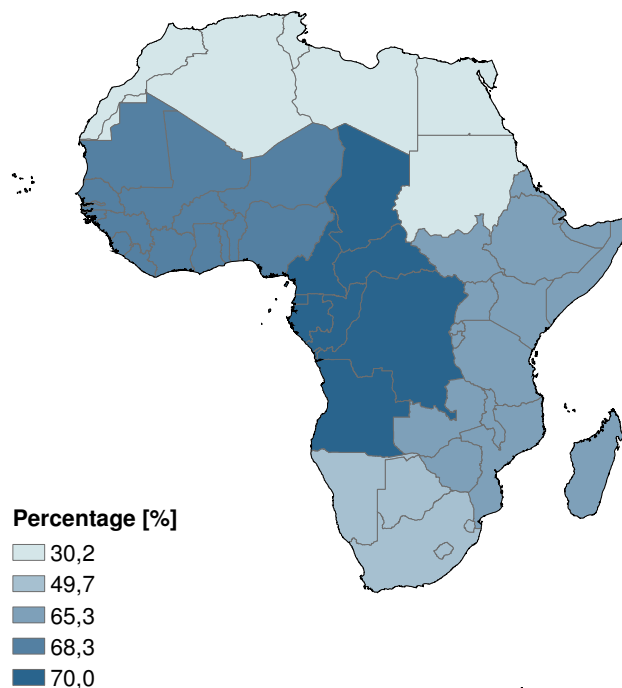


Figure 5.2: Prevalence of severe or moderate food insecurity.

This last argument bridges the question about food production with the one about the impact on water resources caused by the reported increment in yields. In the thirty years going from 2010 to 2040, where the yield increment is located, a strong reduction in uWF can be observed, which suggests a higher efficiency in the use of water resources. At the same time, the CWF increases for all crops, excluded wheat. This is simply due to the parallel rise in the tonnes produces, which derives from the yield growth, since the areas are kept constant. Moreover, CWF growing trends show lower rates than those of yields and, considering the share of rainfed and irrigated areas described in section 4.1 and by figure 4.6a, the recorded increase in CWF is mainly localized on rainfed agriculture. Such consideration opens to the opportunity of expanding current agricultural production by converting shares of cultivated areas from rainfed to irrigated with proper infrastructures for irrigation, where the locally generated runoff is large enough, so as to not compromise the

environmental flow and the downstream flow towards the other cells of the drainage network. According to Elliott et al. (2014), many regions with the largest potential for yield increases from expanded irrigation are also those most likely to have binding constraints on water availability; however, De Angelis et al. (2021) demonstrated how the problem of freshwater shortage in Africa is not only due to the actual lack of water resources, which still occurs and it is worsened by the arid climate, but it is also related to economic water scarcity. This is especially the case of the tropical countries in central Africa, which, although, exhibit large annual availability of rainfall, almost exceeding 2000 mm/yr. Moreover, these areas are crossed by two of the main African rivers, Congo and Niger, they show the highest groundwater recharge rates of all Africa (De Angelis et al., 2021) and the lowest percentage of water stress, as illustrated in figure 5.3, both at 2010 and at 2040. Nevertheless, the *AEI*, illustrated in figure 1.3b, of the countries in central Africa and of those facing

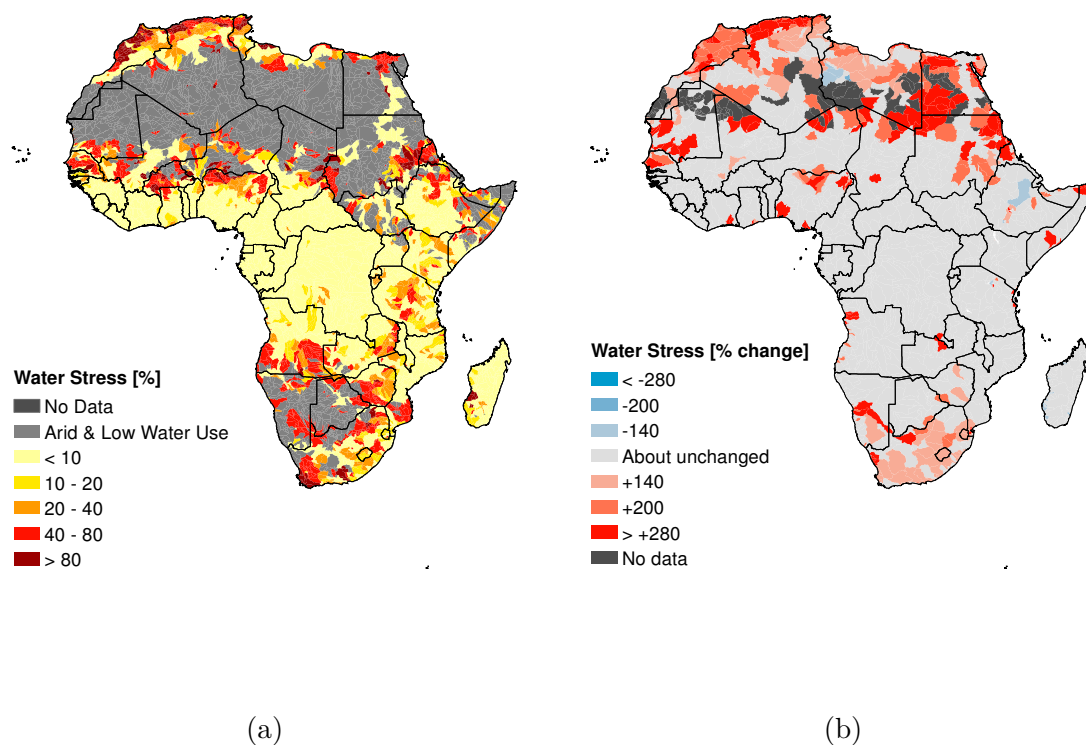


Figure 5.3: Current and projected water stress index in Africa (source: WRI (2021)): (a) Baseline water stress index (2010); (b) Index variation in the projection for year 2040 using the halfway scenario *Business as Usual*.

the gulf of Guinea are minimal and mostly concentrated in Nigeria.

A slightly different picture emerges after 2040. From this moment to 2100, the eventual impacts of climate change become visible. Both CWF and uWF increase, yields fluctuates with positive and negative changes, for reasons discussed in chapter 4, Precipitation patterns change and $ET0$ increases, as shown in figure 2.8. Therefore, the improvements brought by the advanced management assumption might not last indefinitely, or in the more realistic case of a slower advancement, climate change impacts could obstacle or even halt such a process, posing a threat to the food security achievement. Climate change can affect the water availability along the growing season or impact the plant growth by means of high temperatures. The last opportunity to maintain yield improvements under this scenario would be to expand the harvested areas, as it is occurring at the moment from what can be seen from figure 4.5. However, this is a controversial solution. Land clearing is a strong pressure on the environment which causes the loss, fragmentation and degradation of native vegetation, it impacts the local species and the soils, leading to erosion and loss of nutrients. In addition, it is recognised as a driver of climate change, through the emission released in the process and it might cause the trespass over ancestral lands inhabited by local populations.

There is obviously no single solution to this complex and deeply interrelated topic. Given the extension of the African continent, different strategies might be better suited for specific locations and multiple measures might be applied at once aiming to the same purpose.

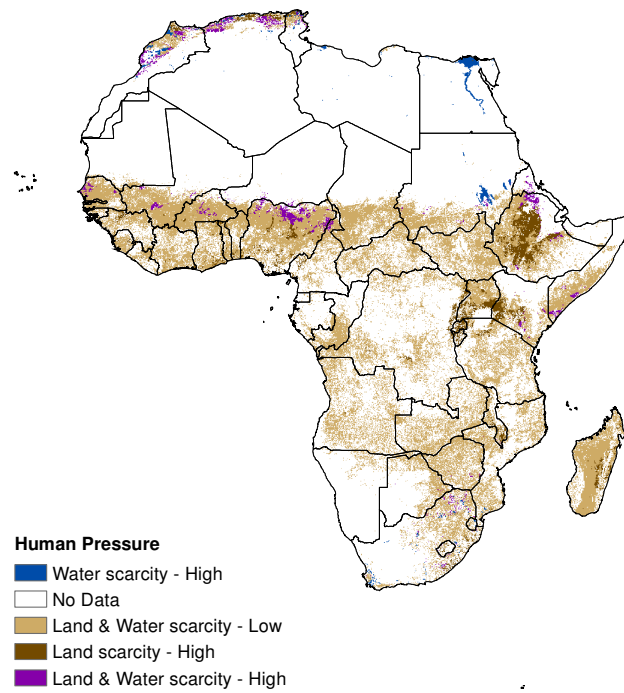


Figure 5.4: Map of land and/or water scarcity pressures on agriculture; taken from FAO (2021)

Chapter 6

Conclusion

The issues of food security and climate change are of primary importance nowadays. Climate change is already affecting every inhabited region across the globe, widespread and rapid changes in the atmosphere, ocean, cryosphere and biosphere have occurred; global temperature and precipitation have increased since 1850, the oceans have warmed and the global mean sea level have risen (IPCC, 2021). Moreover, climate change also affects food production. Warmer mean and extreme temperatures, altered precipitation regimes and drought patterns, elevated atmospheric CO₂ concentrations, among many other mechanisms, already affect agricultural productivity worldwide (Jägermeyr et al., 2021). In parallel to climate change impacts on agriculture, the rising demand for crop production, which stem from increasing human population, meat and dairy consumption, as a consequence of growing affluence, and biofuel consumption (Ray et al., 2013) constitute additional pressures on the sector. Furthermore, world hunger is on the rise after having remained stable for few years, the prevalence of undernourishment increased from 8.4 to 9.9% just in 2020 as a consequence of the global pandemic of COVID-19 (FAO et al., 2021). Africa shows the highest percentage of population suffering from hunger, globally, and many of its regions, due to their current proximity to crop-limiting temperatures thresholds for suitable production, are expected to suffer more negative effects from climate change than mid- and high- latitude regions. The present thesis tries to bridge such matters by placing the discussion at one of the multiple intersections between them. It must be emphasized that, however many socio-economic, political and cultural factors shape the actual changes that occur in the world, this study

only addresses biophysical opportunities and limitations when discussing production increase and resource availability. In this framework, the central questions posed by the present thesis are: (i) What would happen if it was possible to reach an advanced agricultural management on the current cropland by 2040? (ii) Would the production be sufficient to meet the growing food demand? And (iii) How would this impact the water resources?

The *CWF* indicator has been chosen as the meter for this analysis since it unites, in its meaning, information about production, of a crop good in this case, and about the water resources consumption inherent to the production. The future projection add the time variable and allow to simulate the effects of a changing climate on the variable of interest. The *GGCM GAEZ v4* (FAO and IIASA, 2021) has provided the yield component of the *CWF* and its future simulation, while the *ISI-MIP* repository provided the simulations of future climatic variables necessary to the *CWF* model to compute the actual *ET*, the other component necessary to calculate the *CWF*. The computation of the results has been performed by the *CWF* model developed by Tuninetti et al. (2015), aptly modified to produce one baseline scenario set at 2010 and three 30 years long future scenarios, identified by the representative years 2040, 2070 and 2100, for *RCP2.6* and *RCP6.0* and for four different crop: maize, sorghum, soy and wheat. *CWF* has been computed in different forms - namely blue, green, irrigated and rainfed - in order to untangle its dense meaning and better investigate the water use of different types of water supply in African agriculture.

The results obtained show a net decrease, for all crops, of the *uWF* between 2010 and 2040, as a direct consequence of the impressive growth of yield produced by the central assumption of this work: a high input advanced agricultural management over all the continent has been assumed in the future scenarios, in order to study its consequences. Consequently, *CWF* projections between 2010 and 2040 show a positive trend for all crops, wheat excluded. Wheat show a generally different behaviour with respect to the other crops; this has been explained by the fact that the yield growth projected by the high input assumption is in line with the actual yield growth visible until 2019, which suggests a smaller yield gap for this crop.

Additionally, wheat is the crop which shows the highest range of irrigated areas over the total cropland. After 2040 the effects of climate change become visible, causing uWF to rise again and yields to drop. Moreover, the *RCPs* analyzed presents a wider gap between their results the more they approach 2100. The impacts of a changing climate can also be observed in the percentage difference maps, which also show their spatial distribution. Generally, the tropical regions are more negatively affected than the north and the south of the continent. The analysis of the blue WF shows that the main use of water for irrigation occurs along the Nile river and, in the case of Sudan, blue WF is expected to increase, raising concerns for possible conflicts related to the river water use. The production increase observed gives promising results, which seems on track to meet even the highest projection of future food demand and open the possibility to hope for a drastic reduction of food insecurity.

The main limit of this work is the assumption of constant areas at 2010, which forces to neglect the steep expansion observed for all crops between 2010 and 2019. This has been a constraint, since a data set providing future projection of harvested areas is missing in the literature at the moment. However, future works could refine the analysis by including the current cropland expansion and simulating future ones. Moreover, the assumption of advanced management could be represented as an improvement over a longer period of time and a progressive share of irrigated areas could be projected on the current ones, as to show an eventual expansion of irrigated infrastructure.

Bibliography

- M. Aime and A. de Giorgio. *Il grande gioco del Sahel. Dalle carovane di sale ai Boeing di cocaina*. Bollati Boringhieri, 2021.
- T. Allan. *Virtual water: tackling the threat to our planet's most precious resource*. Bloomsbury Publishing, 2011.
- R. G. Allen, L. Pereira, D. Raes, and M. Smith. Crop evapotranspiration: Guidelines for computing crop water requirements. *FAO Irrig. Drain. Pap.*, 56:26–40, 1998.
- A. Bondeau, P. C. Smith, S. Zaehle, S. Schaphoff, W. Lucht, W. Cramer, D. Gerten, H. Lotze-Campen, C. Müller, M. Reichstein, and B. Smith. Modelling the role of agriculture for the 20th century global terrestrial carbon balance. *Global Change Biology*, 13:679–706, 2007. doi: doi: 10.1111/j.1365-2486.2006.01305.x.
- CRU. High-resolution gridded datasets (and derived products), 2021. URL <https://crudata.uea.ac.uk/cru/data/hrg/>. [Accessed: November 2021].
- P. De Angelis, M. Tuninetti, L. Bergamasco, L. Calianno, P. Asinari, F. Laio, and M. Fasano. Data-driven appraisal of renewable energy potentials for sustainable freshwater production in africa. *Renewable and Sustainable Energy Reviews*, 149, 2021. doi: <https://doi.org/10.1016/j.rser.2021.111414>.
- P. D’Odorico, K. F. Davis, L. Rosa, J. A. Carr, D. Chiarelli, J. Dell’Angelo, and M. C. Rulli. The global food-energy-water nexus. *Reviews of geophysics*, 56(3): 456–531, 2018.
- P. D’Odorico, J. Carr, J. D. C. Dalin, M. Konar, F. Laio, and M. Tuninetti. Global virtual water trade and the hydrological cycle: patterns, drivers, and socio-environmental impacts. *Environmental Research Letters*, 14(5), 2019.

- J. Elliott, D. Deryng, C. Müller, K. F. M. Konzmann, D. Gerten, M. G. M. Flörke, Y. Wada, N. Best, S. Eisner, B. M. Fekete, C. Folberth, I. Foster, S. N. Gosling, I. Haddeland, N. Khabarov, F. Ludwig, Y. Masaki, S. Olin, C. Rosenzweig, A. C. Ruane, Y. Satoh, E. Schmid, T. Stacke, Q. Tang, and D. Wisser. Constraints and potentials of future irrigation water availability on agricultural production under climate change. *PNAS*, 111(9):3239–3244, 2014. doi: www.pnas.org/cgi/doi/10.1073/pnas.1222474110.
- FAO. Fao map catalog, 2014. URL <https://data.apps.fao.org/map/catalog/srv/eng/catalog.search#/home>. [Accessed: November 2021].
- FAO. Fao aquamaps, 2021. URL <https://data.apps.fao.org/aquamaps/>. [Accessed: November 2021].
- FAO and IIASA. *Global Agro-Ecological Zones (GAEZ v4) – Data Portal user’s guide*. FAO, 2021.
- FAO, IFAD, UNICEF, WFP, and WHO. *The State of Food Security and Nutrition in the World 2021. Transforming food systems for food security, improved nutrition and affordable healthy diets for all*. FAO, 2021. doi: <https://doi.org/10.4060/cb4474en>.
- FAO/IIASA/ISRIC/ISSCAS/JRC. *Harmonized World Soil Database (version 1.2)*. FAO, 2012.
- FAOSTAT. Faostat, 2021. URL <https://www.fao.org/faostat/en/#data>. [Accessed: September 2021].
- K. Frieler, S. Lange, F. Piontek, C. P. O. Reyer, J. Schewe, L. Warszawski, F. Zhao, L. Chini, S. Denvi, K. Emanuel, T. Geiger, K. Halladay, G. Hurtt, M. Mengel, D. Murakami, S. Ostberg, A. Popp, R. Riva, M. Stevanovic, T. Suzuki, J. Volkholz, E. Burke, P. Ciais¹, K. Ebi, T. D. Eddy, J. Elliott, E. Galbraith, S. N. Gosling, F. Hattermann, T. Hickler, J. Hinkel, C. Hof, V. Huber, J. Jägermeyr, V. Krysanova, R. Marcé, H. M. Schmied, I. Mouratiadou, D. Pierson, D. P. Titensor, R. Vautard, M. van Vliet, M. F. Biber, R. A. Betts, B. L. Bodirsky, D. Deryng, S. Frohking, C. D. Jones, H. K. Lotze, H. Lotze-Campen, R. Sahajpa, K. Thonicke, H. Tian, and Y. Yamagata. Assessing the impacts of 1.5 °c

- global warming – simulation protocol of the inter-sectoral impact model inter-comparison project (isimip2b). *Geosci. Model Dev.*, 10:4321–4345, 2017. doi: <https://doi.org/10.5194/gmd-10-4321-2017>.
- GADM. Global administrative areas, version 3.6, 2018. URL <https://gadm.org/index.html>. [Accessed: September 2021].
- I. Harris, P. Jones, T. Osborn, and D. Lister. Updated high-resolution grids of monthly climatic observations – the cru ts3.10 dataset. *Int. J. Climatol.*, 34: 623–642, 2014. doi: DOI: 10.1002/joc.3711.
- IPCC. *Climate Change 2014: Synthesis Report. Contribution of Working Groups I, II and III to the Fifth Assessment Report of the Intergovernmental Panel on Climate Change [Core Writing Team, R.K. Pachauri and L.A. Meyer (eds.)]*. IPCC, 2014.
- IPCC. *Summary for Policymakers. In: Climate Change 2021: The Physical Science Basis. Contribution of Working Group I to the Sixth Assessment Report of the Intergovernmental Panel on Climate Change [Masson-Delmotte, V., P. Zhai, A. Pirani, S.L. Connors, C. Péan, S. Berger, N. Caud, Y. Chen, L. Goldfarb, M.I. Gomis, M. Huang, K. Leitzell, E. Lonnoy, J.B.R. Matthews, T.K. Maycock, T. Waterfield, O. Yelekçi, R. Yu, and B. Zhou (eds.)]*. In Press, 2021.
- ISIMIP. Inter-sectoral impact model intercomparison project (isimip) repository, 2021. URL <https://gadm.org/index.html>. [Accessed: November 2021].
- J. Jägermeyr, C. Müller, A. C. Ruane, J. Elliott, J. Balkovic, O. Castillo, B. Faye, I. Foster, C. Folberth, J. A. Franke, K. Fuchs, J. R. Guarin, J. Heinke, G. Hoogenboom, T. I. A. K. Jain, D. Kelly, N. Khabarov, S. Lange, T. Lin, W. Liu, O. Milyk, S. Minoli, E. J. Moyer, M. Okada, M. Phillips, C. Porter, S. S. Rabin, C. S. adn J. M. Schneider, J. F. Schyns, R. Skalsky, A. Smerald, T. Stella, H. Stephens, H. Webber, F. Zabel, and C. Rosenzweig. Climate impacts on global agriculture emerge earlier in new generation of climate and crop models. *Nat Food*, 2:873–885, 2021. doi: <https://doi.org/10.1038/s43016-021-00400-y>.

- J. Liu. A gis-based tool for modelling large-scale crop-water relations. *Environmental Modelling & Software*, 24(3):411–422, 2009. doi: <https://doi.org/10.1016/j.envsoft.2008.08.004>.
- J. Liu, J. R. Williams, A. Zehnder, and H. Yang. Gepic – modelling wheat yield and crop water productivity with high resolution on a global scale. *Agricultural Systems*, (94):478–493, 2007. doi: [doi:10.1016/j.agsy.2006.11.019](https://doi.org/10.1016/j.agsy.2006.11.019).
- W. Liu, H. Yang, C. Folberth, X. Wang, Q. Luo, and R. Schulin. Global investigation of impacts of pet methods on simulating crop-water relations for maize. *Agricultural and Forest Meteorology*, 221:164–175, 2016. doi: <https://doi.org/10.1016/j.agrformet.2016.02.017>.
- M. M. Mekonnen and A. Y. Hoekstra. The green, blue and grey water footprint of crops and derived crop products. *Hydrol. Earth Syst. Sci.*, 15(5):1577–1600, 2011.
- C. Müller, J. Elliott, J. Chryssanthacopoulos, A. Arneth, J. Balkovic, P. Ciais, D. Deryng, C. Folberth, M. Glotter, S. Hoek, T. I. R. C. Izaurralde, C. Jones, N. Khabarov, P. Lawrence, W. Liu, S. Olin, T. A. M. Pugh, D. K. Ray, A. Reddy, C. Rosenzweig, A. C. Ruane, G. Sakurai, E. Schmid, R. Skalsky, C. X. Song, X. Wang, A. de Wit, and H. Yang. Global gridded crop model evaluation: benchmarking, skills, deficiencies and implications. *Geosci. Model Dev.*, 10:1403–1422, 2017. doi: [doi:10.5194/gmd-10-1403-2017](https://doi.org/10.5194/gmd-10-1403-2017).
- C. Monfreda, N. Ramankutty, and J. A. Foley. Farming the planet: 2. geographic distribution of crop areas, yields, physiological types, and net primary production in the year 2000. *Global Biogeochem. Cycles*, 22(GB1022), 2008. doi: [doi:10.1029/2007GB002947](https://doi.org/10.1029/2007GB002947).
- M. New, D. Lister, M. Hulme, and I. Makin. A high-resolution data set of surface climate over global land areas. *Clim Res*, 21:1–25, 2002.
- K. W. Oleson, D. M. Lawrence, G. B. Bonan, B. Drewniak, M. Huang, C. D. Koven, S. Levis, F. Li, W. J. Riley, Z. M. Subin, S. C. Swenson, and P. E. Thornton. Technical description of version 4.5 of the community land model (clm). *Tech. Rep., Natl. Center for Atmos. Res.*, (420), 2013.

- F. T. Portmann, S. Siebert, and P. Döll. Mirca2000 global monthly irrigated and rainfed crop areas around the year 2000: A new high resolution data set for agricultural and hydrological modeling. *Global Biogeochem. Cycles*, 24(GB1011), 2010. doi: doi:10.1029/2008GB003435.
- D. K. Ray, N. Ramankutty, N. D. Mueller, P. C. West, and J. A. Foley. Recent patterns of crop yield growth and stagnation. *NATURE COMMUNICATIONS*, 3(1293), 2012. doi: DOI: 10.1038/ncomms2296.
- D. K. Ray, N. D. Mueller, P. C. West, and J. A. Foley. Yield trends are insufficient to double global crop production by 2050. *PLoS ONE*, 6(8), 2013. doi: doi:10.1371/journal.pone.0066428.
- D. K. Ray, P. C. West, M. Clark, J. S. Gerber, A. V. Prishchepov, and S. Chatterjee. Climate change has likely already affected global food production. *PLoS ONE*, 5(14), 2019. doi: <https://doi.org/10.1371/journal.pone.0217148>.
- C. Rosenzweig, J. Elliott, D. Deryng, A. Ruane, C. Müller, A. Arneth, C. F. K. J. Boote, M. Glotter, N. Khabarov, K. Neumann, F. Piontek, T. A. M. Pugh, E. Schmid, E. Stehfest, H. Yang, and J. W. Jones. Assessing agricultural risks of climate change in the 21st century in a global gridded crop model intercomparison. *PNAS*, 111(9):3268–3273, 2014. doi: www.pnas.org/cgi/doi/10.1073/pnas.1222463110.
- H. J. Schellnhuber, K. Frieler, and P. Kabat. The elephant, the blind, and the intersectoral intercomparison of climate impacts. *PNAS*, 111(9):3225–3227, 2014. doi: www.pnas.org/cgi/doi/10.1073/pnas.1321791111.
- S. Siebert and P. Döll. Quantifying blue and green virtual water contents in global crop production as well as potential production losses without irrigation. *J. Hydrol.*, 384(3):198–217, 2010.
- S. Siebert, V. Henrich, K. Frenken, and J. Burke. *Update of the digital global map of irrigation areas to version 5*. Rheinische Friedrich-Wilhelms-Universität, Bonn, Germany and Food and Agriculture Organization of the United Nations, 2013.

- E. H. Sutanudjaja, R. van Beek, N. Wanders, Y. Wada, J. H. C. Bosmans, N. Drost, R. J. van der Ent, I. E. M. de Graaf, J. M. Hoch, K. de Jong, D. K. P. L. López, S. Peßenteiner, O. Schmitz, M. W. Straatsma, E. Vannamettee, D. Wisser, and M. F. P. Bierkens. Pcr-globwb 2: a 5 arcmin global hydrological and water resources model. *Geosci. Model Dev.*, 11:2429–2453, 2018. doi: <https://doi.org/10.5194/gmd-11-2429-2018>.
- S. Tamea, M. Tuninetti, I. Soligno, and F. Laio. Virtual water trade and water footprint of agricultural goods: the 1961–2016 cwasi database. *Earth System Science Data*, 13(5):2025–2051, 2021.
- X. Tian and X. Yu. Crop yield gap and yield convergence in african countries. *Food Security*, 11:1305–1319, 2019. doi: <https://doi.org/10.1007/s12571-019-00972-5>.
- M. Tuninetti, S. Tamea, P. D’Odorico, F. Laio, and L. Ridolfi. Global sensitivity of high-resolution estimates of crop water footprint. *Water Resour. Res.*, 51: 8257–8272, 2015. doi: [doi:10.1002/2015WR017148](https://doi.org/10.1002/2015WR017148).
- M. Turco, E. Palazzi, J. von Hardenberg, and A. Provenzale. Observed climate change hotspots. *Geophys. Res. Lett.*, 42:3521– 3528, 2015. doi: [doi:10.1002/2015GL063891](https://doi.org/10.1002/2015GL063891).
- M. K. van Ittersum, L. G. J. van Bussel, J. Wolfa, P. Grassini, J. van Wart, N. Guilpart, L. Claessens, H. de Groot, K. Wiebe, D. Mason-D’Croz, H. Yang, H. Boogaard, P. A. J. van Oort, M. P. van Loon, K. Saito, O. Adimo, S. Adjei-Nsiah, A. Agali, A. Bala, R. Chikowo, K. Kaizzi, M. Kouressy, J. H. J. R. Makoi, K. Ouattara, K. Tesfaye, and K. G. Cassman. Can sub-saharan africa feed itself? *PNAS*, 113(52):14964–14969, 2016. doi: www.pnas.org/cgi/doi/10.1073/pnas.1610359113.
- L. Warszawski, K. Frieler, V. Huber, F. Piontek, O. Serdeczny, and J. Schewe. The inter-sectoral impact model intercomparison project (isi-mip): Project framework. *PNAS*, 111(9):3228–3232, 2014. doi: www.pnas.org/cgi/doi/10.1073/pnas.1312330110.
- K. G. Wheeler, M. Basheer, Z. T. Mekonnen, S. O. Eltoum, A. Mersha, G. M. Abdo, E. A. Zagona, J. W. Hall, and S. J. Dadson. Cooperative filling approaches for

BIBLIOGRAPHY

the grand ethiopian renaissance dam. *Water International*, 41(4):611–634, 2016.
doi: DOI: 10.1080/02508060.2016.1177698.

WRI. Water resources institute. water risk atlas, 2021. URL
<http://www.wri.org/applications/maps/aqueduct-atlas/>. [Accessed:
November 2021].

Appendix A

Yield spatial variability on Italy and Ethiopia

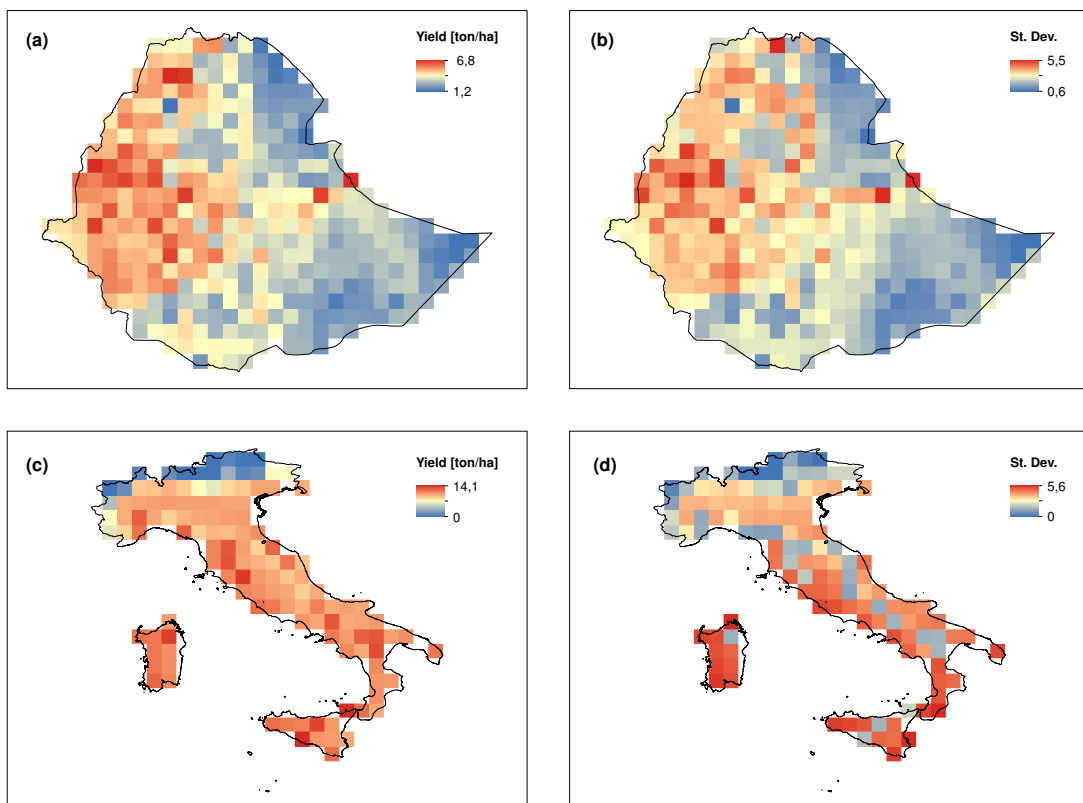


Figure A.1: Spatial variability of irrigated Maize (a) average yield, (b) standard deviation across Ethiopia and (c) average yield, (d) standard deviation across Italy for the year 2000

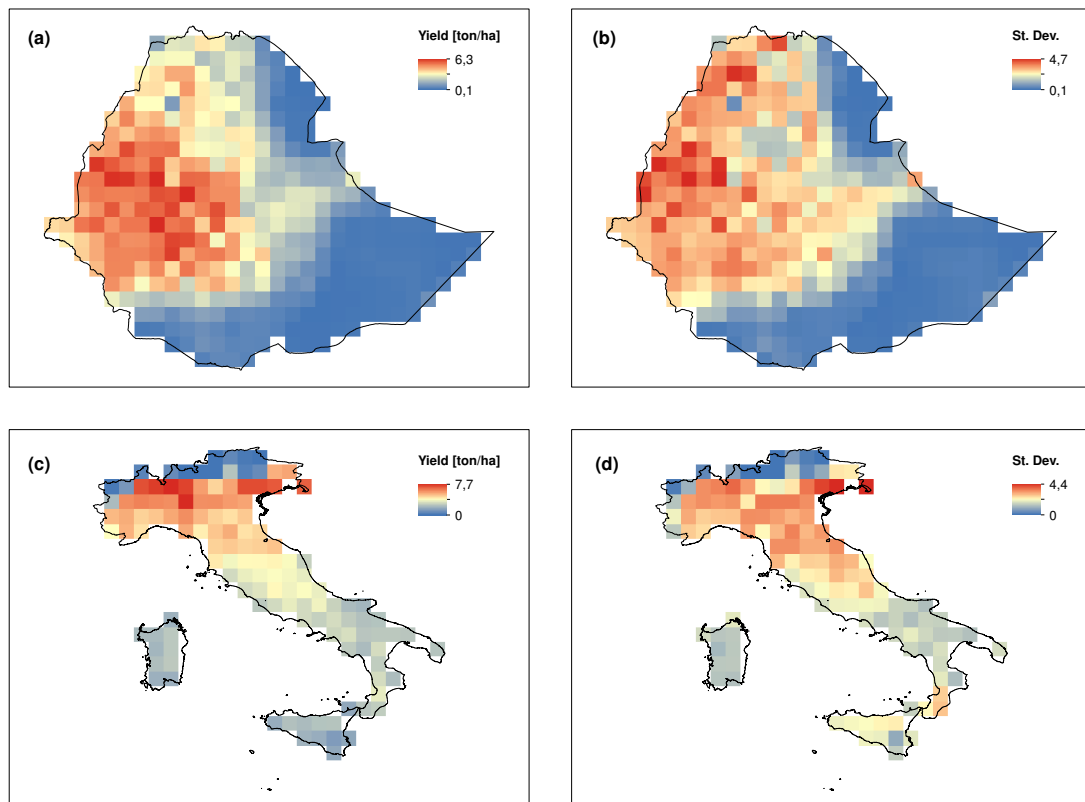


Figure A.2: Spatial variability of rainfed Maize (a) average yield, (b) standard deviation across Ethiopia and (c) average yield, (d) standard deviation across Italy for the year 2000

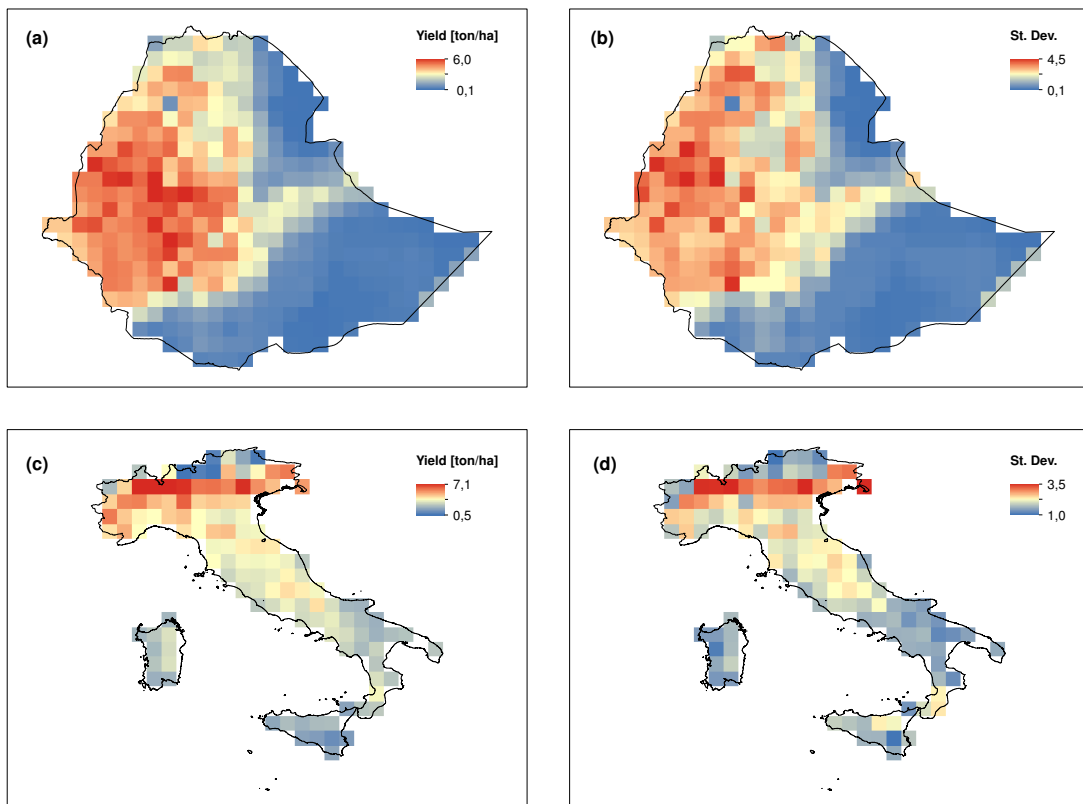


Figure A.3: Spatial variability of rainfed Maize (a) average yield, (b) standard deviation across Ethiopia and (c) average yield, (d) standard deviation across Italy for the year 2099, *RCP6.0*

Appendix B

Country identifier global grid

A global grid containing country-identifying FAO codes in every cells, belonging to the respective country, have been used to perform national aggregation of statistics [e.g. yield national average]. The starting point for the grid production was a single ESRI shapefile with country borders provided by GADM (2018). Consequently, the shapefile was converted to a raster with the proper resolution of 5×5 arc min. The map has been used as a mask to assign yield and area cells to the proper country, in order to produce the above-mentioned scatter-plots.

Appendix C

GGCMs Details

Table C.1: GGCMs detailed parameters description

Model	CLM4.5	GEPIC	PEPIC	LPJmL	GAEZ
Type	Ecosystem	Site-based	Site-based	Ecosystem	AEZ
CO ₂ Effects	n.a.	RUE, TE	RUE, TE	LF, SC	n.a.
Stresses	W, T, H	W, T, H, A, N, P, BD, AL	W, T, H, A, N, P, BD, AL	W, T	W, T, H, PDW
Fertilizer Application	N to meet crop demand	Split N application	N based on ISI-MIP2b, P with no limitation	n.a.	Application depends on input scenario
Spatial Scale	30 x 30 arc min	30 x 30 arc min	30 x 30 arc min	30 x 30 arc min	5 x 5 arc min
Climate Input Variables	T, SH, WS, LwR, SwR, Pr	WS, Tmax, Tmin, RH, SwR, Pr	WS, SH, Tmax, Tmin, RH, SwR, Pr	T, LwR, SwR, Pr	Tmin, Tmax, SF, WS, RH, Pr

Table C.1: GGCMs detailed parameters description

Model	CLM4.5	GEPIC	PEPIC	LPJmL	GAEZ
GCMs	GFDL-ESM2M, HadGEM2-ES, IPSL-CM5A-LR, MIROC5	GFDL-ESM2M, HadGEM2-ES, IPSL-CM5A-LR, MIROC-ESM-CHEM, NorESM1-M			
Crops	Maize, Soy	Maize, Wheat, Soy, Rice	Maize, Wheat, Soy, Rice	Maize, Wheat, Soy, Rice, Millet, Cassava, Sugar beet, Field pea, Rapeseed, Sunflower, Groundnut, Sugarcane	Up to 77 crops
Outputs	Actual yield	Actual yield	Actual yield	Actual yield	Potential yield Attainable yield

Notes for abbreviations:

- CO₂ effects - RUE: Radiation use efficiency; TE: Transpiration efficiency; LF:

Leaf-level photosynthesis; SC: stomatal conductance;

- Stresses - W: water stress; T: temperature stress; H: specific-heat stress; A: oxygen stress; N: nitrogen stress; P: phosphorus stress; BD: bulk density; AL: aluminum stress (based on pH and base saturation); PDW: Pests, diseases and Weeds;
- Fertilizer application - N: Nitrogen; P: Phosphorus;
- Climate input variables - T: temperature; Tmax: maximum temperature; Tmin: minimum temperature; RH: relative humidity; SH: specific humidity; SF: sunshine fraction; WS: wind speed; LwR: long wave radiation; SwR: short wave radiation; Pr: precipitation;